Economic Geology, v. 105, pp. 467–508

Iron Formation: The Sedimentary Product of a Complex Interplay among Mantle, Tectonic, Oceanic, and Biospheric Processes *

Andrey Bekker,[1,†] John F. Slack,[2] Noah Planavsky,[3] Bryan Krapež,[4] Axel Hofmann,[5] Kurt O. Konhauser,[6] and Olivier J. Rouxel[7,8]

[1]*Department of Geological Sciences, University of Manitoba, Winnipeg, Manitoba R3T 2N2, Canada*

[2]*U.S. Geological Survey, National Center, Mail Stop 954, Reston, Virginia 20192*

[3]*Department of Earth Sciences, University of California, Riverside, 900 University Ave., Riverside, California 92521*

[4]*The Institute for Geoscience Research, Curtin University, GPO Box U1987, Perth, Western Australia 6845, Australia*

[5]*School of Geological Sciences, University of KwaZulu-Natal, Durban 4041, South Africa*

[6]*Department of Earth and Atmospheric Sciences, University of Alberta, Edmonton, Alberta T6G 2E3, Canada*

[7]*Department of Marine Chemistry and Geochemistry, Woods Hole Oceanographic Institution, Mail Stop 25, 266 Woods Hole Road, Woods Hole, Massachusetts 02543*

[8]*Université Européene de Bretagne, IUEM European Institute for Marine Studies, Technopôle Brest-Iroise, Place N. Copernic, 29280 Plouzané, France*

Abstract

Iron formations are economically important sedimentary rocks that are most common in Precambrian sedimentary successions. Although many aspects of their origin remain unresolved, it is widely accepted that secular changes in the style of their deposition are linked to environmental and geochemical evolution of Earth. Two types of Precambrian iron formations have been recognized with respect to their depositional setting. Algoma-type iron formations are interlayered with or stratigraphically linked to submarine-emplaced volcanic rocks in greenstone belts and, in some cases, with volcanogenic massive sulfide (VMS) deposits. In contrast, larger Superior-type iron formations are developed in passive-margin sedimentary rock successions and generally lack direct relationships with volcanic rocks. The early distinction made between these two iron-formation types, although mimimized by later studies, remains a valid first approximation. Texturally, iron formations were also divided into two groups. Banded iron formation (BIF) is dominant in Archean to earliest Paleoproterozoic successions, whereas granular iron formation (GIF) is much more common in Paleoproterozoic successions. Secular changes in the style of iron-formation deposition, identified more than 20 years ago, have been linked to diverse environmental changes. Geochronologic studies emphasize the episodic nature of the deposition of giant iron formations, as they are coeval with, and genetically linked to, time periods when large igneous provinces (LIPs) were emplaced. Superior-type iron formation first appeared at ca. 2.6 Ga, when construction of large continents changed the heat flux at the core-mantle boundary. From ca. 2.6 to ca. 2.4 Ga, global mafic magmatism culminated in the deposition of giant Superior-type BIF in South Africa, Australia, Brazil, Russia, and Ukraine. The younger BIFs in this age range were deposited during the early stage of a shift from reducing to oxidizing conditions in the ocean-atmosphere system. Counterintuitively, enhanced magmatism at 2.50 to 2.45 Ga may have triggered atmospheric oxidation. After the rise of atmospheric oxygen during the GOE at ca. 2.4 Ga, GIF became abundant in the rock record, compared to the predominance of BIF prior to the Great Oxidation Event (GOE). Iron formations generally disappeared at ca. 1.85 Ga, reappearing at the end of the Neoproterozoic, again tied to periods of intense magmatic activity and also, in this case, to global glaciations, the so-called Snowball Earth events. By the Phanerozoic, marine iron deposition was restricted to local areas of closed to semiclosed basins, where volcanic and hydrothermal activity was extensive (e.g., back-arc basins), with ironstones additionally being linked to periods of intense magmatic activity and ocean anoxia.

Late Paleoproterozoic iron formations and Paleozoic ironstones were deposited at the redoxcline where biological and nonbiological oxidation occurred. In contrast, older iron formations were deposited in anoxic oceans, where ferrous iron oxidation by anoxygenic photosynthetic bacteria was likely an important process. Endogenic and exogenic factors contributed to produce the conditions necessary for deposition of iron formation. Mantle plume events that led to the formation of LIPs also enhanced spreading rates of midocean ridges and produced higher growth rates of oceanic plateaus, both processes thus having contributed to a higher hydrothermal flux to the ocean. Oceanic and atmospheric redox states determined the fate of this flux. When the hydrothermal flux overwhelmed the oceanic oxidation state, iron was transported and deposited distally from hydrothermal vents. Where the hydrothermal flux was insufficient to overwhelm the oceanic redox state, iron was deposited only proximally, generally as oxides or sulfides. Manganese, in contrast, was more mobile. We conclude that occurrences of BIF, GIF, Phanerozoic ironstones, and exhalites surrounding VMS systems record a complex interplay involving mantle heat, tectonics, and surface redox conditions throughout Earth history, in which mantle heat unidirectionally declined and the surface oxidation state mainly unidirectionally increased, accompanied by superimposed shorter term fluctuations.

† Corresponding author: e-mail, bekker@cc.umanitoba.ca

* A digital supplement to this paper is available at <http://www.geoscienceworld.org/> or, for subscribers, on the SEG website, <http://www.segweb.org>.

0361-0128/10/3884/467-42

Submitted: February 22, 2009
Accepted: March 16, 2010

Introduction

GIANT hematite and martite-goethite iron ores (≥56% Fe) derived from iron formations rank among the largest ore deposits and are the principal source of iron for the global steel industry. Given their economic importance, iron formations have been extensively studied during the past one hundred years, but many aspects of their sedimentary origin remain enigmatic because modern analogues are unknown. How these deposits were upgraded to iron ore also remains an intriguing question (e.g., Morey, 1999; Taylor et al., 2001). However, as Precambrian studies advance and become more closely coupled with modern biogeochemical work, our understanding of iron formations also improves. Iron formations were deposited for more than three billion years, but as the Earth system changed fundamentally, so too did the style of iron-formation deposition. Aspects of, and changes in, the Earth system that are most relevant to the deposition of iron formation include volcanism, evolution of the biosphere, and ocean composition (e.g., Huston and Logan, 2004; Holland, 2005). In this review, we discuss interplays among these factors and their respective links to the deposition of iron formation.

The abundance of iron formations in Precambrian successions was used in early studies as an argument for an anoxic state of the atmosphere and ocean (e.g., Cloud, 1973). It is generally accepted that accumulation of such large masses of iron required the transport of Fe(II); in solution Fe(III) is essentially insoluble at circumneutral pH values in the presence of even traces of oxygen. Although earlier models generally invoked a terrestrial source of iron for iron formations, the discovery in the late 1970s of modern sea-floor hydrothermal systems shifted emphasis to the deep ocean as the most likely source (e.g., Isley, 1995). Based on the depositional setting of and microfossil work on Paleoproterozoic iron formations in the Animikie basin of the Lake Superior region, Cloud (1965) argued for a role of cyanobacteria in iron precipitation, a model that quickly gained wide acceptance for Precambrian iron formations. Cloud (1965, 1973) suggested that the redox state of the ocean-atmosphere system was maintained at low levels of free oxygen, primarily by the reducing potential of the oceans and continuous iron-formation deposition. Subsequently, it became clear that the Animikie iron formations were deposited well after the GOE at ca. 2.4 Ga (e.g., Bekker et al., 2004), and that many of the Gunflint-type microfossils, interpreted earlier as oxygenic photosynthesizers, were likely metabolic iron oxidizers (Golubic and Seong-Joo, 1999; Planavsky et al., 2009).

Precise geochronologic constraints also challenged the earlier assumption that iron formations were continuously deposited before the rise of atmospheric oxygen (e.g., James, 1983). Deposition of large, economically important iron formations was restricted in time and coincided with mantle plume breakout events, as recorded by the secular distribution of large igneous provinces (LIPs), dike swarms, and submarine-emplaced mafic volcanic rocks (e.g., Klein and Beukes, 1992; Isley and Abbott, 1999). These events not only provided the dissolved ferrous iron for iron formation, but they also tempered the oceanic redox state and its chemistry by changing the flux of reductants such as H_2 and H_2S. In addition, higher oceanic spreading rates, increased submarine and subaerial volcanic activity, and an enhanced production of volcanogenic massive sulfide (VMS) deposits are predicted consequences of mantle plume breakout events (e.g., Barley et al., 2005).

Emerging age constraints also provide insights into other puzzles of iron-formation genesis. For example, if the oceanic and atmospheric redox states are major controls on iron transport and deposition, then why were giant BIFs deposited at ca. 2.45 Ga? It appears that deposition of these iron formations occurred shortly before the GOE, thus suggesting a genetic link. If atmospheric oxygen rose during the early Paleoproterozoic, then why is there a second peak in iron-formation deposition at ca. 1.88 Ga? This pulse of iron-formation deposition seemingly occurred during a mantle plume breakout event, again suggesting a link. The disappearance of iron formations at ca. 1.8 Ga has been explained by either complete ocean oxidation (Holland, 1984) or by development of sulfidic conditions in the deep ocean (Canfield, 1998; Poulton et al., 2004). Neither of these models fully addresses the mechanism that caused the ocean redox state prior to 1.88 Ga to change back to anoxic ferruginous conditions and, subsequently at ca. 1.8 Ga, to either fully oxic or sulfidic conditions. A suboxic redox state after ca. 1.8 Ga was proposed by Slack et al. (2007, 2009) based on Ce anomalies and abundant hematite and magnetite in VMS-related, deep-water, oxide-facies exhalites of late Paleoproterozoic and Mesoproterozoic age.

It has long been argued that Archean and Paleoproterozoic (e.g., 1.88 Ga) iron formations were deposited in entirely different settings and have different compositions and textures (e.g., Klein and Beukes, 1992). Archean iron formations consist predominantly of interbanded iron- and silica-rich layers and were generally, but not universally, deposited in relatively deep water settings, as they typically lack evidence for wave or storm action. The 1.88 Ga iron formations were in contrast deposited close to or above storm and fair-weather wave base and commonly have granular, possibly clastic, textures. These differences reflect not only distinctions in their depositional settings but also different mechanisms for iron oxidation and precipitation. Following a gap between ca. 1.8 and 0.7 Ga, iron formations reappeared at the end of the Neoproterozoic, apparently related to global Snowball Earth events (Hoffman et al., 1998). These are mineralogically simple iron and silica oxide deposits that, in places, also contain economic manganese concentrations (Klein and Beukes, 1992). Phanerozoic iron formations, termed ironstones, are by contrast relatively rare, being temporally linked to marine anoxic events. They comprise iron silicates and oxides without the chert enrichment characteristic of Precambrian deposits but with appreciable phosphorous contents. Significantly, Archean, Paleoproterozoic, and Phanerozoic iron formations and ironstones are temporally associated with organic matter-rich black shales (e.g., van Houten and Arthur, 1989; Simonson, 2003). In contrast, other Phanerozoic examples of Fe-Si–rich rocks, commonly termed umber, generally developed above volcanic rocks and probably formed through diffuse sea-floor hydrothermal venting, although direct precipitation from seawater as hydrothermal plume fallout has also been suggested (Elderfield et al., 1972; Alt, 2003; Little et al., 2004).

Tectonic processes, in addition to mantle plume breakout events, imposed a major control over the deposition and preservation of iron formations. The growth of continents created a crucial shallow-water depository (Simonson, 2003), because before large landmasses developed considerable freeboard, iron formations may have been deposited in close association with volcanic edifices and seemingly were smaller as a result. The Mesoproterozoic and early Paleoproterozoic (ca. 2.45–2.22 Ga) gaps in the record of iron formation closely coincide with inferred pauses in global plate tectonic activity (Silver and Benn, 2008; Condie et al., 2009). On the other hand, tectonic settings, such as isolated to semi-isolated back-arc, rift, or foreland basins, have been invoked to explain the iron source, basin-scale water column redox state, and deposition of iron formation (e.g., Ohmoto et al., 2006; Beukes and Gutzmer, 2008). Indeed, with high-precision geochronology, it is possible now not only to correlate iron formations of similar ages in different basins but also to establish that iron-formation deposition in one basin coincided with the lack of iron enrichment in another basin. It is difficult, however, at this point to separate basin and paleogeographic controls from those determined by ocean circulation and upwelling processes for Precambrian basins.

The ocean chemical redox states as established by oxygen, sulfate, and nitrate contents determine whether iron and manganese can be transported in solution within the ocean. In addition, secular changes in seawater silica concentrations influenced the composition of iron formations, specifically their silica and phosphorous contents. It is generally accepted that seawater silica contents were high during the Precambrian but it is unclear whether silica in seawater declined dramatically at the beginning of the Phanerozoic (Siever, 1992) or if silica concentrations remained high until the Cretaceous when diatoms began to remove silica from seawater (Grenne and Slack, 2003). Exhalites that formed distal to deep-water VMS deposits help in evaluating ancient ocean redox states, including open-marine settings (Slack et al., 2007, 2009). This information can be compared directly with inferences from correlative shallow-water iron formations in order to constrain the redox conditions of the global ocean.

In this review, we place the deposition of iron formations in a framework of broader changes in tectonics, mantle plume activity, and oceanic and atmospheric redox states in order to assemble a new integrated model for their deposition. In contrast to most previous studies, we suggest that no single parameter controlled iron-formation deposition. Rather, complex give-and-take relationships among all of these parameters determined the time intervals and environments in which iron formations were deposited through Earth history, as well as changes in their mineralogy and composition. Figure 1 shows the global distribution of large and giant iron formations (≥1,000 Gt) and selected smaller deposits discussed below.

Definition of Iron Formation

The term iron formation is restricted to stratigraphic units composed of layered, bedded, or laminated rocks (Figs. 2-4) that contain 15 percent or more iron, in which the iron minerals are commonly interlayered with quartz, chert, or carbonate (James, 1954; Gross, 1980). James (1954) defined four facies of iron formation: silicate, carbonate, oxide, and sulfide. Sulfide-facies iron formation is pyritic carbonaceous shale or slate and not a type of iron formation. Barren or mineralized, sea-floor hydrothermal iron-rich exhalites and sulfidic cherts are in some cases also assigned to the iron-formation category and host some important gold deposits in Archean terranes. The former, in many cases, represent VMS deposits, whereas the latter could be either exhalites or hydrothermally replaced iron formation (Groves et al., 1987); these also should be excluded from iron formations sensu stricto. As a result, many Archean (sulfide-facies) iron formations described in the literature and shown in geologic maps are not true iron formations (Hofmann et al., 2003).

All other facies are generally interbedded with variably recrystallized chert (Simonson, 2003). Oxide-facies iron formation consists predominantly of magnetite or hematite, whereas carbonate-facies varieties contain siderite or ankerite as major constituents. The mineralogy of silicate-facies iron formations is more complex and depends to a large extent on the degree of postdepositional metamorphism. Under relatively low grade metamorphic conditions, at the biotite zone and lower, greenalite, minnesotaite, stilpnomelane, chamosite, ripidolite (Fe chlorite), riebeckite, and ferri-annite may be present. At higher grades, cummingtonite, grunerite, pyroxene, garnet, and fayalite can occur.

Primary Iron Mineralogy, Diagenesis, and Metamorphism

Original mineral phases in BIFs and also in GIFs have not been unequivocally identified, although some investigators have established the presence of possible original granular textures, such as microspheres 540 μm in diameter (Ayres, 1972), 120 to 200 nm in diameter nanospheres (Ahn and Buseck, 1990), and primary microplaty hematite (Han, 1988). How granular textures in BIF and GIF are related is not established, particulary because primary iron minerals in BIF are much smaller and far less common. Fine-grained ferric oxyhydroxides, siderite, and precursor clays to stilpnomelane and chlorite have long been considered the original minerals that formed during deposition or early diagenesis. Magnetite has also been interpreted to have formed during early diagenesis (e.g., Johnson et al., 2008a) but in most cases it is unambiguosly a late-stage mineral, as discussed below. Greenalite may have been the precursor diagenetic mineral to stilpnomelane, an iron-rich, alumina-poor metamorphic mineral of the biotite zone, although not all stilpnomelane is a transformation product of original clay minerals. Greenalite was probably the diagenetic transformation of an original iron-rich, alumina-poor smectite (i.e., nontronite). Most euhedral rhombic ankerite, ferroan dolomite, and siderite formed during burial after the formation of chert, but before burial stylolitization, although some euhedral iron-rich carbonate is much younger. The formation of stilpnomelane, chlorite, minnesotaite, riebeckite, crocidolite, and most hematite and magnetite postdates burial stylolitization, whereas some hematite is much younger (Ayres, 1972) and probably postdates regional metamorphism (e.g., Morey, 1999; Taylor et al., 2001).

In BIFs, fine-grained compact hematite occurs as rare 5- to 40-μm spheroids that contain 1 μm pore-filling inclusions of early diagenetic silica (Trendall and Blockley, 1970; Ayres,

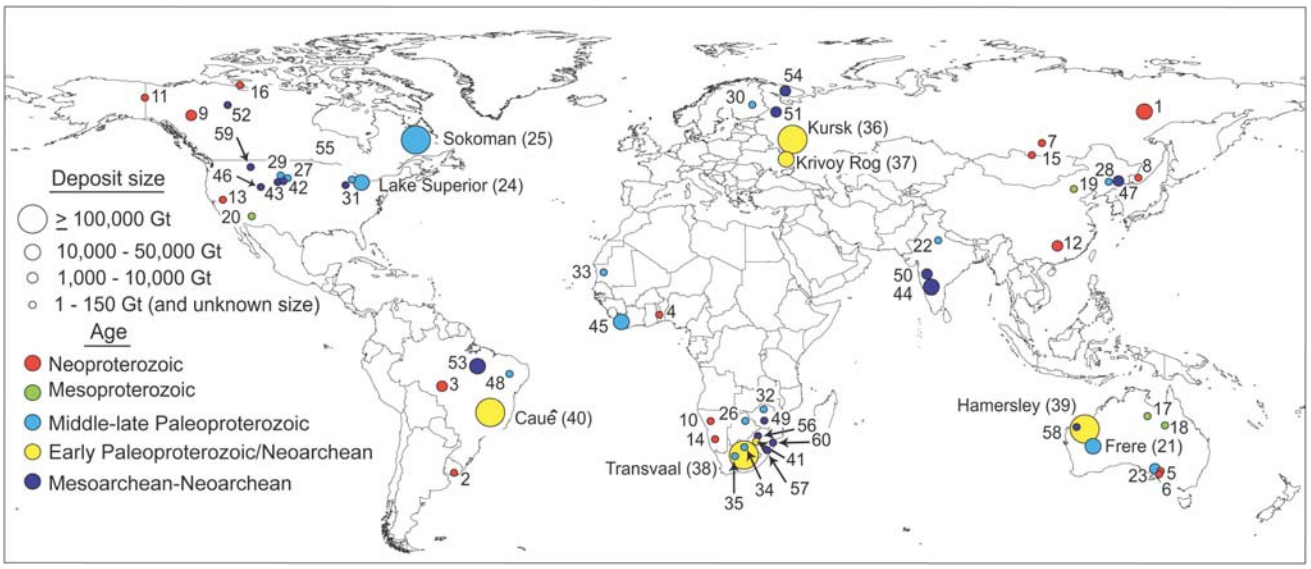

FIG. 1. Major sediment-hosted iron formations of the world, including BIF, GIF, and Rapitan-type iron formations. Also shown are several ironstones. Iron deposits are distinguished on the basis of size and age. Key to numbered iron-rich sedimentary units and areas (see App. 2 and text for information on age constraints and on stratigraphic and geographic position): 1 = Maly Khinghan Formation, 2 = Yerbel Formation, 3 = Jacadigo Group, 4 = Bisokpabe Group, 5 = Holowilena Ironstone, 6 = Braemar Iron Formation, 7 = Yamata Formation, 8 = Lake Khanka Formation, 9 = Rapitan Formation, 10 = Chuos Formation, 11 = Upper Tindir Group, 12 = Fulu Formation, 13 = Kingston Peak Formation, 14 = Numees Formation, 15 = Mugur Formation, 16 = Aok Formation, 17 = Corcoran and McMinn Formations, 18 = Mullera Formation, 19 = Chuanlinggou Iron Formation, 20 = Pike's Peak Iron Formation, 21 = Frere Formation, 22 = Alwar Group, 23 = Hutchison Group, 24 = Lake Superior region (includes five large iron formations), 25 = Sokoman Iron Formation, 26 = Shoshong Formation, 27 = Rochford Formation, 28 = Liaohe Group, 29 = Estes Formation, 30 = Pääkkö Iron Formation, 31 = Glen Township Formation, 32 = Lomagundi Group, 33 = Ijil Group, 34 = Hotazel Iron Formation, 35 = Timeball Hill Formation, 36 = Kursk Supergroup, 37 = Krivoy Rog Supergroup, 38 = Transvaal Province, 39 = Hamersley Province (includes six large iron formations), 40 = Cauê Formation, 41 = Penge Iron Formation, 42 = Benchmark Iron Formation, 43 = Nemo Iron Formation, 44 = Mulaingiri Formation, 45 = Nimba Itabirite, 46 = Atlantic City Iron Formation, 47 = Anshan, 48 = Caldeirão belt, 49 = Manjeri Iron Formation, 50 = Bababudan Group, 51 = Gimola terrane, 52 = Central Slave Cover Group, 53 = Carajás Formation, 54 = Olenegorsk Formation, 55 = Steep Rock Group, 56 = West Rand Group, 57 = Pongola Supergroup, 58 = Cleaverville Formation, 59 = Indian Creek Metamorphic Suite, 60 = Moodies Group.

1972). These spheroids are similar to hematite spheroids in modern iron oxide deposits of the Red Sea (Taitel-Goldman and Singer, 2002) and are possibly early diagenetic transformations of original particles of ferric oxyhydroxides. Similar-sized spheroids of siderite are either original or early diagenetic particles. Other spheroids, now composed of stilpnomelane, chert, or even greenalite, may be original granules, but their precursor compositions are unknown (Ayres, 1972). Neither granular textures nor hematite spheroids have been universally recognized from Archean Algoma-type BIFs.

Granules within GIFs are composed of chert and iron oxide, iron carbonate, or iron silicate. The granules are considered detrital, with some, both well-rounded and angular, being derived by sedimentary reworking of iron-rich mudstone and arenite (Simonson and Goode, 1989). Many well-rounded granules resemble peloids (Simonson, 2003) and possibly were originally composed of iron-rich clay. Oolitic banding in granules is relatively rare in late Paleoproterozoic GIFs but common in younger deposits (e.g., Harms, 1965). Iron silicates (greenalite), siderite, chert, and hematite formed early in the diagenetic history of GIFs (LaBerge, 1964), but the composition of the granules at the time of their deposition is unknown. Whether in BIF or GIF, granules range from grain to matrix supported, with no evidence that they were compacted during burial. It appears that a matrix of chert was early cement that protected the granules from compaction and preserved "floating" textures.

As stated above, although Fe oxides can form early in an iron formation's diagenetic history, most hematite and also magnetite is postdepositional in origin and linked with iron enrichment leading to ore genesis, even in sections distal to iron orebodies. The source of iron for the growth of postdepositional hematite, and also magnetite and iron-rich carbonate, currently is not known with certainty. Iron formations upgraded to hematite and martite-goethite ores are some of the largest known orebodies. Their origin remains controversial, but hydrothermal processes are well documented (Taylor et al., 2001). Ore hematite is prismatic or platy, and commonly occurs with bladed carbonate minerals, but is considerably finer grained distal to ore. An interpretation that platy hematite was depositionally or diagenetically early is suspect, because it is the typical form of ore generation hematite. Indeed, geochronologic studies of xenotime and monazite paragenetic with hematite and martite-goethite orebodies formed during hydrothermal alteration of iron formation indicate that iron-ore formation was a long-lived and multistage process (Rasmussen et al., 2007). Within the iron orebodies of the Hamersley Province, hematite-carbonate alteration occurred

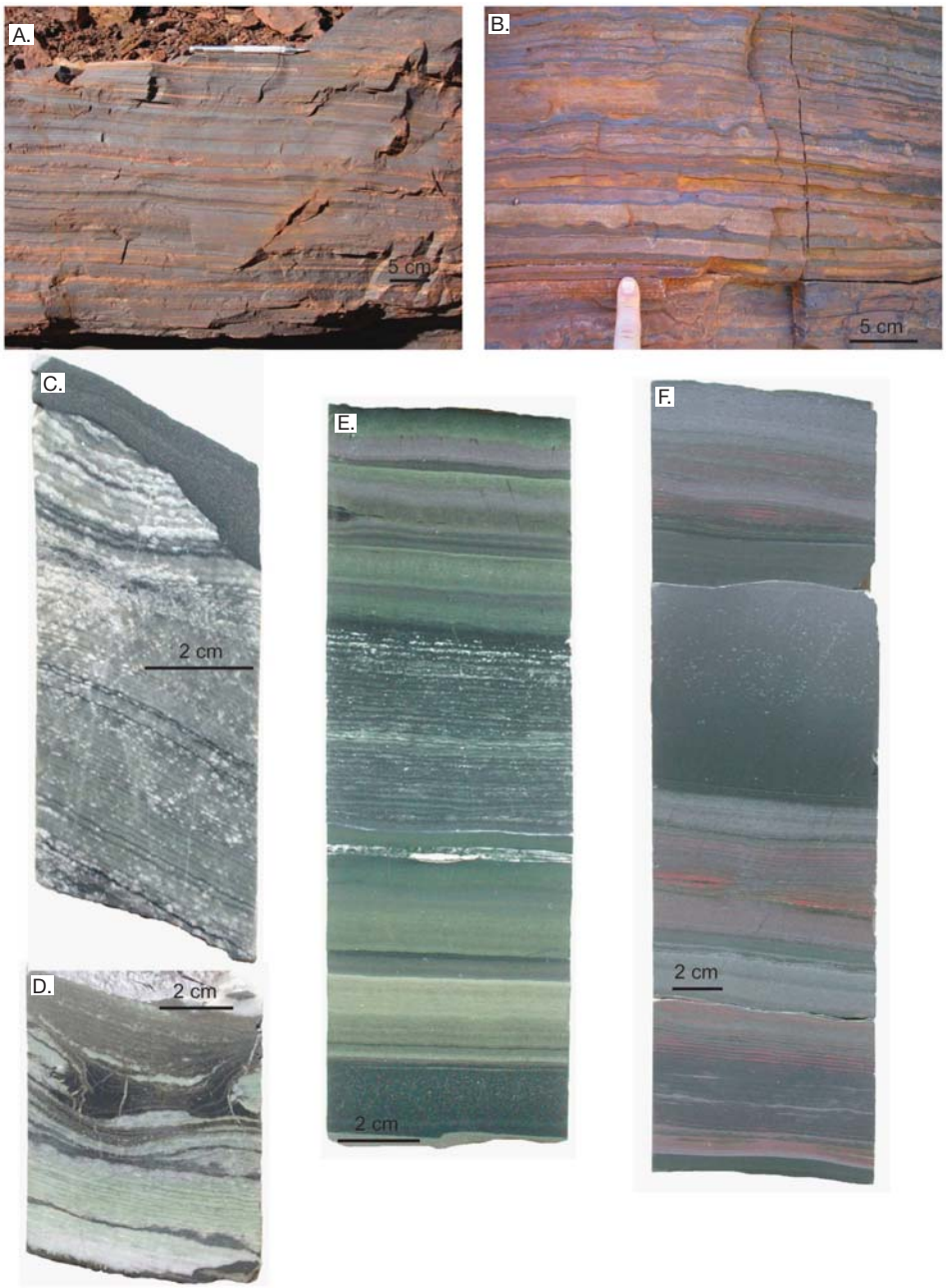

FIG. 2. A. Laminated martite (magnetite replaced by hematite) and chert BIF of the Nimingarra Iron Formation from near Goldsworthy, North Pilbara greenstone belt; the iron formation is a stratigraphic equivalent of the Cleaverville Formation and shows the typical shaley structure of Algoma-type BIF. B. Layers of magnetite and laminated chert of BIF in the Dales Gorge Member, Dales Gorge, Karijini National Park, Hamersley Province. The magnetite bands are laminated to vaguely laminated to massive and even at the small scale truncate laminations (primary layering) in the chert. C. Erosional truncation of laminations in bedded chert at the contact between the DB9 (below) and the DS10 (above) macrobands of the Dales Gorge Member from drill hole DDH44 at Paraburdoo, Hamersley Province. The cloudy white mineral obscuring laminae in the chert is diagenetic rhombic ankerite-ferroan dolomite. D. Remnants of shale (black) and chert-shale microbands and/or lamina sets (green), emphasizing the replacement origin of chert, in the DS6 macroband of the Dales Gorge Member from drill hole S96-03, Tom Price, Hamersley Province. E. Rhythms in BIF resembling thinly bedded density-current deposits (cf. turbidites), the lowest (dark) unit contains detrital rounded and tabular grains. The green color is ferrostilpnomelane. Coarse structure in the chert interval is typical of early (precompaction) diagenetic chert and comprises irregular laminae of chert and relict laminae of ferric-stilpnomelane, obscured by rhombic carbonate. Sample is of the Joffre Member in drill hole DD98SGP001, Silvergrass, western Hamersley Province. F. Graded massive to plane-laminated bed of stilpnomelane-rich tuffaceous siltstone-mudstone within BIF of the Joffre Member in drill hole DD98SGP001, Silvergrass, western Hamersley Province. The lower part of the section is similar to the rhythmic bedding in (E), but ferrostilpnomelane (green) has been oxidized to ferricstilpnomelane (dark), and magnetite euhedra have been replaced by hematite (red lines), although much magnetite remains. White-speckled appearance of the tuffaceous bed is due to fine-grained, diagenetic rhombic ankerite-ferroan dolomite.

at temperatures of ~250°C under high fluid pressures (Taylor et al., 2001).

In BIFs and GIFs, magnetite typically replaced or overgrew early hematite and siderite, and most rhombic, iron-rich carbonate (Ayres, 1972; Ewers and Morris, 1981), and has several forms: (1) disseminated grains within, but obscuring sedimentary laminae, (2) laminated bands, (3) layer-discordant veins and bands, (4) cleavage fillings, and (5) coarse grains in iron ore. Much, if not all, disseminated magnetite formed during deep-burial diagenesis or later. Ewers and Morris (1981) reported for the Dales Gorge Member of the Brockman Iron Formation in the Hamersley Province that most magnetite overgrows fine-grained hematite, but textural evidence can be ambiguous because much diagenetic magnetite is overgrown by postmetamorphic hematite. Ayres (1972) reported that magnetite euhedra predate rhombic carbonate but postdate matrix chert, although ongoing petrographic work contradicts that observation because euhedral magnetite is younger than burial-related rhombic carbonate. In contrast, laminated bands of magnetite postdate burial stylolites and destroy primary layering; Krapež et al. (2003) referred to such laminated bands as iron proto-ore (Fig. 3C-E). Discordant veins, laminae, and cleavage fillings of magnetite cut these bands. Magnetite is also an ore mineral, showing preserved transformations from proto-ore to ore magnetite, ore hematite to ore magnetite, and ore magnetite to ore hematite, but ore-generation magnetite also occurs in settings distal to ore.

Banding and lamination are the typical structures of BIFs, occurring at many scales as originally defined by Trendall and Blockley (1970), namely microbanding, mesobanding, and macrobanding. In terms of modern terminology, microbanding means lamina sets (i.e., paired laminae), mesobanding means sets, cosets, or bedsets (i.e., genetically linked sets) or even beds, and macrobanding means parasequences and parasequence sets (i.e., genetically linked bedsets and beds). Sequence-stratigraphic terminology is equally applicable to BIFs and GIFs of all ages and is more useful for comparisons to other sedimentary facies than the microband, mesoband, and macroband terminology.

Whereas much banding and lamination is sedimentary (Fig. 2A, E-F), not all is (Fig. 3C-E), and care must be taken with description and interpretation. In BIFs of the Hamersley Province, laminated bands of magnetite constitute the magnetite mesobands of Trendall and Blockley (1970). Other mesoband types comprise chert-magnetite, chert-hematite, chert-siderite, chert-iron silicate, and chert and riebeckite, but all may contain magnetite. All of the mesoband types formed prior to regional folding. Chert-hematite, chert-siderite, chert-iron silicate, and chert mesobands are sedimentary layers, albeit the mineralogy is not original. Graded beds of resedimented tuffaceous sandstone or mudrock are common (Fig. 2F) but were not included in the mesoband categories of Trendall and Blockley (1970). Chert mesobands are bedded chert or the seafloor hardgrounds of Krapež et al. (2003). They often preserve eroded upper surfaces, testifying to their early lithification (Fig. 2C). Chert-magnetite mesobands with disseminated magnetite are also sedimentary layers, but chert-magnetite mesobands with millimeter- to centimeter-sized lenses of chert enveloped and truncated by laminated magnetite preserve only relics of original sedimentary layers (Fig. 3C-E). Sedimentary layers of chert-iron silicate ± magnetite show the same type of destruction by laminated magnetite.

Planar and internally laminated magnetite mesobands, referred to as planar laminated magnetite bands, are paraconcordant with bedding, but it is moot whether they are sedimentary layers (Fig. 3C). Anastomosing laminated magnetite bands clearly truncate sedimentary layering (Fig. 3D). Field exposures (Fig. 3E) show that preserved relics of the precursor rock are truncated intervals of bedded chert, and the geometrical arrangement of chert bodies defines an imbricate structure. Offsets within and between chert bodies have normal rotational sense and define laminated magnetite as a ductile listric mineral foliation. In planar laminated magnetite bands, the deformation fabric approaches concordancy with sedimentary layering. Proto-ore formation included near-total replacement of the microlaminated chert matrix of BIF and the partial destruction of bedded chert (cf. Klein and Beukes, 1989). These types of laminated magnetite, whether layer-concordant or -discordant, are present in BIFs and GIFs and must not be confused with sedimentary layering.

In the Hamersley and Transvaal BIFs, sodium-rich iron amphiboles formed late in proto-ore genesis (Trendall and Blockley, 1970; Beukes, 1973) involving either complete or partial replacement of chert and chert-magnetite mesobands by riebeckite or by formation of crocidolite veins in overpressured zones. Some of this crocidolite was mined for asbestos. Riebeckite formation predates regional folding but may have been synmetamorphic in origin, whereas overpressure zones are related to regional folding.

Superior- and Algoma-Type Iron Formations in the Precambrian Rock Record

The division of iron formations into Superior- and Algoma-type was made on the basis of their interpreted depositional settings (Gross, 1980). Superior-type iron formations were regarded to have been deposited in near-shore continental-shelf environments because they are typically interbedded with carbonates, quartz arenite, and black shale, but with only minor amounts of volcanic rocks (Gross, 1980). Algoma-type iron formations are generally hosted in volcanic rocks and, in some cases, in graywacke and apparently formed by exhalative hydrothermal processes close to volcanic centers. Based on geochemical signatures, Barrett et al. (1988a) argued that some Algoma-type deposits formed within restricted basins like the modern Red Sea. Algoma-type iron formations are present in volcano-sedimentary sequences of greenstone belts ranging in age from Eoarchean to late Paleoproterozoic (Goodwin, 1973; James, 1983; Isley and Abbott, 1999; Huston and Logan, 2004). Granular iron formations are generally absent within Algoma-type deposits, which are typically mesobanded to microbanded (Fig. 2A). Iron formations older than 3.0 Ga have generally been described as Algoma-type, which possibly reflects the absence of preserved cratonic successions prior to this time. Mineralogically, Algoma- and Superior-type iron formations are similar.

Algoma-type iron formations are thinner and smaller in lateral extent relative to Superior-type iron formations and

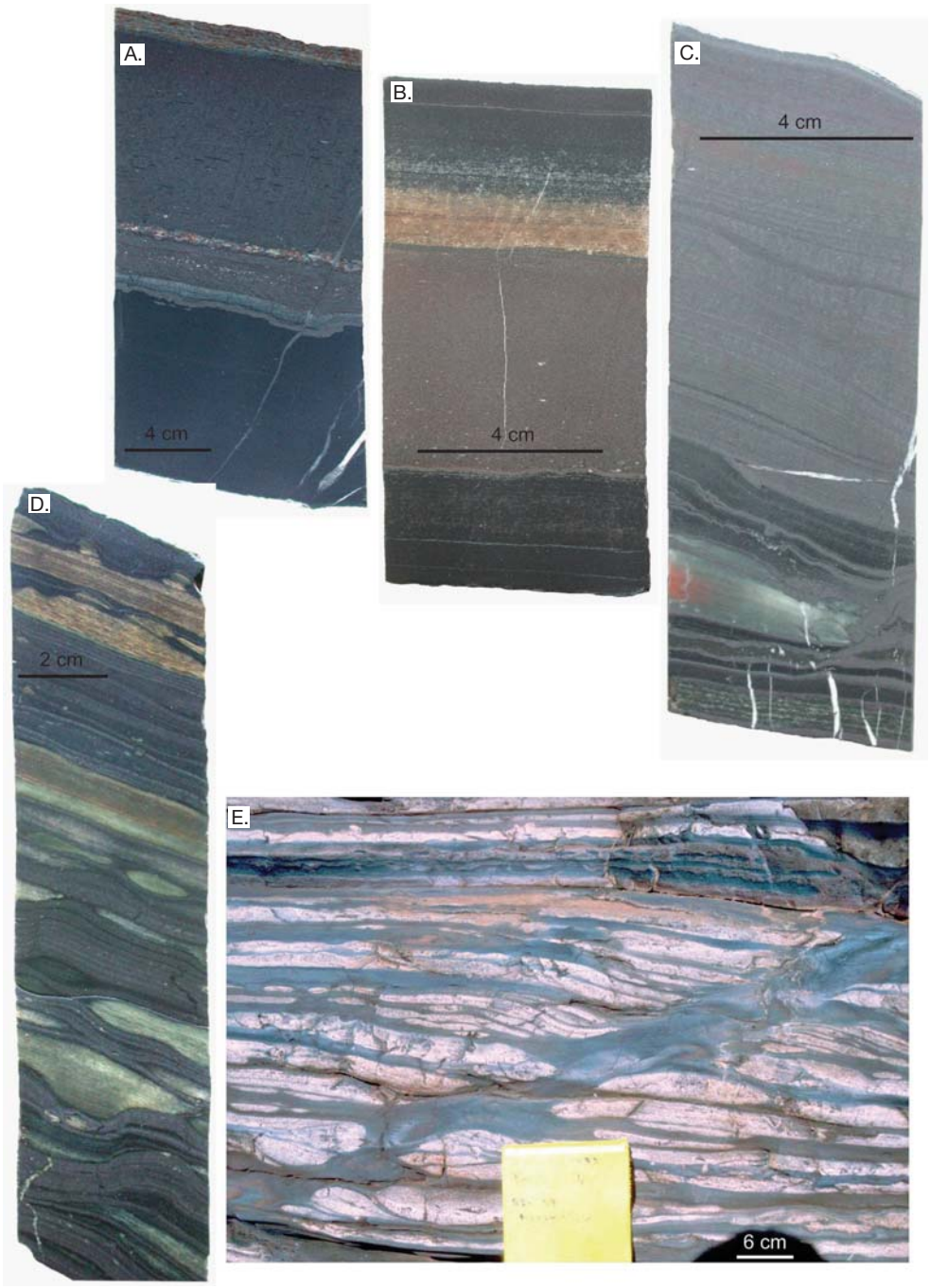

FIG. 3. A. Massive, graded bed composed of detrital tabular and rounded grains of mudstone and/or shale, in a cherty matrix with euhedral grains of magnetite, from BIF of the DB15 macroband, Dales Gorge Member, drill hole DD98SGP001, Silvergrass, western Hamersley Province. The blue color is due to fine-grained, metamorphic riebeckite. B. Similar graded bed in BIF of the DB14 macroband, Dales Gorge Member, drill hole DD98SGP001, Silvergrass, western Hamersley Province. C. Typical form of laminated magnetite in Hamersley BIF, showing apparent primary lamination, which in fact is discordant to bedding, and structural truncation of chert lenses; note weak alteration of magnetite to hematite (red). Whether discordant or paracordant, it is not obvious that laminated magnetite had a sedimentary precursor. Broken black layer near the base of the core interval is the remnant of a stilpnomelane-rich tuff. Sample is from the Colonial Chert Member in drill hole DDH44 at Paraburdoo, Hamersley Province. D. More obvious truncation of early diagenetic bedded chert by laminated bands of magnetite; brown and green colors in chert are the variably oxidised stilpnomelane, representing relict shale within the chert. This is the typical form of BIF in the Dales Gorge Member, showing how BIF rarely fits its traditional description in its type area. Sample is from the DB13 macroband of the Dales Gorge Member in drill hole DDH44 at Paraburdoo, Hamersley Province. E. Planar, anastomosing, and highly discordant bands of magnetite that truncate and structurally "erode" layers of early diagenetic chert, in the type section of BIF of the Joffre Member at Joffre Falls, Karijini National Park, Hamersley Province. Note the normal listric dislocation of chert layers by the highly discordant band of magnetite. Such structural disruption of BIF is commonplace.

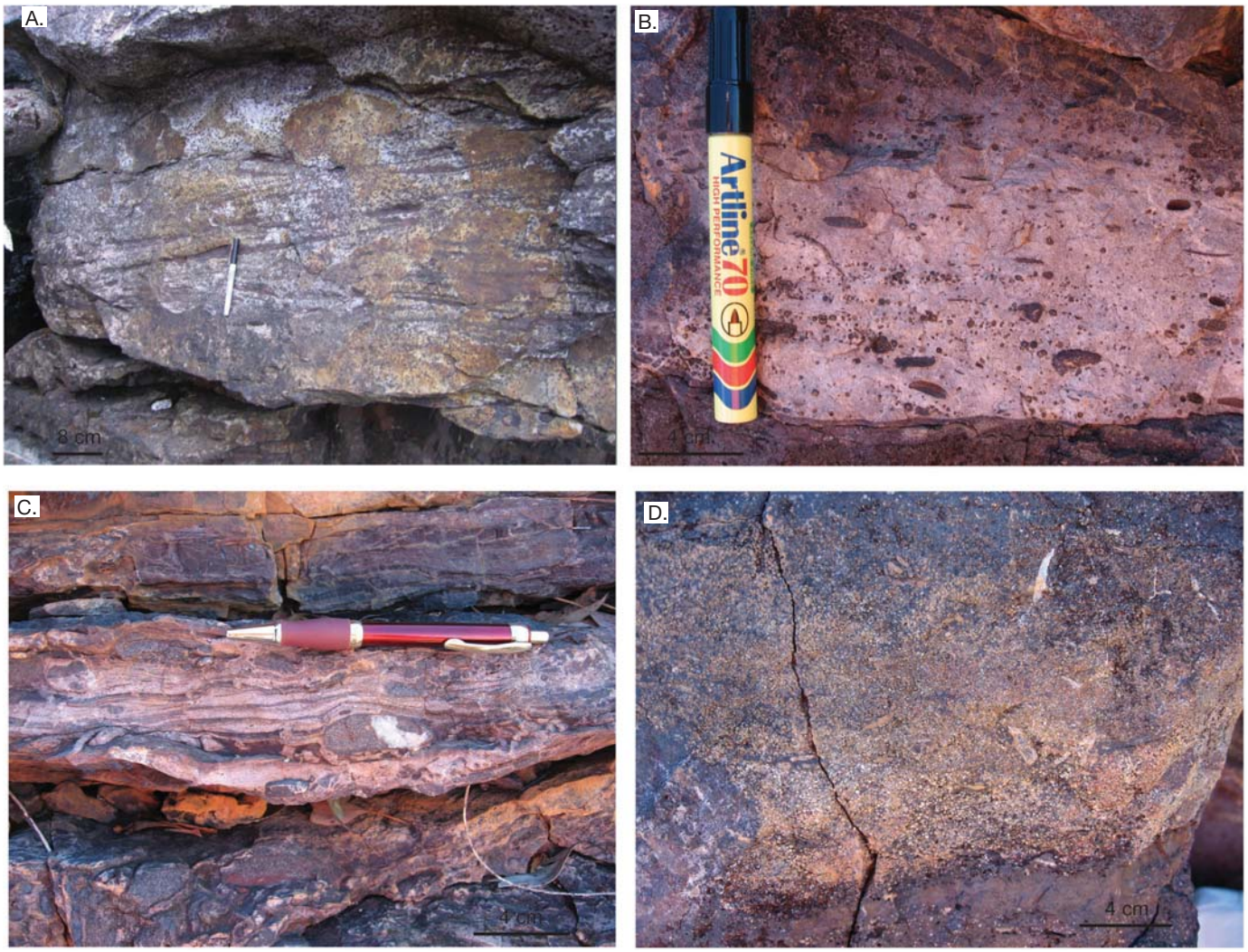

FIG. 4. A. Trough crossbedded GIF of the ca. 1.88 Ga Temicamie Iron Formation, Mistassini basin, Quebec. B. Quartz-rich sandstone overlying ooidal ironstone and containing rounded clasts of ooidal ironstone as well as ironstone ooids and pelloids; Train Range Member of the Mullera Formation, Constance Range, Northern Territory-Queensland border. C. Same location and unit as in (B), showing large clasts of cemented ooidal ironstone in quartz-rich sandstone and wavy heavy mineral bands composed of hematite. D. Same location and unit as in (B) and (C), showing a typical bed of ooidal ironstone.

rarely exceed 10^7 Mt (Huston and Logan, 2004), although the former are more abundant in terms of numbers of deposits and geographic distribution (Beukes and Gutzmer, 2008). Typical Algoma-type iron formations are less than 50 m thick and rarely extend for more than 10 km along strike. However, these characteristics do not indicate that all Algoma-type iron formations were originally smaller, as most have been affected by deformation and tectonic dismemberment, implying that their true size and extent are likely underestimated in global compilations of iron formations (Gole and Klein, 1981). By contrast, Superior-type BIFs are more laterally extensive. They are also considerably larger, with some major units containing an estimated 10^{14} Mt initially at 15 wt percent Fe (James, 1983; Isley, 1995).

Huston and Logan (2004) pointed out that the largest peak in Algoma-type BIF deposition corresponds to a major plume event at 2.75 to 2.70 Ga, but that not all plume events correspond to Algoma-type BIF deposition. Barley et al. (1998) related Archean BIF deposition to the interplay among tectonics, magmatism, and eustacy. Algoma-type BIFs were regarded to reflect intrabasinal pulses of magmatic and hydrothermal activity during the deposition of volcano-sedimentary greenstone successions, whereas Superior-type BIFs formed on continental shelves during periods of global high sea levels and pulses of enhanced magmatic and hydrothermal activity. This model indicates that conditions for the deposition of Algoma-type iron formations were favorable during much of the Archean, occurring whenever environmental conditions allowed. If this model is correct, then a distinction between Superior and Algoma types of iron formation has some merit. For example, the geochemistry of Algoma-type iron formations may reflect local volcanic or hydrothermal conditions, rather than being representative of the large-scale chemistry of the oceans during their formation. In contrast, the deposition of Superior-type iron formations reflects processes that probably acted on a global scale (Huston and

Logan, 2004), although potential influence by nearby cratonic areas needs to be also considered.

Clear differentiation between Superior and Algoma types of iron formation is difficult in Archean successions affected by strong deformation and shearing that resulted in tectonic dismemberment or imbrication of genetically unrelated packages. For example, iron formations interbedded with quartz arenites and carbonates are locally interlayered with thick packages of mafic-ultramafic extrusive rocks. Although some of these sequences may represent primary stratigraphic units that were deposited in extensional continental or arc settings (e.g., Srinivasan and Ojakangas, 1986), others could have formed by tectonic imbrication of cratonic cover sequences and overlying piles of mafic-ultramafic rocks (e.g., Dirks et al., 2002).

Depositional Setting and Sequence Stratigraphic Framework of Iron Formations

The depositional settings of iron formations range from relatively deep water for BIFs to above storm- and fair-weather wave-base for GIFs. Both varieties, particularly if they constitute large deposits, formed in open-marine environments during high sea level (cf. Simonson and Hassler, 1996; Krapež et al., 2003; Fralick and Pufahl, 2006). Iron formations are commonly either overlain or underlain by organic matter-rich and sulfidic shales and, in some cases, are interstratified with them. These shales are shallower water equivalents of Archean and some Paleoproterozoic BIFs (e.g., Klein and Beukes, 1989, 1992; Beukes et al., 1990; Simonson and Hassler, 1996).

The most detailed sedimentologic studies of BIFs have been conducted in the Hamersley Province of Australia and the Transvaal and Griqualand West basins of South Africa. The classical description of BIFs as laminated units was based on those localities. Studies of BIFs of the Hamersley Province documented iron minerals and chert in paired layers that vary from microbands 0.2 to 2.0 mm in thickness to mesobands 10 to 50 mm in thickness. Trendall and Blockley (1970) suggested that mesobands and microbands could possibly be correlated basin-wide, which led to the inference that BIFs are chemical varves precipitated on a deep-water shelf (Trendall, 1973). However, it is now well established that only chert mesobands can be correlated (Krapež et al., 2003). Whereas microbanding is obvious in drill core intervals, in field exposures it has little to no lateral continuity. Through facies and sequence-stratigraphic analysis, Krapež at al. (2003) and Pickard et al. (2004) subsequently concluded that all chert in BIFs was early diagenetic in origin and, moreover, that chert mesobands are siliceous equivalents of modern-day sea-floor hardgrounds (Fig. 2C). Ferric oxyhydroxide particles, which probably comprised an initial iron component in BIF, are highly reactive toward dissolved silica (e.g., Konhauser et al., 2007b), implying that the silica component in BIF was scavenged from seawater during particle sedimentation and resting at the sediment-water interface, and was later released during diagenesis when ferric oxyhydroxides transformed to stable crystalline compounds (Slack et al., 2007; Fischer and Knoll, 2009). Much silica was also bound within the structure of originally deposited clay minerals. The implication is that chert was not a direct chemical precipitate from seawater, but rather a pore-filling cement and sediment replacement; that is, chert in BIFs is not a diagenetic replacement of earlier precipitated silica from seawater. Bedded chert can clearly be seen to be a replacement, preserving relics of a precursor sediment within lamina sets and discontinuous bands (Fig. 2D).

Fine-grained spheroids of hematite and siderite are distributed along laminae in bedded chert and within the chert matrix of BIFs. Assuming that these lamina sets in BIFs originated from a process similar to that responsible for lamina sets in lithofacies interbedded with BIFs, they can be assumed to have a density current origin (Krapež et al., 2003). The density current interpretation is supported by the presence of two bedding styles of mesobands in BIFs: microbanded and tabular-bedded (Fig. 3A-B); the latter typically is massive or weakly laminated (Ewers and Morris, 1981). Massive mesobands grading upward into microbanded mesobands resemble density-current intervals and are preserved at various scales (Figs. 2E-F, 3A-B). Rare preservation of erosional truncation of draped lamination (Krapež et al., 2003) also supports the density-current interpretation (Fig. 5).

Depositional sequences in the Dales Gorge Member of the Hamersley Province comprise lowstand density-current deposits of dolostone, graded mudrock, and rare conglomerate, the so-called DS macrobands, overlain by a condensed section of BIF, the so-called DB macrobands. The architecture establishes deposition on the basin floor, beyond a slope environment (Krapež et al., 2003). Bedded chert defines the top of every depositional sequence by sharp eroded contacts with overlying dolostone or mudrock and gradational contacts into underlying BIF. In contrast, the contacts from lowstand mudrock to condensed-section BIF are transitional, with upward continuity of parasequences (Krapež et al., 2003). Bedded chert intervals at the top of many depositional sequences are compound, containing multiple 5- to 10-cm-thick relics of stilpnomelane-rich shale. The presence of these compound intervals indicates that ambient suspension sediments during sediment starvation were not BIF, and that BIF deposition ceased prior to the end of depositional cycles. Depositional sequences characterized by this lowstand-condensed section architecture are preserved throughout all of the Hamersley Province and also have been documented in the Transvaal Province (e.g., Beukes and Gutzmer, 2008); it appears to be the common architecture of all deep-water BIFs.

Lowstand deposits change from dolostone-mudrock to shale-only toward the southwest in the Hamersley Province, indicating a paleoslope to the southwest (Simonson et al., 1993). Lowstand deposits in those distal sections contain BIF units that are identical to BIF in the condensed sections. This pattern suggests that precursor sediments to BIF characterized basin sedimentation not only during rising and high sea level but also during some lowstands beyond the limits of shelf-derived resedimented sediments.

The following arguments provide evidence that the precursor sediments to Dales Gorge BIF were not ambient iron-rich pelagites: (1) suspension-deposited sediments in lowstand deposits were siliciclastic, calcareous, carbonaceous, or volcaniclastic mudstone; (2) suspension-deposited sediments in condensed sections and compound hardgrounds at the top of depositional sequences were iron-poor hemipelagites; and (3)

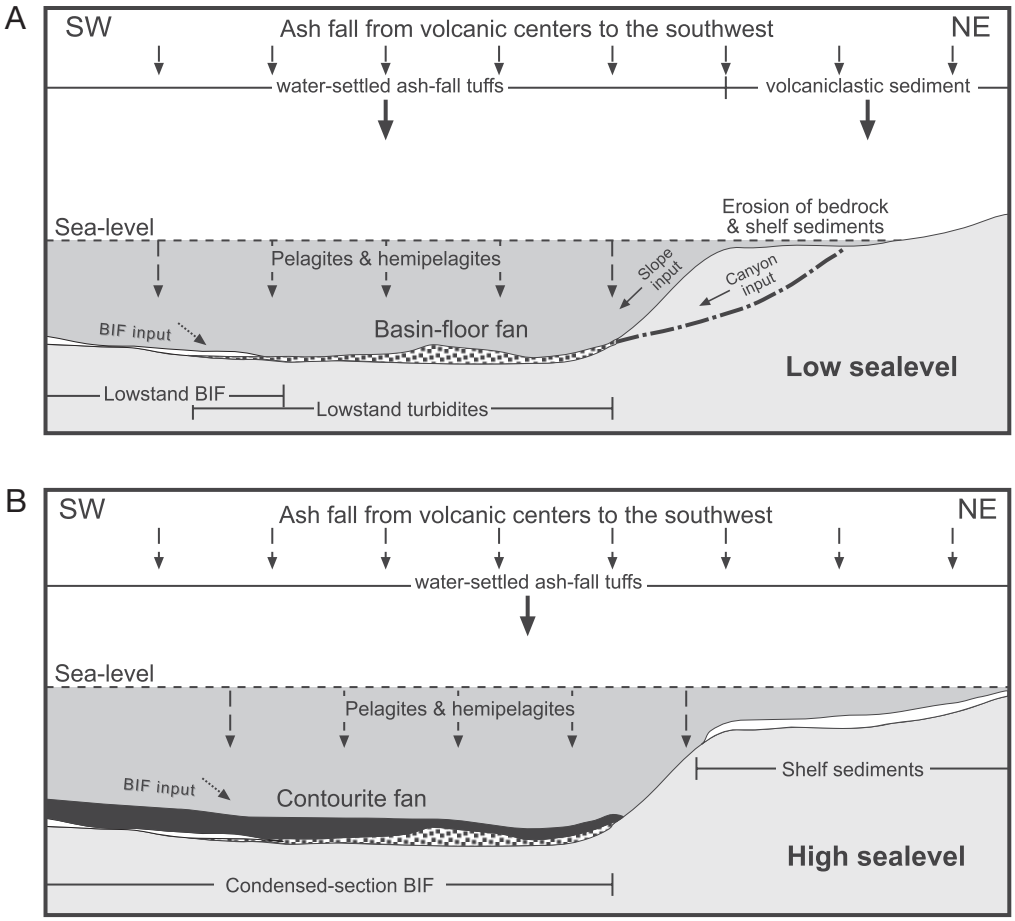

FIG. 5. Depositional models for Hamersley-type BIF (modified from Krapež et al., 2003). During low sea level (A), shelf sediments (a mixture of carbonates, and volcaniclastic and siliciclastic detritus) are resedimented to the basin floor where they accumulate on mound-shaped, basin-floor fans. Coeval precursor sediments to BIF accumulate on the sea floor beyond the influence of shelf-derived sediments. During rising and high sea level (B), sediments accumulate on the shelf and are not resedimented to the basin floor. Consequently, the area of BIF deposition covers the entire basin floor, draping over the basin-floor fans as contourite fans. The source of the precursor sediments to BIFs was not the shelf but an intrabasinal factory, probably submarine to shallow-water volcanic edifices or platforms. A complex interplay exists among sea-level change, sedimentation patterns, and volcanism, because peak production of volcanism-related BIF relates to increasing sea-floor volcanism that feeds back into sea-level rise.

no evidence exists for BIF drapes on hardground surfaces (Krapež et al., 2003). The last point is important because hardgrounds developed during periods, and in areas, of sediment starvation. It appears, therefore, that deposition of the precursor sediments to BIF was restricted to sea-floor areas beyond the limits of resedimented shelf sediments and was dominant during rising and high sea level but ceased prior to the end of depositional cycles. The precursor sediments to BIF almost certainly were sourced within the basin realm but not from the shelf environment that produced lowstand sediments. This model for deposition of Dales Gorge BIF (Krapež et al., 2003) is applicable to many other BIFs such as the correlative Transvaal (South Africa), Krivoy Rog (Ukraine), Kursk Magnetic Anomaly Russia), and Quadrilátero Ferrífero (Brazil) iron formations. It is not applicable to shallow-water BIFs, such as those in the Pongola and Witwatersrand Supergroups (Beukes and Cairncross, 1991), where responses to rising and falling sea level differed according to the classic sequence-stratigraphic profile (see below).

The GIFs are clastic sedimentary rocks that are mainly restricted, at least in their preservation, to Paleoproterozoic continental basins. Those basins surrounding the Superior craton of North America constitute the type area, where two lithofacies are recognized: slaty and cherty (Ojakangas, 1983). The slaty lithofacies is iron-rich shale comprised of alternating, millimeter-scale layers of iron oxides or silicates and chert and consisting of parallel- and wavy-laminated, iron-rich mudstone interbedded with lenses of grainstone. Lamina sets are similar to those in BIF; gently dipping erosive truncations draped by mudstone are also present (Pufahl and Fralick, 2004).

The cherty lithofacies is a grainstone with a cherty cement; in situ and reworked stromatolites are common (Ojakangas, 1983; Pufahl and Fralick, 2004). This lithofacies is comprised of interconnecting lenses of trough cross-stratified grainstone. The largest lenses typically have a basal layer of intraformational breccia derived from the reworking of iron-rich mudstone. Millimeter- to centimeter-scale, grain-size grading in iron-rich shales indicates that the depositional process was

gravity settling. A siliciclastic component to the mudstone and/or shale supports suspension deposition from density currents. Density current settling is a typical process on current-, wave-, and storm-dominated shorelines, such that microgradedsets of mudstone are the ambient sedimentary style. Granular beds within the mudstone sequences were deposited by traction currents. Sets are channel-shaped, with internal trough cross-stratification. Wave- and current-formed sedimentary structures and hummocky cross-stratification are abundant (e.g., Ojakangas, 1983; Pufahl and Fralick, 2004), establishing that the depositional environment was a shallow-water shelf disturbed by storms. The environment was also coeval with bimodal volcanism, indicating almost certainly a volcano-tectonic influence. In general, the pattern is one of alternating units of storm-influenced event beds and background density-current deposits, passing upward into shallow-water grainstones of the cherty lithofacies (Fig. 6A). The sequence-stratigraphic architecture is one of upward thickening and upward coarsening, reflecting deposition during rising and high sea level on a shelf. Although contrasting with the sequence architecture of BIFs, the two styles are linked and are in agreement with a classic sequence-stratigraphic profile, defined by GIFs on the shelf and BIFs in a deep-water setting. For GIFs of the Superior craton, the transiton between pairs of slaty and cherty lithofacies is a unit of convolute iron formation (Fig. 6A), which Pufahl and Fralick (2004) interpreted to record seismic shaking during active subsidence.

Sequence stratigraphic models for Phanerozoic and some Mesoproterozoic iron formations are slightly different because iron formation is a lithofacies within siliciclastic depositional sequences. Maynard and Van Houten (1992) suggested that oolitic ironstones were deposited during still-stand following the peak of regression and prior to the peak of transgression (Fig. 6B). The ironstones are capped by a hardground, which in the Mesoproterozoic oolitic iron formations of northern Australia is recognized by ooids, granules, and intraclasts floating in an early diagenetic chert matrix and/or cement (Harms, 1965). Cherty hardground records the peak of siliciclastic sediment starvation on the shelf, thereby representing a maximum flooding surface. Oolitic iron formation within siliciclastic depositional sequences, therefore, formed during transgression, rather than still-stand. Not only would peak flooding be the time of high organic productivity and

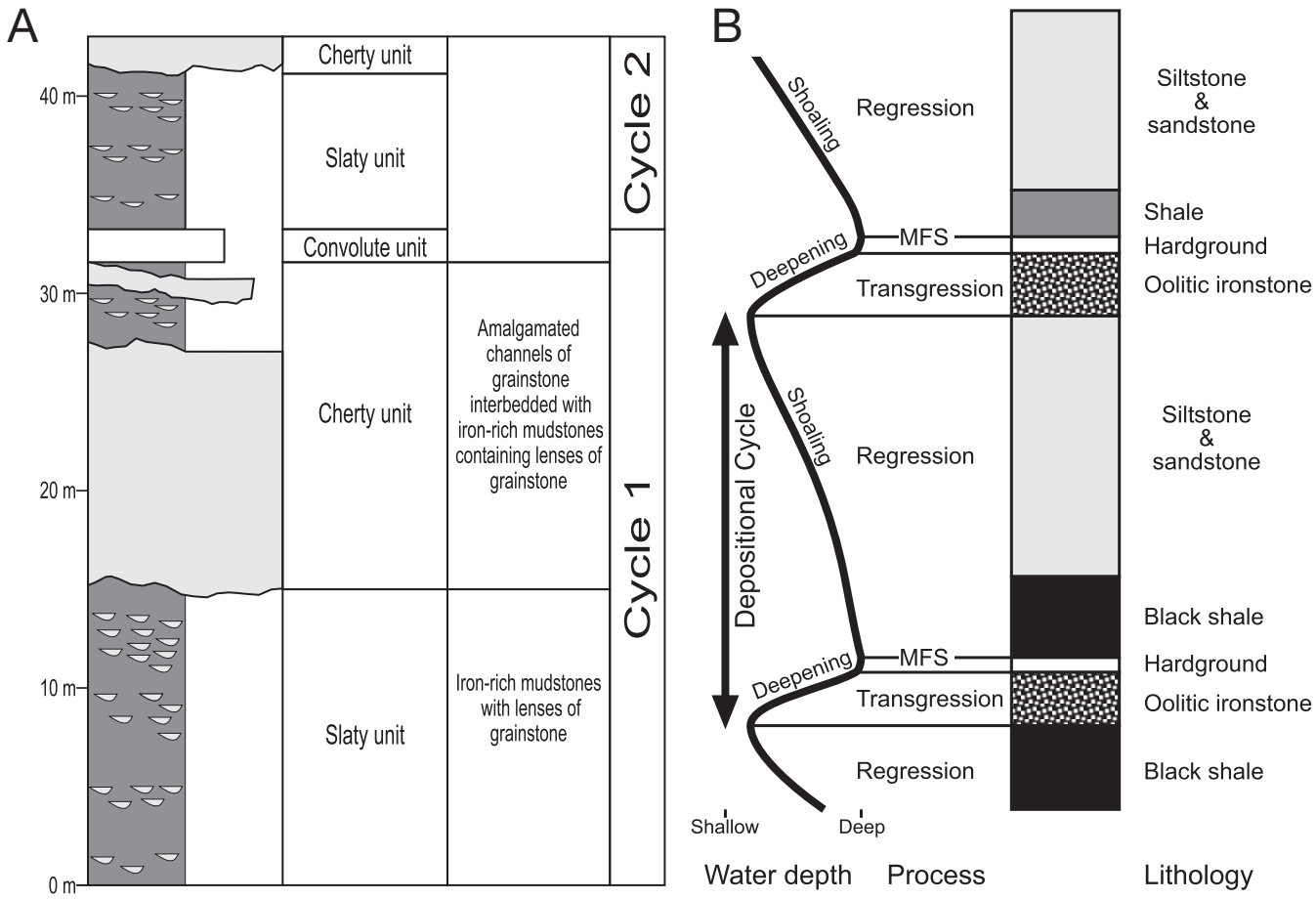

Fig. 6. A. Statigraphic profile showing facies composition of depositional cycles in granular iron formations of the Lake Superior area (after Pufahl and Fralick, 2004). Each cycle shallows upward from laminated iron-rich mudstones to amalgamated channel fills of grainstone, with seismically disturbed bedding (convoluted units) present at the top of each sequence. B. Generalized sequence-stratigraphic model for Phanerozoic oolitic ironstones (modified from Maynard and Van Houten, 1992). Rather than oolitic ironstones forming during still-stand at the peak of regression, they probably formed during transgression prior to maximum flooding.

anoxia on the shelf, it would likely also be the period of maximum ingress of basinal waters, which suggests that a basinal supply of Fe(II) was important.

Oxidation Mechanisms: Biological Versus Nonbiological

The basic conditions leading to deposition of iron formations in ancient oceans are generally agreed upon; that is, the precursor to iron formations precipitated from seawater containing micromolar (<100 μmol) levels of ferrous iron (Holland, 1973, 1984). An amplified marine reservoir of dissolved iron was possible due to the following: (1) a reducing atmosphere or one with a low oxidizing potential (Holland, 1984; Bekker et al., 2004), (2) low marine sulfate and sulfide concentrations (Habicht et al., 2002), and (3) a high hydrothermal iron flux (Kump and Seyfried, 2005). The presence of hematite BIF indicates that some form of oxidative mechanism existed in Precambrian oceans to convert dissolved Fe(II) into solid-phase ferric-rich iron particles that then settled and accumulated on the sea floor. The caveat is, however, that BIFs must contain original grains of hematite and that cannot be proven in many sequences.

The specific mechanisms involved in the deposition of iron formations (Fig. 7) remain poorly resolved despite more than a century of investigation (e.g., Ohmoto et al., 2006; Beukes and Gutzmer, 2008). Given that BIF deposition spans major evolutionary changes in Earth's surface composition, from an early anoxic atmosphere dominated by CO_2 and CH_4 to an atmosphere that became partially oxygenated and CO_2 rich (e.g., Bekker and Kaufman, 2007), it is likely that BIFs formed via different mechanisms during the Precambrian. Mechanisms most widely supported in the literature are briefly discussed below.

Oxidation of Fe(II) by cyanobacterial O_2

The traditional model for BIF deposition invokes inorganic oxidation of dissolved Fe(II) with photosynthetically produced oxygen by cyanobacteria (Fig. 7A). Historically, cyanobacteria were assumed to be the primary producers utilizing oxygenic photosynthesis in the Archean oceans, because compelling evidence for an eukaryotic fossil record before ~1.9 Ga is absent (Han and Runnegar, 1992; Knoll et al., 2006). These prokaryotic microbes likely flourished in the photic zone of near-coastal waters, where Fe(II) and nutrients were made available by a combination of continental weathering and upwelling of deep currents containing a hydrothermal component (Cloud, 1973):

$$2Fe^{2+} + 0.5O_2 + 5H_2O \leftrightarrow 2Fe(OH)_3 + 4H^+. \quad (1)$$

Under an anoxic atmosphere, the required oxygen would have been confined to localized "oxygen oases," although some workers have suggested that the oceans were stratified, with a thin oxic zone overlying an anoxic and ferruginous water column (e.g., Klein and Beukes, 1989). In either case, BIF deposition with oxygen necessitates the existence of oxygenic photosynthesis at that time. Several lines of evidence tentatively suggest that oxygenic photosynthesis evolved during the Neoarchean, including these: 2.7 Ga stromatolitic assemblages of the Tumbiana Formation in Western Australia in which the microbial mat community probably was comprised of cyanobacteria (Buick, 1992); and the presence of ^{13}C-depleted kerogens in ca. 2.7 Ga shales and carbonates that suggests a microbial community comprised of cyanobacteria and aerobic methanotrophs (Eigenbrode and Freeman, 2006; Eigenbrode et al., 2008; but see for a different interpretation Hinrichs, 2002, and for a different oxidation mechanism Beal et al., 2009). The existence of organic matter-rich shales alone may also indicate the presence of oxygenic photosynthesis (cf. Buick, 2008). However, at present, direct "smoking gun" evidence for oxygenic photosynthesis during the Archean is absent.

Metabolic iron oxidation

Metabolic ferrous iron oxidation is the other most commonly invoked mechanism of iron-formation deposition (Fig. 7B). The potential importance of microaerophilic microbial iron oxidizers in iron-formation deposition has been recognized for almost a century, mainly due to the common occurrence of "iron bacteria" such as *Leptothrix* and *Gallionella* in iron-rich ground-water seeps and freshwater streams (e.g., Harder, 1919). Recent efforts have sought to unravel the importance of these microbes in laboratory and modeling-based studies and through geochemical investigations of iron formations.

Microaerophilic Fe(II) oxidizers utilize oxygen, carbon dioxide, and water, and the reaction can be summarized as:

$$6Fe^{2+} + 0.5O_2 + CO_2 + 16H_2O \leftrightarrow [CH_2O] + 6Fe(OH)_3 + 12H^+. \quad (2)$$

Known microaerophilic Fe(II) oxidizers are *Proteobacteria*, but the metabolic pathway appears to be nested within several different clades of this broad grouping of bacteria. Interestingly, microaerophilic Fe(II) oxidizers have been recently discovered to be widespread in marine systems. For example, a strain of bacteria that is morphologically indistinguishable but phylogenetically distinct from *Gallionella* was found to be abundant at the Loihi seamount iron-rich hydrothermal vents (Emerson and Moyer, 2002). Under low oxygen conditions, microaerophilic microbial Fe(II) oxidizers can dominate the iron cycle, because the rate of microbial oxidation can be more than fifty times faster than abiotic rates (e.g., Søgaard et al., 2000). Additionally, Fe(II)-oxidizing bacteria are present and may be abundant at the chemocline in ferruginous lakes, where iron-rich sediments are deposited (e.g., Pavin Lake, France; Lehours et al., 2007).

Anoxygenic photosynthetic oxidation, photoferrotrophy, a recently discovered means of metabolic Fe(II) oxidation, was linked to iron-formation deposition by Garrels and Perry (1974) nearly 20 years before organisms capable of this type of metabolism were cultured (Widdel et al., 1993). Anoxygenic photosynthesis uses Fe(II) rather than H_2O as an electron donor, producing Fe(III) rather than dioxygen (Ehrenreich and Widdel, 1994):

$$4Fe^{2+} + 11H_2O + CO_2 \leftrightarrow [CH_2O] + 4Fe(OH)_3 + 8H^+. \quad (3)$$

In the past 20 years, a number of experimental studies have confirmed that various purple and green bacteria can use Fe(II) as a reductant for carbon dioxide fixation (e.g., Widdel et al., 1993; Heising et al., 1999; Straub et al., 1999). One of the most attractive aspects of this concept is that it explains

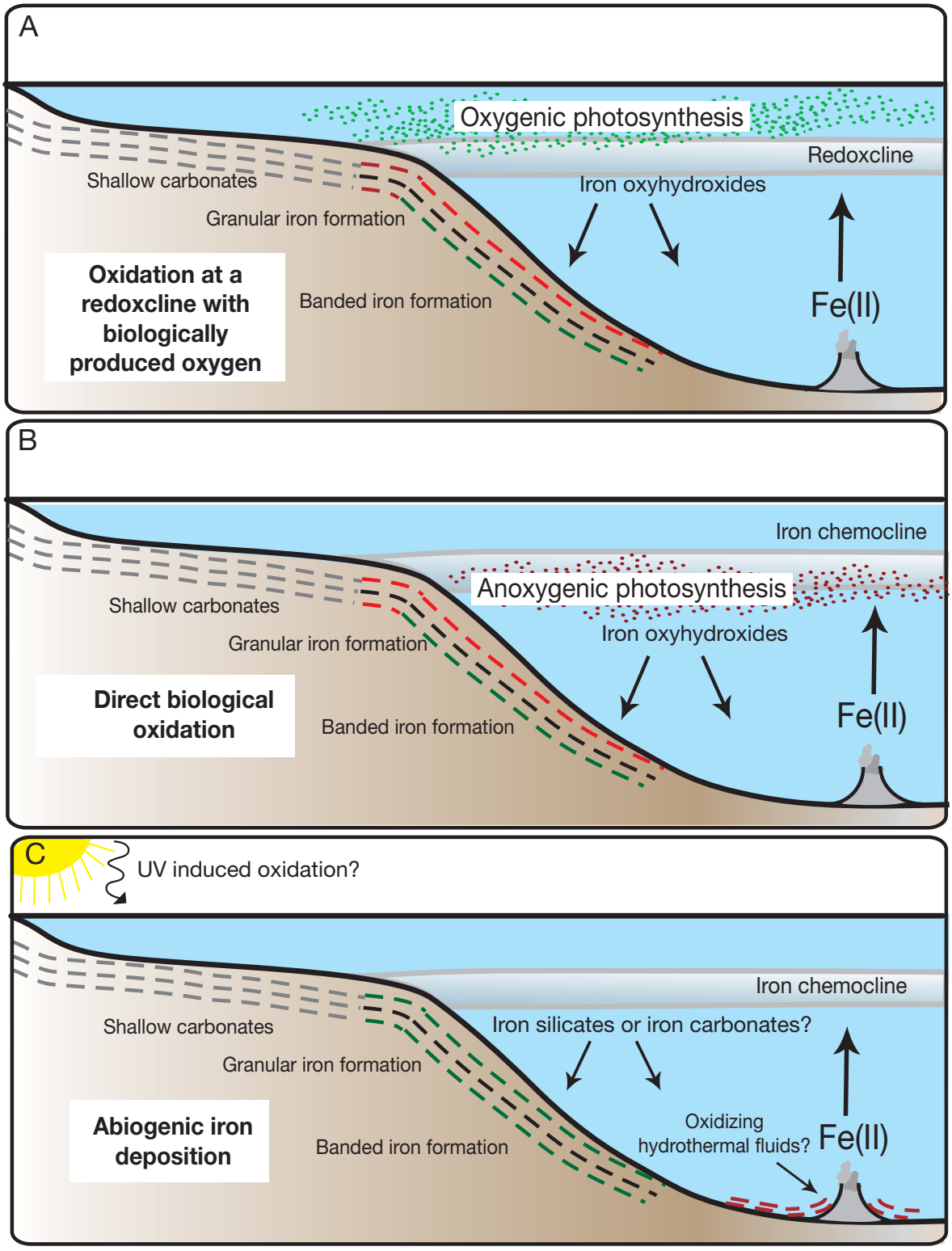

FIG. 7. Simplified models for the deposition of Archean and Paleoproterozoic iron formations. Marked gradients in iron concentrations existed in both Archean and Proterozoic oceans in which iron-formation deposition occurred. Oxygen oases in shallow-water environments (A), above the redoxcline, generated by oxygenic photosynthesis were originally held responsible for deposition of iron formation (Cloud, 1973). However, during the Archean even shallow-water settings may have been reducing with respect to iron. In this case, it is unlikely that oxidation with dissolved divalent oxygen was an important process; anoxygenic photosynthesis (B) was probably the dominant means of ferrous iron oxidation. Photochemical oxidation of iron was also inferred (C) but is now considered insignificant.

BIF deposition in the absence of molecular oxygen using the abundant availability of Fe(II), light, and carbon dioxide at that time. It has even been demonstrated by ecophysiological laboratory experiments in combination with modeling that these phototropic bacteria would have been capable of oxidizing enough Fe(II) to fully account for all of the primary ferric iron deposited as BIF precursor sediment, despite their extremely rapid accumulation rates (Konhauser et al., 2002; Kappler et al., 2005). Interestingly, growth experiments suggest that the phototrophs can potentially oxidize Fe(II) effectively at as much as a few hundred meters of water depth, and as such, they could easily have oxidized all of the upwelling Fe(II) before the iron made contact with the overlying oxygenated waters if these existed in Archean oceans (Kappler et al., 2005).

It has been demonstrated that two Fe(II)-rich lakes (Lake Matano in Indonesia and Lake La Cruz in Spain) contain phototrophic Fe(II)-oxidizing bacteria in the photic zone of the water column (Crowe et al., 2008; Walter et al., 2009). Additionally, phylogenetic analysis of the enzymes involved in the bacteriochlorophyll biosynthesis shows that anoxygenic photosynthetic lineages are more deeply rooted than the oxygenic cyanobacterial lineages (Xiong, 2006). Based on modern systems, there is compelling evidence that metabolic microbial iron oxidation was an important process in deposition of iron formations. It has to be noted that there is little paleontological or chemical evidence for existence of Fe(II)-oxidizing phototrophs during the Archean. However, ocean or basin-scale paleoredox studies may help to untangle the importance of different oxidative mechanisms. Most Archean and early Paleoproterozoic iron formations do not indicate a distinct redoxcline or an oxide shuttle from shallow- to relatively deep water environments, which has recently been used to question the classical models for BIF deposition based on iron oxidation through mixing of oxic and anoxic waters (e.g., Planavsky et al., 2008). Consequently, Fe(II) oxidation in suboxic or anoxic waters, where microbial oxidation would be important, was probably common in Archean and early Paleoproterozoic oceans (cf. Planavsky et al., 2008).

UV photooxidation of Fe(II)

As an alternative to biological models for Fe(II) oxidation, Cairns-Smith (1978) proposed that ferrous iron could have been photo-oxidized by the high flux of ultraviolet photons that would have reached Earth's surface prior to the rise of atmospheric oxygen and prior to the development of a protective ozone layer (Fig. 7C). This reaction proceeds readily in acidic waters exposed to wavelengths in the range of 200 to 300 nm:

$$2Fe^{2+}_{(aq)} + 2H^{+} + h\upsilon \rightarrow 2Fe^{3+}_{(aq)} + H_2. \quad (4)$$

Braterman et al. (1983) further explored the viability of the photochemical oxidation model at circumneutral pH and over a range of UV wavelengths (217–406 nm). Based on a quantum yield determined from proton flux, they suggested that at pH >6.5 the presence of the dissolved ferrous iron species $Fe(OH)^{+}$ is important because it is oxidized by photons of λ = 300 to 450 nm, a wavelength region where the solar flux is more intense and where seawater is more transparent, as compared to λ <300 nm. The dissolved ferric iron formed is subsequently hydrolyzed and precipitated as ferric oxyhydroxide. Extrapolating from these experiments, a mean photochemical oxidation rate of 0.5 mol Fe(II) m^2 yr^{-1} has been estimated at rapid upwelling rates (4,000 m yr^{-1}), indicating that this process alone could have accounted for deposition of as much as 1.8×10^{14} mol Fe(III) annually (François, 1986). Other estimates place the total amount of Fe(II) photo-oxidized annually at 2.3×10^{13} mol (Braterman and Cairns-Smith, 1986). These rates are much greater than annual rates inferred during deposition of the largest Archean and Paleoproterozoic BIFs (Pickard, 2002, 2003).

Importantly, these earlier photochemical models focused on determining the rates of Fe(II) photooxidation at, or close to, thermodynamic equilibrium conditions with 0.02 mM Fe and under rather simplistic geochemical conditions in which other ions were unavailable for reaction with dissolved Fe(II). In this regard, Konhauser et al. (2007a) performed a series of experiments designed to mimic conditions in a photic zone proximal to a seamount-type vent system effusing elevated concentrations of Fe(II) into seawater saturated with respect to amorphous silica and calcite. Under those conditions, the photochemical contribution to solid-phase precipitation was negligible compared to the formation of the ferrous silicate mineral greenalite or the ferrous carbonate siderite. Many iron formations are composed predominantly of iron carbonates or iron silicates, which have been widely suggested to be abiotic marine precipitates (e.g., Ohmoto et al., 2004). However, based on petrographic and isotopic constraints, siderite in iron formations is a diagenetic, or later, mineral phase. In experiments where Fe(II) was exposed to either phototrophic Fe(II)-oxidizing bacteria or dioxygen, ferric oxyhydroxide formed considerably faster than through UV photooxidation. Collectively, these experiments suggest that the precursor sediments to oxide-facies BIFs were the product of rapid, nonphotochemical oxidative processes, the most probable candidates being direct or indirect biological oxidation. However, additionally experimental work on UV photooxidation in complex seawater solutions is needed to rule out that photochemical oxidation was an important mechanism in iron formation genesis.

In addition, Foustoukos and Bekker (2008) argued that some deep-water Algoma-type iron formations deposited in association with VMS deposits formed by oxidation during phase separation into vapor and brine, with hydrogen and HCl removed into the vapor phase, leaving oxidizing and alkaline conditions in the brine. Transition metals would form chlorocomplexes and would then be enriched in the brine. This model, although not yet supported by either detailed modeling or empirical data, warrants serious consideration because it has the potential to explain enigmatic associations of Archean jasper and oxide-facies iron formation with some Cu-rich VMS deposits that formed in anoxic deep waters.

Geochemistry

Trace elements

Trace element studies of iron formations have focused on the source of iron and the relative contribution of hydrothermal fluids and seawater. Trace metal concentrations, their ratios, and correlations among concentrations of elements are consistent with a mainly hydrothermal source modified by mixing with seawater (e.g., Gross, 1993).

In natural systems where trace element sequestration by authigenic hydrous ferric oxides (HFO) results from a continuum of adsorption and coprecipitation reactions, lumped-process distribution coefficient models can be used to relate the concentration of an element in the HFO precipitate to the dissolved concentration present at the time of precipitation. This predictive aspect of HFO sorption reactions has been exploited to better understand ancient seawater composition and nutrient limitations on Precambrian primary productivity. Sequestration of bioessential nutrients during HFO precipitation in the water column and their eventual accumulation as iron-rich sediment likely provide a means to trace past ocean chemistry (e.g., Bjerrum and Canfield, 2002; Konhauser et al., 2007b).

One particularly compelling example is how molar Ni/Fe ratios preserved in BIFs over time may yield insights into ancient marine microbial productivity. Konhauser et al. (2009) observed that the nickel content of BIFs changed dramatically over time, from iron-normalized concentrations of greater than 0.0004 *M* Ni/Fe between 3.8 and 2.7 Ga, dropping to about one-half that value between 2.7 and 2.5 Ga, and then slowly approaching modern values (<0.0001) by 0.55 Ga. The large drop in nickel availability in the oceans at 2.7 Ga would have had profound consequences for microorganisms that depended on it, specifically methane-producing bacteria, methanogens. These bacteria have a unique nickel requirement for many of their essential enzymes (Jaun and Thauer, 2007), and a deficiency in the metal could have decreased the metabolism and populations of these methane producers. Crucially, methanogens have been implicated in controlling oxygen levels on early Earth because the methane they produced was reactive with oxygen and kept oxygen levels low. So as long as methane was abundant, oxygen could not accumulate in the atmosphere, and indeed, it is considered that methane production must have dropped to enable the rise of atmospheric oxygen at ca. 2.4 Ga, during the GOE (Zahnle et al., 2006).

Rare earth elements

Rare earth elements (REEs) are one of the most commonly used geochemical tools to understand the origin and deposition of iron formations, and other iron oxide-rich sedimentary rocks (e.g., Freyer, 1976; Klein and Beukes, 1989; Derry and Jacobsen, 1990; Bau and Dulski, 1996; Frei et al., 2008). At the heart of REE studies in iron formation is the assumption that there is minimal fractionation of REE during precipitation of ferric iron oxides and oxyhydroxides. Iron formations are, therefore, inferred to have trapped a REE signature of seawater at the site of Fe precipitation. This assumption is supported by both experimental studies and results from natural systems. For example, Mn-poor hydrothermal plume particles in modern hydrothermal systems record a seawater REE pattern (e.g., Sherrell et al., 1999). The REEs in iron oxide-rich sediments appear to be rock buffered under most early- to late-stage diagenetic and metamorphic alteration conditions (Bau, 1993). Hence, iron formations are likely to preserve their primary REE pattern during burial and exhumation. However, for iron formations that have undergone relatively high degrees of metamorphism, at amphibolite facies and above, or have been affected by high fluid/rock conditions during metamorphism, REE patterns must be used with caution for inferring primary depositional redox states (Bau, 1993; Slack et al., 2009).

There have been two central facets in REE studies of iron formations: tracing iron sources and deciphering oxidation mechanisms responsible for iron deposition. More specifically, most REE studies of iron formations have focused on Eu anomalies as tracers of hydrothermal input and Ce anomalies as redox proxies. Therefore, REE studies are an important component of our understanding of aspects of iron formations that are central to this review; that is, the timing and causes of iron-formation deposition, depositional mechanisms, and the evolution of iron oxide-rich sedimentary environments through time.

Europium enrichments in sediments that were apparently precipitated from seawater indicate a strong influence of hydrothermal fluids on the dissolved REE load of seawater (Derry and Jacobsen, 1990). The disparate behavior of Eu from neighboring REEs in hydrothermal fluids is linked to Eu(III) reduction under high-temperature (>250ºC) and low-Eh conditions (Klinkhammer et al., 1983). It is generally assumed that iron and REEs will not be fractionated during transport from spreading or other exhalative centers and, therefore, a large positive Eu anomaly indicates that the iron present in the protolith is hydrothermally derived (e.g., Slack et al., 2007). The recognition by Huston and Logan (2004) that shale-normalized Eu anomalies of Algoma-type iron formations are generally much larger than those of Superior-type iron formations, when both sample sets were screened to minimize detrital influences, led these workers to suggest that the latter contain a smaller hydrothermal component. This interpretation is consistent with the large dilution of hydrothermal fluids by seawater in modern plumes (typical dilution factor of 10^4; German and Von Damm, 2004) and a decrease in the magnitude of Eu anomalies with distance from ancient hydrothermal vents (Peter et al., 2003). As a result of these factors, the distribution and composition of Superior-type iron formations are considered to more accurately reflect the nature of coeval deep seawater (Huston and Logan, 2004). Large positive Eu anomalies are a common feature of Phanerozoic and Proterozoic distal hydrothermally sourced sedimentary rocks, generally interpreted to record a localized hydrothermal flux (e.g., Peter et al., 2003).

Redox-oriented REE studies are founded on extensive work on water column REE behavior in modern anoxic basins. In general, oxygenated marine settings show a strong negative Ce anomaly when sample REE data are normalized to shale composites ($Ce_{(SN)}$), whereas suboxic and anoxic waters lack large negative $Ce_{(SN)}$ anomalies (German and Elderfield, 1990; Byrne and Sholkovitz, 1996). Oxidation of Ce(III) greatly reduces Ce solubility, resulting in preferential removal onto Mn-Fe oxyhydroxides, organic matter, and clay particles (Byrne and Sholkovitz, 1996). In contrast, suboxic and anoxic waters lack significant negative $Ce_{(SN)}$ anomalies due to reductive dissolution of settling Mn-Fe–rich particles (German et al., 1991; Byrne and Sholkovitz, 1996). Similarly, light REE depletion develops in oxygenated waters due to preferential removal of light versus heavy REEs onto Mn-Fe oxyhydroxides and other particle-reactive surfaces, and the ratio of light to heavy REEs markedly increases across redox boundaries

owing to reductive dissolution of Mn-Fe oxyhydroxides (German et al., 1991; Byrne and Sholkovitz, 1996). In many basins, the $Ce_{(SN)}$ anomaly and the light to heavy REE ratio return to nearly the shale composite value across the Mn and Fe redox boundaries. In some basins, even positive $Ce_{(SN)}$ anomalies and light REE enrichment develop in anoxic and suboxic waters (De Baar et al., 1988; Bau et al., 1997; De Carlo and Green, 2002). Redox-induced shifts in REE patterns in some modern stratified basins are directly linked to Mn cycling in the suboxic zone (German et al., 1991; De Carlo and Green, 2002).

There is no evidence for deviation from trivalent Ce behavior in many Archean and early Paleoproterozoic iron formations (e.g., Bau and Dulski, 1996; Alexander et al., 2008; Frei et al., 2008), suggesting that the water column from which ferric oxides and oxyhydroxides may have precipitated was reducing with respect to manganese (cf. Bau and Dulski, 1996). In support of this model, a recent survey of 18 Paleoproterozoic and Archean iron formations found that bulk samples of iron formation lack significant Ce anomalies (Fig. 8) until after the GOE at ca. 2.4 Ga (Planavsky et al., 2008).

There also appear to be differences in trivalent REE behavior in iron formations before and after the rise of atmospheric oxygen. Archean and early Paleoproterozoic iron formations are characterized by consistent depletion in light REE (Planavsky et al., 2008). This feature contrasts markedly with late Paleoproterozoic iron formations that show significant ranges in light to heavy REE ($Pr/Yb_{(SN)}$) ratios, both below and above the shale composite value (Fig. 9). The range of light to heavy REE and Y/Ho ratios in late Paleoproterozoic iron formations reflects varying contributions of REE + Y from Mn and Fe oxyhydroxide precipitation and dissolution. This interpretation implies deposition of late Paleoproterozoic (ca. 1.9 Ga) iron formations in basins having varying redox conditions and a strong redoxcline separating the oxic upper part of the water column from the suboxic to anoxic deeper part (Planavsky et al., 2009). A similar Mn redoxcline was absent in Archean oceans (Bau and Dulski, 1996; Planavsky et al., 2008).

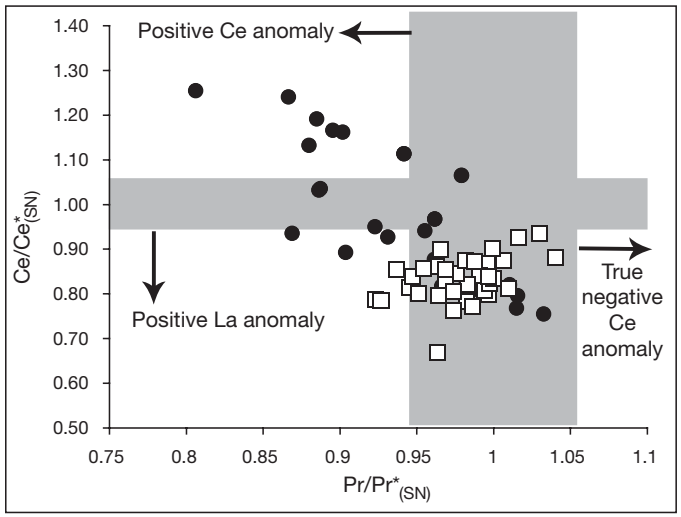

FIG. 8. Plot of Ce_{SN} and Pr_{SN} anomalies for a set of late Paleoproterozoic (●) and Archean and early Paleoproterozoic (□) iron formations (modified from Planavsky et al., in prep.). Positive Ce anomalies are only present in late Paleoproterozoic iron formations, whereas all shown iron formations lack true negative Ce anomalies. True negative Ce anomalies are defined by Ce/Ce^*_{SN} ($Ce_{SN}/(0.5(Pr_{SN} + La_{SN})$ and Pr/Pr^*_{SN} ($Pr_{SN}/(0.5Ce_{SN} + 0.5Nd_{SN})$) values above and below unity, respectively. This approach, first described by Bau and Dulski (1996), discriminates between positive La and true negative Ce anomalies.

Numerous studies report deviations from trivalent Ce behavior in Archean and early Paleoproterozoic iron formations (e.g., Klein and Beukes, 1989; Ohmoto et al., 2006). Although the significance of each reported case of negative or positive Ce anomalies in Archean rocks needs to be discussed individually, it is important to note that Ce anomalies in iron formations can arise from analytical artifacts and diagenetic alteration. Many previous REE studies are plagued by inaccurate and incomplete measurements (e.g., Klein and Beukes, 1989). Additionally, negative Ce anomalies were found in single samples, but no studies have documented consistent Ce anomalies for a suite of representative samples. At least some of the negative Ce anomalies, therefore, might reflect metamorphic or recent weathering-related redistribution of REEs between metamorphic minerals and compositionally different layers or between the soil horizon and bedrock (e.g., Braun et al., 1990; Slack et al., 2009). In this regard, it is noteworthy that analytically reliable bulk compositions of Archean and early Paleoproterozoic iron formations older than the 2.4 Ga do not provide evidence for an oxidative Ce cycle (e.g., Planavsky et al., in prep.).

Stable Isotopes

Light stable isotopes of oxygen and carbon and, to a lesser extent, hydrogen, sulfur, and nitrogen have been widely used to understand the genesis of iron formations, fundamental constraints on Precambrian paleoenvironments, and the evolution of life (e.g., Becker and Clayton, 1972; Goodwin et al., 1976; Thode and Goodwin, 1983; Walker, 1984; Baur et al., 1985; Beaumont and Robert, 1999; Shen et al., 2006; Hren et al., 2009). Following analytical advances in stable isotope geochemistry, new isotope tracers are now available, including the two major elements in iron formations, iron and silicon, as well as trace elements such as chromium and uranium. Although still in its infancy, the growing field of nontraditional stable isotope geochemistry will certainly open new avenues for investigations of iron formations.

Traditional light stable isotopes

Carbon isotopes have long been used as a tool to understand the genesis of iron formations. Most carbon isotope studies of iron formations have focused on the carbonate fraction, due in part to the low organic carbon content in iron formations. The most extensive carbon isotope studies of iron formations have been undertaken on the low metamorphic grade deposits of the Transvaal Supergroup in South Africa (e.g., Beukes and Klein, 1990; Fischer et al., 2009), the Brockman Iron Formation in Western Australia (e.g., Becker and Clayton, 1972, Baur et al., 1985), and the ca. 1.88 Ga Biwabik and Gunflint Iron Formations in the United States and Canada (Perry et al., 1973; Winter and Knauth, 1992). In addition, numerous siderite-rich iron formations have been analyzed for carbonate carbon isotopes (e.g., Ohmoto et al., 2004). Based on a recent compilation by Johnson et al.

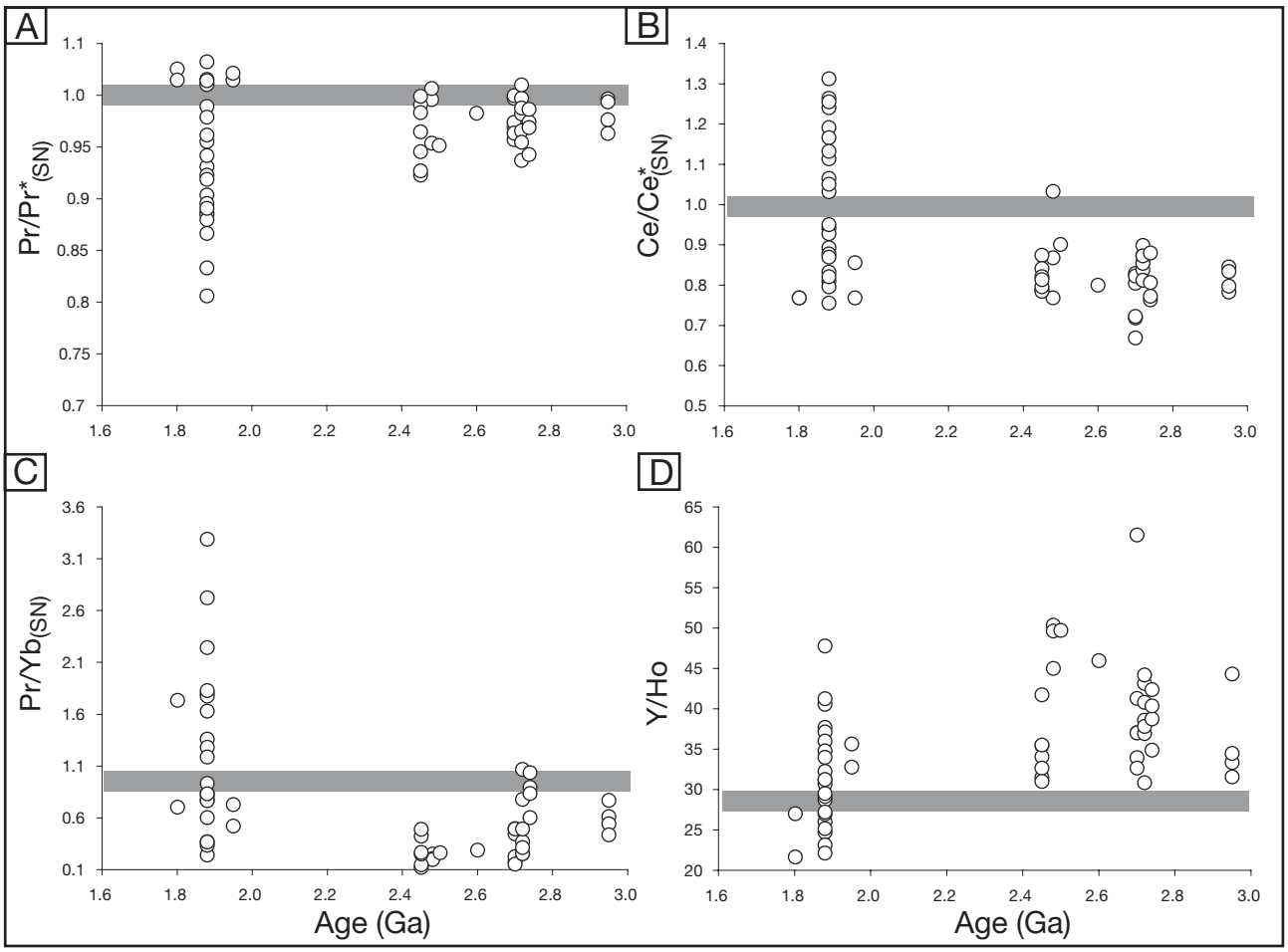

FIG. 9. Secular trends in REE + Y characteristics in a set of 18 Archean and Paleoproterozoic iron formations (modified from Planavsky et al., in press). A. Pr anomalies ($Pr_{SN}/(0.5(Ce_{SN} + Nd_{SN})$. B. Ce anomalies ($Ce_{SN}/(0.5(Pr_{SN} + La_{SN})$. C. Light to heavy REE ratios (Pr/Yb_{SN}). D. Y/Ho ratios. Black bar indicates PAAS shale composite values. Positive Ce_{SN} anomalies are not present in Archean iron formations but are common in late Paleoproterozoic iron formations. Archean iron formations are characterized by higher Y/Ho ratios and lower light to heavy REE ratios than those of the shale composite; late Paleoproterozoic iron formations have a large range of Y/Ho and light to heavy REE ratios. Observed secular trend in REE + Y characteristics is best explained by the absence of a Fe-Mn redoxcline in the Archean oceans prior to the rise of atmospheric oxygen (see text for details).

(2008a), carbonates in iron formations are isotopically light, with $\delta^{13}C$ values ranging from +2.4 to –20.0 per mil, whereas organic carbon isotope values are also ^{13}C depleted, with values as light as –41.4 per mil PDB. Studies of carbonates from the Brockman Iron Formation (Baur et al., 1985) show that isotopically light carbon and oxygen isotope values correlate with concentrations of iron. The negative carbonate carbon isotope values are commonly interpreted as evidence for direct carbonate (siderite) precipitation from an iron-rich water column, stratified with respect to carbon isotope composition of total dissolved inorganic carbon (e.g., Beukes and Klein, 1990; Winter and Knauth, 1992). Although a several per mil stratification in carbon isotope composition of dissolved inorganic carbon is present in the modern ocean (e.g., Kroopnick, 1985), a much smaller gradient is observed in the early Precambrian rock record and is expected under the high pCO_2 conditions required to compensate for a lower solar luminosity (Hotinski et al., 2004). As another caveat on those interpretations, however, petrographic documentation (e.g., Ayres, 1972) establishes that almost all iron-rich carbonates in iron formations grew during burial diagenesis and, therefore, were unlikely to have precipitated in the water column (see, e.g., how iron-rich carbonate in Fig. 2C occludes laminae). Formation of ^{13}C-depleted carbonates is also considered to result from either a fermentative metabolism and anaerobic respiration in the water column or a hydrothermal flux derived from deep waters dominated by submarine magmatic activity. The former interpretation was suggested by Perry et al. (1973) and, later, by Walker (1984) who proposed that the markedly light carbon isotope values of siderite reflect diagenetic ferruginous carbonate formation linked to organic matter remineralization, with ferric oxides being the terminal electron acceptor. Fischer et al. (2009) provided support for this model by questioning the presence of strong dissolved inorganic carbon isotope gradients between the shallow and deep waters.

An alternative to these two canonical models is that the light carbon isotope ratios in iron carbonates of iron formations are

linked to methane oxidation. It has been recently documented at modern marine methane seeps (Beal et al., 2009), as has commonly been predicted on thermodynamic considerations, that bacteria are capable of linking methane oxidation to ferric iron reduction. Methanogenesis was a widespread metabolic pathway in sulfidic shales rich in organic matter within iron-formation sequences, as well as in precursor sediments for iron formations in Archean and Paleoproterozoic oceans (e.g., Konhauser et al., 2005). In this scenario, methane and carbon dioxide produced in sediments during early diagenesis diffused upward. While carbon dioxide was released back to the water column, methane was biologically oxidized with ferric oxides, producing both ferrous iron and bicarbonate, which would precipitate as iron-rich carbonates. The presence of markedly negative carbonate carbon isotope values ($\delta^{13}C < -10‰$ PDB) is consistent with methane cycling having mediated carbonate precipitation, given that methane is much more isotopically depleted than is typical organic matter. This process could also create organic matter with extremely depleted $\delta^{13}C$ values without aerobic processes.

The oxygen isotope composition of chert in iron formations, particularly coupled to other isotope proxies, such as Si, H, and Fe, have been used to address such issues as ocean temperatures during the Precambrian (Knauth and Lowe, 2003; Robert and Chaussidon, 2006; Hren et al., 2009), the oxygen isotope compositions of Precambrian seawater (Perry, 1967), ocean silica sources (Robert and Chaussidon, 2006; van den Boorn et al., 2007; Steinhoefel et al., 2009), and metamorphic overprints in iron formations (Valaas Hyslop et al., 2008). Assuming that oxygen isotope values of Precambrian oceans were similar to those of ice-free modern oceans (Knauth and Lowe, 2003) and that postdepositional isotope exchange was minimal, bulk oxygen isotope composition of chert might be a useful paleothermometer because isotope fractionation between silica and seawater is dependent on temperature. Under this assumption, low oxygen isotope values of 3.4 to 3.2 Ga cherts were interpreted as evidence for hot early oceans, with seawater temperatures of 55° to 85°C (Knauth and Lowe, 2003). This was later supported by the Si isotope record and its covariation with the oxygen isotope record (Robert and Chaussidon, 2006). However, a study of isotope compositions of the ca. 3.42 Ga Buck Reef chert in South Africa (Hren et al., 2009), previously studied by Knauth and Lowe (2003), questioned this interpretation. Hren et al. (2009) explored the temperature dependence of $\delta^{18}O$ and δD fractionation in order to calculate $\delta^{18}O$ values of ambient fluid during transformation to microcrystalline quartz, finding that the Paleoarchean ocean was isotopically depleted relative to the modern ocean and thus was far cooler (<40°C) than previously envisaged. In using these and similar arguments, the assumption has generally been made that chert represents a marine chemical precipitate, and that its isotopic composition directly reflects the composition and temperature of the Archean ocean at the time of deposition. This is, however, unlikely for Paleoarchean cherts within volcano-sedimentary sequences of greenstone belts, because their origin was closely linked to syndepositional, low-temperature hydrothermal processes on the sea floor (Hofmann and Bolhar, 2007; Hofmann and Harris, 2008). Temperature estimates obtained from stable isotope paleothermometry, therefore, reflect the temperature of chert precipitation as a result of mixing of hydrothermal waters with colder seawater. The diagenetic origin of bedded cherts in Hamersley-like BIFs also questions the meaning of these data.

Sulfur isotope compositions of sulfidic shales rich in organic matter interbedded with Neoarchean and Paleoproterozoic iron formations were extensively studied to constrain biological sulfur cycling, sources of sulfur, and ocean redox structure (e.g., Goodwin et al., 1976; Thode and Goodwin, 1983; Cameron, 1983; Grassineau et al., 2002). The results were used to infer low (<200 μM) seawater sulfate content in the Archean ocean (Habicht et al., 2002). An increase in the range of sulfur isotope values in ca. 2.7 Ga black shales interbedded with iron formations has been interpreted as an expression of dissimilatory bacterial sulfate reduction or redox cycling in the Archean oceans (Goodwin et al., 1976; Grassineau et al., 2002). Studies of multiple sulfur isotopes have shown that the range of $\delta^{34}S$ values alone in sediments deposited before the GOE cannot be used to support either of these two interpretations, because photochemical processes in an anoxic atmosphere significantly fractionate sulfur isotopes (Farquhar et al., 2000). Indeed, the same Archean sedimentary units have been shown to contain a large signal of mass-independent fractionation in sulfur isotopes, arguing for the role of photochemical processes and against oxygenated surface environments. Although biological sulfur cycling was probable in the Archean oceans, it is difficult to constrain its role with sulfur isotopes alone. Multiple sulfur isotope analyses of sulfur extracted from iron formations also show a large range of mass-independent fractionations (Farquhar and Wing, 2005; Kaufman et al., 2007; Partridge et al., 2008), suggesting that small amounts of sulfur compounds derived from photochemically oxidized sulfur species coprecipitated with iron formations.

Much less data are available for nitrogen isotope composition of iron formations, most likely due to their low nitrogen contents. However, ammonium might substitute for the potassium ion in the original clay minerals (cf. Williams and Ferrell, 1991) within iron formations, such as in the sedimentary precursor to stilpnomelane, making iron formations a prospective lithology for nitrogen isotope studies. Nitrogen isotope data for organic matter-rich shales, cherts, and iron formations suggest a bimodal pattern with a change occurring across the Neoarchean-Paleoproterozoic boundary, interpreted as reflecting progressive oxidation of surface environments (Beaumont and Robert, 1999; Shen et al., 2006; Garvin et al., 2009; Godfrey and Falkowski, 2009). The older record is marked by negative and highly positive nitrogen isotope values, which are generally related to bacterial nitrogen fixation as a principal pathway for biogeochemical nitrogen cycling in anoxic oceans where nitrification with oxygen as an electron acceptor was limited or absent. A shift to predominantly positive nitrogen isotope values in Neoarchean samples is related to an emergence of nitrification and denitrification processes coeval with the appearance of oxidized environments in the ocean (Garvin et al., 2009; Godfrey and Falkowski, 2009). Interestingly, 2.7 and 2.5 Ga iron formations also contain nitrogen with highly positive isotope values (Beamont and Robert, 1999; Shen et al., 2006). Considering

that these iron formations were deposited in deep-water anoxic environments, it is highly unlikely that any levels of nitrate were exported into these environments from locally oxygenated settings, where they could have gained positive nitrogen isotope values due to Rayleigh distillation associated with nitrate reduction. On another hand, it is plausible that oxidized nitrogen species were produced during early diagenesis when organic matter and ammonium were biologically remineralized, with oxidized iron species acting as electron acceptors. Released oxidized nitrogen compounds would have been quickly reduced in the water column into dinitrogen gas, whereas a minor remaining fraction would have been incorporated into organic matter with its highly fractionated nitrogen isotope values reflecting Rayleigh distillation processes. A strong case has recently been made that sulfate-reducing ammonium oxidation occurs in modern marine sediments (Schrum et al., 2009). Ammonium oxidation coupled to Fe(III) reduction might, therefore, also be a feasible metabolic pathway. Calculations of the potential Gibbs free energy for this reaction under a wide range of conditions are needed to further evaluate the potential importance of this process.

Nontraditional stable isotopes in iron formations: iron isotopes

Stimulated by the potential of using iron isotopes to trace biogeochemical cycling of iron on early Earth, studies of the iron isotope composition of iron formations have generated great interest in recent years (Beard et al., 1999; Johnson et al., 2003, 2008a, b; Dauphas et al., 2004; Rouxel et al., 2005; Planavsky et al., 2009; Steinhoefel et al., 2009). Experimental investigations have highlighted the importance of Fe redox cycling, mineral precipitation and dissolution, and microbial processes as factors contributing to iron isotope compositions (e.g., Beard et al., 1999; Bullen et al., 2001; Johnson et al., 2002, 2008b). Therefore, it is expected that iron isotopes may provide valuable constraints on both biotic and abiotic redox processes recorded in iron formations.

A compilation of bulk-rock and mineral-specific δ^{56}Fe values in Archean and Paleoproterozoic BIFs (Fig. 10) shows an overall variation between –2.5 and +2.7 per mil, which encompasses most of the natural range in iron isotope values. Although magnetite, carbonates (siderite and ankerite), and pyrite have both positive and negative δ^{56}Fe values, iron oxides generally have the highest δ^{56}Fe values, whereas carbonate minerals have subcrustal δ^{56}Fe values. Microanalytical techniques, such as laser ablation MC-ICP-MS (Frost et al., 2007) and ion microprobe (Whitehouse and Fedo, 2007), have established that iron isotope heterogeneity and intermineral fractionations can be preserved during diagenesis and metamorphism. Most iron isotope studies have been done on the giant 2.5 Ga deposits of the Hamersley and Transvaal provinces (Johnson et al., 2003, 2008a), which contain sequences that have been metamorphosed to only the biotite zone. Other studies have focused on younger iron

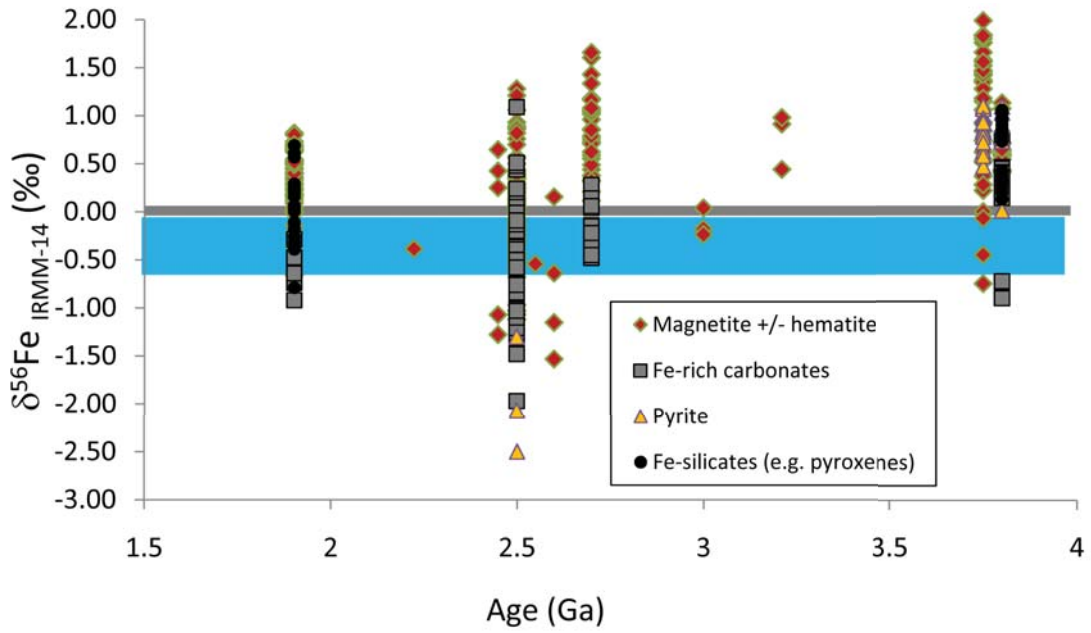

FIG. 10. Secular variations in δ^{56}Fe values for Archean and Paleoproterozoic iron formations. Data include bulk mineral analyses (magnetite, hematite, Fe-rich carbonates: ankerite and siderite, pyrite, and metamorphic Fe silicates) and in situ analysis (magnetite) using laser-ablation MC-ICP-MS and ion-microprobe. A total of 490 datapoints is shown including 83 analyses of the 1.88 Ga GIFs from the Animikie basin, North America (Frost et al., 2007; Valaas Hyslop et al., 2008; Planavsky et al., 2009), 138 analyses of the ca. 2.5 Ga Brockman Iron Formation, Western Australia (Johnson et al., 2008), 58 analyses of the 2.5 Ga Transvaal Supergroup BIF, South Africa (Johnson et al., 2003), 27 analyses of BIF from the Shurugwi and Belingwe greenstone belts, Zimbabwe (Steinhoefel et al., 2009; Rouxel et al., 2005), 137 analyses of the Eoarchean Isua, Akilia, and Innersuartuut BIFs and metamorphic rocks (Dauphas et al., 2004, 2007; Whitehouse and Fedo, 2007), and 45 analyses of Paleoproterozoic and Archean BIFs (Rouxel et al., unpu. data). Gray line and blue area represent average δ^{56}Fe values for igneous rocks and range of δ^{56}Fe values for hydrothermal sources, respectively (e.g., Beard et al., 2003; Rouxel et al., 2008).

formations from the Animikie basin (ca. 1.88 Ga Gunflint and Biwabik Iron formations: Frost et al., 2007; Planavsky et al., 2009), as well as on Paleoarchean 3.8 Ga iron formations from Isua, and the Nuvvuagittuq greenstone belt in northern Quebec (Dauphas, 2004, 2007; Whitehouse and Fedo, 2007). Limited data are also available on iron formations from the ca. 2.7 Ga Belingwe and Shurugwe greenstone belts of Zimbabwe (Rouxel et al., 2005; Steinhoefel et al., 2009).

A central tenant to understanding the genesis of iron formations, as stressed above, is identifying mechanisms that caused the oxidation of ferrous iron in Precambrian oceans. During anoxygenic photosynthesis and oxygen-mediated oxidation, net shifts in δ^{56}Fe values of 1.5 and 0.8 per mil have been documented under experimental conditions between precipitated Fe oxyhydroxides and dissolved Fe(II) (Bullen et al., 2001; Croal et al., 2004; Balci et al., 2006). Preliminary experiments performed to characterize the isotopic fractionation of iron during photooxidation (Staton et al., 2007) yield an isotopic shift of about 2.5 per mil. This shift is comparable to the fractionation between Fe(II) and Fe(III) hexaquo complexes (Welch et al., 2003) but larger than the effect typically seen during overall Fe(II) oxidation and precipitation at near-neutral pH. Assuming that Fe(II) in the Archean oceans had the same isotopic composition as Fe(II) released in modern hydrothermal systems, averaging about –0.3 per mil (Beard et al., 2003; Severmann et al., 2004, 2008; Rouxel et al., 2008), abiotic or biotic Fe oxidation in Precambrian oceans would have resulted in iron oxyhydroxides with δ^{56}Fe values of about 0.5 to 1.2 per mil. Higher δ^{56}Fe values up to ~2.7 per mil, such as those measured for Isua magnetite (Whitehouse and Fedo, 2007), are also theoretically possible considering the 3 per mil fractionation between dissolved Fe(II) and Fe(III) (Welch et al., 2003). In contrast, lower to near-zero δ^{56}Fe values of iron oxides resulted from partial oxidation of remaining iron in solution that experienced Rayleigh distillation during transport from hydrothermal vents in a redox-stratified ocean (Dauphas et al., 2004; Rouxel et al., 2005; Planavsky et al., 2009; Steinhoefel et al., 2009).

Because dissimilatory iron reduction was a widespread form of metabolism on early Earth (Vargas et al., 1998), the ferric iron component in iron formations was potentially actively recycled through dissimilatory iron reduction during diagenesis, providing that organic matter was available (Konhauser et al., 2005). Iron isotope fractionations during diagenesis of iron formations have been recently investigated using in situ δ^{56}Fe analysis. For example, Steinhoefel et al. (2009) studied iron isotope systematics of ca. 2.7 Ga iron formation from the Shurugwi greenstone belt, Zimbabwe. They showed that magnetite has relatively uniform δ^{56}Fe values of about 0.9 per mil, but has intracrystal zonation, suggesting fractionation during magnetite formation. Iron carbonates were also relatively uniform at near-zero values, with siderite and ankerite showing iron isotope values of +0.4 and –0.7 per mil, respectively. The data are consistent with a diagenetic origin of the magnetite precursor and iron carbonates by the reaction of organic matter with ferric oxyhydroxides catalyzed by Fe(III)-reducing bacteria. However, Steinhoefel et al. (2009) favored an alternative scenario involving abiotic reaction of organic carbon and Fe(III) during low-grade metamorphism.

The ubiquitous presence of magnetite and siderite in the Hamersley and Transvaal Iron Formations, with δ^{56}Fe values as low as –2.1 per mil (Fig. 10), has been interpreted as evidence for bacterially mediated Fe(III) reduction during diagenesis (Johnson et al., 2003, 2008a, b). These data might be also compatible with the formation of those minerals during burial. In this case, δ^{56}Fe values of magnetite might be inherited from a ferric oxide/oxyhydroxide precursor that formed through complete oxidation of hydrothermal Fe(II), followed by conversion to magnetite through interaction with Fe(II) formed by dissimilatory iron reduction. Similarly, the peak in δ^{56}Fe values at ~–0.5 per mil for siderite (Fig. 10) is interpreted to be controlled by dissolved iron in seawater with near-zero δ^{56}Fe values (Johnson et al., 2008a). Lower δ^{56}Fe values in carbonates may also indicate a higher proportion of iron from dissimilatory iron reduction incorporated during diagenesis of the iron formation. In principle, partial iron oxidation in the water column also fractionates dissolved iron in seawater toward negative δ^{56}Fe values through reservoir effects (Rouxel et al., 2005). For example, a Rayleigh fractionation mechanism involving between 50 and 80 percent of dissolved iron oxidation may explain isotopically enriched iron oxides in iron formations (as high as +0.8‰) and negative δ^{56}Fe values in seawater (as low as –2.2‰). Regardless of the exact mechanism, the magnetite inventory in the ca. 2.5 Ga Hamersley and Transvaal Iron Formations has average δ^{56}Fe values of approximately 0 per mil (Johnson et al., 2008a), which suggests that the iron ultimately was derived from oceanic crust and is hydrothermal in origin. Limited input of isotopically negative diagenetic iron was derived from continental margin sediments, as suggested for modern redox-stratified basins (Severmann et al., 2008). However, the study of Johnson et al. (2008a) focused only on mineralogically pure microlaminae and, therefore, is likely a poor estimate for the bulk isotopic composition of iron formations.

Paleoarchean iron formations from Isua and the Nuvvuagittuq greenstone belt in northern Quebec (Dauphas, 2004, 2007; Whitehouse and Fedo, 2007) are characterized by only positive δ^{56}Fe values. Because negative δ^{56}Fe values are relatively common in Neoarchean iron formations, it is premature to draw robust conclusions regarding secular changes in biogeochemical cycling of iron from iron isotope data. It seems, however, that the range of iron isotope values in iron formations decreases significantly after the GOE at ca. 2.4 Ga (Rouxel et al., 2005; Johnson et al., 2008a, b; Planavsky et al., 2009). Based on δ^{56}Fe record of iron formations and black shales, Johnson et al. (2008a, b) argued for an emergence of dissimilatory iron reduction early in Earth history, with a pronounced peak between ca. 2.7 and 2.5 Ga, which is coincident with the most negative δ^{56}Fe values in sedimentary rocks. It was further argued that the increase in seawater SO_4^{2-} by ca. 2.3 Ga may have restricted dissimilatory iron reduction in extent, due to complete titration of hydrothermal Fe(II) to pyrite in a deep-water anoxic water column. However, it is unclear why late Paleoproterozoic (1.88 Ga) depositional systems such as in the Animikie basin, where iron was clearly in excess of sulfate, would differ from Archean systems. In addition, a growing body of evidence suggests the development of at least local sulfidic conditions as early as 2.7 Ga (Scott et al., 2008; Reinhard et al., 2009), contemporaneous with highly negative δ^{56}Fe values in

iron formations (Rouxel et al., 2005; Johnson et al., 2008b). Ocean redox evolution is a more likely explanation for the presence of markedly negative δ^{56}Fe values in Archean shales and iron formations. Within an anoxic ocean, hydrothermally derived iron could undergo partial oxidation via anoxic processes over a significant depth range, thus allowing for burial of isotopically heavy iron. This burial would leave behind an iron reservoir with negative iron isotope values that was titrated at the later stage in iron transport, when hydrothermal plumes crossed the chemocline between iron- and sulfur-rich waters and approached shallow-water environments where sulfidic shales rich in organic matter were deposited (Fig. 11; Rouxel et al., 2005). In contrast, after the GOE, anoxic deep waters developed only locally and episodically and iron oxidation was focused at a prominent dynamic redocline separating anoxic ferruginous and oxic shallow waters (cf. Planavsky et al., 2009).

Other isotope systems

High-precision isotopic measurements of nontraditional isotope systems, such as chromium (Frei et al., 2009), uranium (Weyer et al., 2008), and germanium (Rouxel et al., 2006), have also revealed small, but significant, mass-dependent fractionations in iron formations and cherts. For example, the chromium isotope composition of iron formations has been explored to constrain biogeochemical cycling of chromium in Precambrian surface environments and oceans (Frei et al., 2009) in order to provide an independent secular record of the redox state of the atmosphere and oceans. Other isotope systems such as nickel (Cameron et al., 2009) have a great potential as environmental proxy and will be undoubtedly used in future investigations.

Influence of Hydrothermal Processes on Ocean Composition and Organic Productivity

Archean and Paleoproterozoic iron formations are commonly interbedded with or adjacent to sulfidic shale rich in organic matter, whereas similar shales appear to be underrepresented in the Archean record beyond stratigraphic intervals that contain iron formations (Condie et al., 2001). This intimate association is rather enigmatic and, to date, has not been satisfactorily addressed. During the Phanerozoic, the genetic connection between black shales and mantle plume events has generally been explained by sea-level rise and a higher flux of reductants into the ocean, creating extensive ocean areas with anoxia and euxinia where higher rates of organic matter burial reflect higher preservation potential. This explanation does not apply, however, to the Archean oceans that were persistently anoxic. In order to explain the origin of these organic matter-rich shales, we infer higher primary productivity driven by higher nutrient fluxes, either from the deep ocean or the continents.

In nearly all modern aquatic systems, primary production of organic matter is limited by either phosphorus or bioavailable nitrogen (Tyrrell, 1999). Iron formations may hold the key to understanding Earth's earliest phosphorous cycle. For example, P/Fe molar ratios in BIFs have been used to infer the concentration of dissolved phosphorous during the Precambrian in seawater because dissolved phosphate partitions onto ferric hydroxides in a predictable manner (Bjerrum and Canfield, 2002). In this regard, low P/Fe ratios in iron formations might provide empirical evidence for a small, biologically available phosphorus reservoir (Bjerrum and Canfield, 2002). In modern oceans, reactive phosphorus is delivered to sediments predominately with organic matter (Föllmi, 1996). Orthophosphate coprecipitates with iron oxides, and oxide-bound phosphorous is the other substantial flux of reactive phosphorus to sediments (Wheat et al., 1996). In contrast to modern oceans, during some of the Archean and Paleoproterozoic, especially during peak times of iron-formation deposition, iron oxide-bound phosphate may have been the dominant phosphorous sink (Bjerrum and Canfield, 2002). If this interpretation is correct, then low dissolved phosphorus concentrations in the early oceans could have severely limited primary productivity and organic matter burial (Bjerrum and Canfield, 2002). High dissolved silica concentrations may, however, have prevented iron oxides from being a major dissolved phosphate sink (Konhauser et al., 2007b). At dissolved

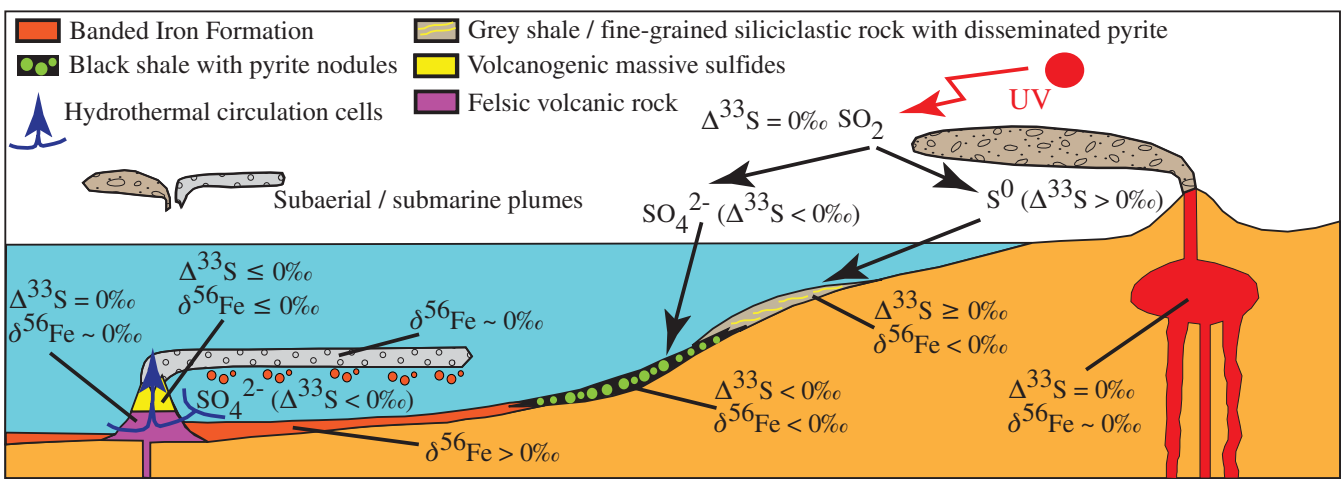

FIG. 11. Schematic diagram illustrating iron and multiple sulfur isotope compositions of depositional environments that were influenced by photochemical mass-independent sulfur isotope fractionation in the Archean anoxic atmosphere during the ca. 2.7 Ga mantle plume breakout event (modified from Bekker et al., 2009).

silica concentrations of >0.05 mM, silica competes with phosphate for sorption sites on ferric oxyhydroxides, which are considered as poorly crystalline precursors to some iron minerals in iron formations (Konhauser et al., 2007b). Iron-silica coprecipitation also decreases the point-of-zero net charge of precipitating ferric oxyhydroxides (Konhauser et al., 2007b), rendering them less reactive to dissolved anions. Dissolved silica concentrations during the Archean are considered to have been at least six times those in the oceans now, based on petrographic data indicating that early Precambrian seawater was at saturation with the silicon dioxide polymorph, cristobalite (Siever, 1992). Additionally, high levels of carbonate saturation during the Precambrian (cf. Grotzinger, 1990) would have inhibited carbonate fluorapatite formation. Carbonate ion substitution into carbonate fluorapatite scales with the ambient carbonate ion activity and increases solubility of the precipitating carbonate fluorapatite (Jahnke, 1984). Substitution of higher levels of carbonate ion into the fluorapatite structure, therefore, rather counterintuitively results in an exponential increase in levels of dissolved phosphorous needed for carbonate fluorapatite precipitation (Jahnke, 1984). Authigenic carbonate fluorapatite precipitation is the largest burial flux for phosphorous in modern oceans (Ruttenberg and Berner, 1993). Combined, these two factors suggest higher, rather than lower dissolved Archean phosphorous concentrations.

If phosphorous content was not the controlling factor for Archean primary productivity, could nitrogen be the culprit? In the Archean anoxic ocean, dinitrogen was seemingly fixed by diazotrophic cyanobacteria, whereas ammonium produced during organic matter remineralization was assimilated by other organisms (Garvin et al., 2009; Glass et al., 2009; Godfrey and Falkawski, 2009). Both nitrogen fixation and ammonium assimilation are operated by enzymes, which are dependent on bioessential trace metals, such as Fe, V, and Mo, as metal cofactors (Glass et al., 2009). Both the V and Mo dissolved loads were generally low or negligible in the early oceans because under an essentially anoxic atmosphere these metals are insoluble (Scott et al., 2008). Iron concentrations, in contrast, were high and iron was likely utilized by diazotrophs on early Earth for nitrogen fixation and ammonium assimilation (Glass et al., 2009). Iron availability enhances nitrogen fixation and photosynthesis in modern environments (e.g., Berman-Frank et al., 2001, 2007); however, Fe-Mo nitrogenase is one hundred times as efficient as the Fe-Fe nitrogenase in dinitrogen fixation (Zerkle et al., 2006). Therefore, nitrogen limitation of primary productivity was much more probable than phosphorous limitation in the early oceans. However, nitrogen stress was likely partially alleviated during mantle plume breakout events when iron formations were deposited.

The emerging picture is of coupled enhanced primary productivity and deposition of iron formations initiated by mantle plume breakout events. Related changes in the atmosphere and terrestrial settings are also relevant. The subaerial volcanism that occurred during these events would have delivered large amounts of SO_2 and CO_2 to the atmosphere. Enhanced weathering under greenhouse conditions yielded bicarbonates and nutrients, such as phosphorus and, to a lesser extent, nitrogen, to the oceans and, at the same time, sulfur photolyzed in the atmosphere into elemental sulfur and sulfate aerosols was concentrated in shallow-marine environments. As a result, iron oxyhydroxides would precipitate in deeper water environments and would oxidize organic matter in these settings, whereas anoxic and, possibly, sulfidic conditions would develop in correlative shallow-water environments where iron-depleted hydrothermal plumes would still deliver some reactive iron (Fig. 11; Rouxel et al., 2005; Bekker et al., 2009). A dynamic chemocline would therefore develop between anoxic ferruginous deep waters and anoxic sulfidic shallow waters and would persist until hydrothermal iron and atmospheric and/or terrestrial sulfur fluxes subsided, switching to an unstratified, fully anoxic ocean.

If this model is valid, then it has some implications for the rise of atmospheric oxygen. Once extensive oxidative continental weathering was initiated, it would provide abundant Mo to the oceans to activate the much more efficient Mo nitrogenase enzyme. However, an initial increase in primary productivity in this scenario might be linked with pulsed, global, and long-lived hydrothermal iron delivery to the oceans during deposition of iron formations shortly after the Archean (Isley and Abbott, 1999; Condie et al., 2001; Barley et al., 2005). Although iron formations were deposited and LIPs formed before then, both processes are not comparable in scale or extent with those at 2.5 to 2.45 Ga (Heaman, 1997; Isley and Abbott, 1999; Condie et al., 2001; Barley et al., 2005). Higher seawater iron concentrations during that time period would have removed any iron limitation-induced stress connected to nitrogen assimilation and fixation. An iron flux may have enhanced nitrogen fixation by Fe-Fe nitrogenase, thereby partially relieving nitrogen limitation and increasing primary productivity by photosynthetic cyanobacteria. Iron limitation under anoxic conditions is certainly counterintuitive but is not impossible, given that before widespread use of a diverse range of trace metals (e.g., Mo, V, Zn) as cofactors, iron stress would have been much higher than in modern ecosystems. Additionally, the lower efficiency of Fe-Fe nitrogenase relative to other trace metal-based enzymes would have further increased Fe demand. For instance, as stated above, the Fe-Fe nitrogenase is one hundred times less efficient than the Fe-Mo nitrogenase (Zerkle et al., 2006).

Consistent with the model, the oldest positive carbon isotope excursion is in carbonates of the ca. 2.48 Ga Tongwane Formation, South Africa, which sits above an iron formation (Bekker et al., 2001). Mass independent sulfur isotope fractionations, a proxy for atmospheric redox state, declined shortly after deposition of the ca. 2.5 to 2.45 Ga iron formations. Coincident with this shift is the onset of glaciations related to the rise of atmospheric oxygen and the oxidation of atmospheric methane, which was an important greenhouse gas during the Archean (Bekker and Kaufman, 2007). Higher net oxygen production would not only have provided the oxygen required to remove iron from seawater but would also have allowed a terrestrial flux of dissolved Mo to the oceans. Under these conditions, Fe-Mo nitrogenase would have replaced the less efficient Fe-Fe nitrogenase, lifting nitrogen limitation and leading to irreversible atmospheric oxidation. The rise of atmospheric oxygen in this model might have been brought on by an enhanced flux of reductants from the mantle.

Secular Trends for Exhalites, Iron Formations, and VMS Deposits

Relationship among mantle plume breakout events, iron-formation deposition, and VMS mineralization

Secular trends in the distribution of Precambrian iron formations and VMS deposits (Fig. 12) have been discussed by numerous workers (e.g., Veizer, 1976; James, 1983; Meyer, 1988; Isley and Abbott, 1999; Huston and Logan, 2004; Huston et al., 2010). Whereas the deposition of iron formations has been genetically linked to mantle plume breakout events and mafic volcanism (Isley and Abbott, 1999), the largest VMS deposits are genetically linked to bimodal arc volcanism (Franklin et al., 2005). Significantly, hydrothermal systems that produce VMS deposits also deliver iron and manganese to the deep ocean (e.g., German and Von Damm, 2004). As far as iron in hydrothermal plumes was derived by hydrothermal leaching of submarine volcanic rocks in the deeper part of the ocean to form iron formation, accompanying VMS deposits should have formed contemporaneously near the volcanic source. Exhalites that formed in stratigraphic association with VMS deposits are useful in providing a record of deep-water ocean redox states (Slack et al., 2007). The following section explores secular trends of sea-floor hydrothermal exhalites and iron formations to infer ocean redox state during their deposition.

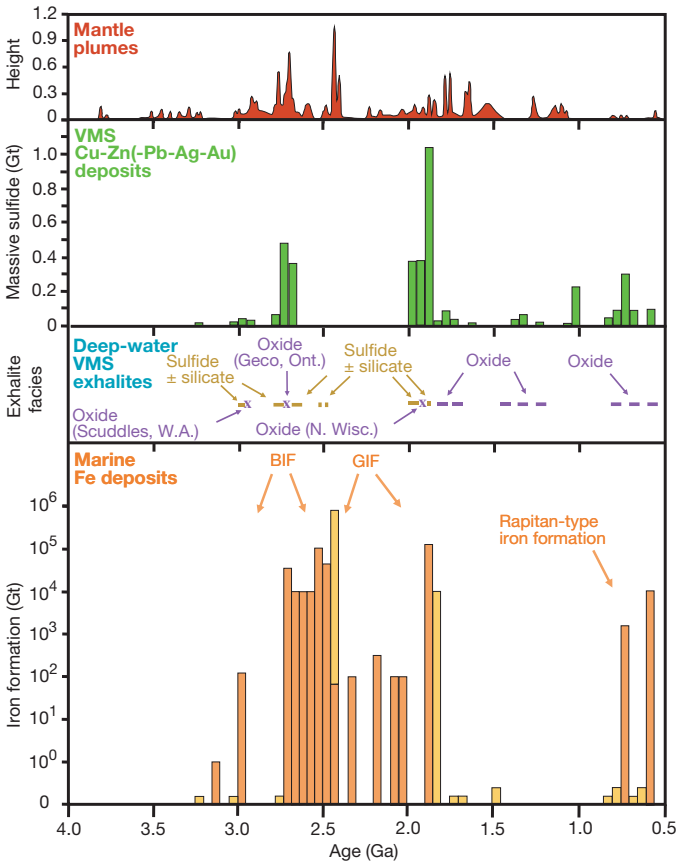

FIG. 12. Secular distributions of mantle superplume breakout events and selected marine mineral deposits during the Precambrian. Distribution of mantle superplumes is from Abbott and Isley (2002) in which the y-axis (height) is the sum of Gaussian time series for high Mg rocks and layered intrusions, flood basalts, and dikes. Distribution of marine Fe deposits is plotted as amount of iron formation in billion metric tons (Gt), integrated over time intervals of 50 m.y. (data in App. 2); apparently small deposits that lack published tonnage data are assigned a size of 0.2 Gt; deposits having poor age control are included as pale orange bars. Time periods dominated by banded iron formation (BIF), granular iron formation (GIF), and Rapitan-type iron formation are shown schematically (see text). Distribution of VMS deposits is similarly plotted in Gt for time intervals of 50 m.y. (data in Franklin et al., 2005, App. A2). Secular facies variation of exhalites associated with deep-water, Cu-rich VMS deposits is from Slack and Cannon (2009).

Secular patterns in Precambrian VMS-related exhalites

Constraints on the redox state of the deep ocean during the Precambrian can be derived from the mineralogy and geochemistry of exhalites related to the formation of Cu-rich VMS deposits. Such exhalites are generally stratiform layers or lenses as much as several meters thick in the hanging wall of VMS deposits or along strike at approximately the same stratigraphic level (e.g., Sangster, 1978; Spry et al., 2000). Exhalites also occur with some sediment-hosted, stratiform Zn-Pb deposits. Based on abundant lithological and geochemical data, exhalites are widely interpreted as precipitates from sea-floor hydrothermal vents and plumes (Kimberley, 1989; Isley, 1995; Peter, 2003; Grenne and Slack, 2005). Exhalites vary greatly in mineralogy and composition, mostly consisting of silica in the form of chert or microcrystalline quartz and iron oxides (e.g., hematite, magnetite), silicates (e.g., greenalite, stilpnomelane, grunerite), carbonates (e.g., siderite, ankerite), or sulfides (e.g., pyrite, pyrrhotite); other exhalites may contain abundant Ba (barite), Mn (spessartine), P (apatite), or F (fluorite). Slack et al. (2007) first proposed using Precambrian Fe-rich exhalites as proxies for the redox state of coeval deep seawater. This approach is limited to VMS deposits that contain appreciable Cu (>1 wt %) in chalcopyrite, given that chalcopyrite-rich deposits form at ≥300°C (Hannington et al., 1995, 2005). This minimum temperature of 300°C, together with the average salinity of 3*M* NaCl equiv measured in high-temperature, sea-floor hydrothermal fluids (e.g., Von Damm, 1995), suggests that Cu-rich massive sulfide deposits form at water depths of >850 m. At shallower depths, hydrothermal fluids having approximately this salinity and temperatures of ≥300°C will boil in the subsurface (Bischoff and Rosenbauer, 1987) and will not precipitate Cu-rich massive sulfides on or near the sea floor. Although 850 m is much shallower than the ~3.8-km average depth of the modern ocean, it is far deeper than the approximate 200-m base of modern photic zones and is below the 600-m sea-floor depth that characterizes the edge of continental margins.

Several precautions must be taken when using exhalites as proxies for the redox state of ancient deep seawater. First, exhalites must be spatially linked to relatively Cu rich VMS deposits (Slack et al., 2007), because Cu-poor, Zn- and Pb-rich mineralization on the sea floor can form at shallow depths of 100 to 500 m, based on elevated solubilities of Zn and Pb in chloride complexes of VMS hydrothermal fluids at temperatures of 150° to 200°C (Large, 1992; Hannington et al., 1995). Exhalites related to sediment-hosted, stratiform Zn-Pb deposits (Leach et al., 2005) similarly are not meaningful in this context, as this deposit type chiefly forms in restricted basins that lack communication with the global ocean (Slack et al., 2007). Second, the exhalites must occur at or near the

stratigraphic level of the Cu-rich VMS deposit to ensure that they formed from the same hydrothermal system and not as separate systems that existed during periods of different water depths. Third, exhalites must be laterally extensive for >100 m along strike, in order to reflect precipitation from hydrothermal fluids that mixed with bottom waters near a vent or in a hydrothermal plume, as in modern VMS systems (German and Von Damm, 2004); smaller occurrences of isolated exhalites that lack stratigraphic continuity were probably deposited from diffuse, low-temperature (<50°C) fluids (Hein et al., 1999; Koschinsky et al., 2002) that may not record the redox state of coeval deep seawater. Fourth, it is important to exclude from consideration magnetite-rich lenses that formed by subsea-floor replacement and not as true exhalites, such as in the Gossan Hill VMS deposit in Western Australia (Sharpe and Gemmell, 2002), possibly as a result of nonredox transformations by hydrothermal fluids beneath the sea floor (Ohmoto, 2003) or by phase separation into vapor and brine in hydrothermal system (cf. Foustoukos and Bekker, 2008). Similarly, magnetite-rich zones in epigenetic iron oxide-copper-gold (IOCG) deposits that formed in continental, rather than submarine settings (Williams et al., 2005) should also be excluded from this analysis. Finally, care must be taken to ensure that the observed mineralogy and geochemistry of the exhalites reflect primary depositional conditions and not effects of later alteration, diagenesis, metamorphism, or weathering (Slack et al., 2009).

Appendix 2 lists mineralogical and geochronological data for 45 exhalites related to Precambrian Cu-rich VMS deposits worldwide. This compilation, updated from that in Slack and Cannon (2009, table DR2), reveals a secular pattern in which exhalites older than ca. 1.85 Ga mostly consist of sulfidic shales, barren sulfides, pyritic chert, or pyritic tuff, whereas those younger than ca. 1.85 Ga mainly contain iron oxide varieties such as jasper, hematite iron formation, or magnetite iron formation (Fig. 12). Archean and early Paleoproterozoic reduced-facies exhalites suggest deposition under anoxic and possibly sulfidic bottom waters based on geochemical and thermodynamic arguments (Huston and Logan, 2004; Ohmoto et al., 2006).

The late Paleoproterozoic marks a fundamental shift in the nature of VMS-related exhalites, recording a protracted period during which oxide-facies varieties were deposited episodically in 1.84 to 1.70 Ga volcanic and volcano-sedimentary sequences. The presence of abundant hematite or magnetite within these exhalites and their high Fe(III)/Fe(II) ratios rule out sulfidic bottom waters during mineralization, requiring at least suboxic conditions (<5 μM O_2) in coeval deep seawater (Slack et al., 2007). For hematite-rich exhalites such as jasper or iron formation, protoliths are interpreted to be amorphous ferric oxyhydroxides, based on analogy with precipitates from modern sea-floor hydrothermal vents and plumes (Grenne and Slack, 2005; Slack et al., 2007). Magnetite in ancient exhalites could reflect precursors of mixed ferrous-ferric "green rust" compounds such as $Fe(OH)_2$ that formed in anoxic seawater (Murray, 1979). However, these precursors are considered unlikely because Archean and Paleoproterozoic seawater, as well as diagenetic pore fluids, probably were saturated in $FeCO_3$ before saturation in $Fe(OH)_2$ was reached, owing to high atmospheric pCO_2 during this time period and resulting bicarbonate saturation in coeval seawater (Slack et al., 2009, and references therein). Geochemical data for REE in late Paleoproterozoic hematite- and magnetite-rich exhalites show small negative to small positive Ce anomalies based on shale normalization, in contrast to the larger negative Ce anomalies that characterize modern oxyhydroxide deposits, thereby also ruling out fully oxic conditions for deep seawater during VMS and related exhalite mineralization (Slack et al., 2007, 2009).

During the Mesoproterozoic (1.60–0.9 Ga), VMS mineralization decreased substantially in magnitude compared to the late Paleoproterozoic (Fig. 12). Some Cu-rich deposits within this time period are known, several of which have related exhalite units (App. 2) that range in age from 1395 to ca. 1000 Ma. Deposition of similar oxide-facies exhalites continued during the Neoproterozoic, producing jasper, magnetite iron formation, and hematite iron formation at or near several VMS deposits ca. 900 to 600 Ma.

Some exceptions exist to the pattern of sulfidic exhalites genetically linked to Archean and early Paleoproterozoic Cu-rich VMS deposits (Fig. 12; App. 2). These include magnetite iron formation, hematite iron formation, and jasper at the following deposits: 2960 Ma Scuddles, Western Australia; 2720 Ma Geco and Willroy, Ontario; ca. 2530 Ma Wutai, Shanxi Province, China; and ca. 1870 Ma Bend and Eisenbrey, Wisconsin. The presence of abundant Fe(III) in hematite or magnetite within these >1850 Ma deposits might reflect the following processes (Slack and Cannon, 2009): (1) deposition from S-poor seawater (Huston and Logan, 2004), (2) hydrothermal plumes that rose above the chemocline (Ohmoto et al., 2006), (3) phase separation during boiling of the hydrothermal fluids (Foustoukos and Bekker, 2008), (4) deposition during a transitory period in deep-ocean oxidation, and (5) deposition within a local oxygenated basin.

The lack of Cu-rich VMS deposits during some periods of Earth history precludes use of exhalites for evaluating the redox state of coeval deep oceans. For example, several VMS deposits have been documented in sequences >3000 Ma, including the oldest 3465 Ma deposits at Big Stubby and Lennons Find in the Pilbara craton of Western Australia, but these deposits contain abundant Zn and Pb, with little or no elevated Cu contents (Huston et al., 2002; Franklin et al., 2005, App. 1). The oldest Cu-rich VMS deposit with a genetically linked exhalite unit is the 2.97 Ga Miranda deposit in South Africa (Slack and Cannon, 2009, table DR2). Noteworthy is a major gap of ~620 m.y. in exhalite data from ca. 2530 until 1910 Ma, during which 16 VMS deposits are known (Franklin et al., 2005, App. 1), but none has a reported exhalite. Other major gaps in the record of Precambrian deep-marine exhalite mineralization of this type are ca. 1700 to 1400 and ca. 1000 to 770 Ma (App. 2).

Exhalites related to stratiform Pb-Zn deposits in predominantly metasedimentary sequences provide insights into redox conditions within restricted shallow-marine settings. Proterozoic deposits of this type formed by synsedimentary processes within intracratonic rift basins (e.g., Leach et al., 2005). Some stratiform Pb-Zn deposits of late Paleoproterozoic or Mesoproterozoic age contain exhalites, including magnetite iron formation, within the mineralized sequences or along strike from the orebodies. Examples of such magnetite

iron formations are at the large Dariba Zn-Pb-Ag deposit (ca. 1800 Ma) in the Bhilwara belt of Rajasthan, India (Deb and Pal, 2004; Deb and Thorpe, 2004), the giant ca. 1685 Ma Broken Hill Pb-Zn-Ag deposit in New South Wales, Australia (Lottermoser, 1989; Page et al., 2005), and the large ca. 1200 Ma Aggeneys and Gamsberg Pb-Zn-Ag deposits in Namaqua Province, South Africa (Stalder and Rozendaal, 2004; Cornell et al., 2009). Magnetite iron formation also occurs regionally in strata broadly correlative with the host rocks to some of these Pb-Zn deposits, such as in the Bhilwara belt in Rajasthan (Deb and Pal, 2004), the Broken Hill Group in the Broken Hill district, New South Wales (Barnes, 1988), and the Soldiers Cap Group that hosts the large ca. 1675 Ma Cannington Ag-Pb-Zn deposit in Queensland (Giles and Nutman, 2003; Hatton and Davidson, 2004). Settings of the deposits and iron formations range from siliciclastic-volcanic basin (Broken Hill), to siliciclastic-volcanic slope and platform (Bhilwara belt, Soldiers Cap Group), to wholly siliciclastic platform (Aggeneys, Gamsberg). Although water depths during formation of Pb-Zn and Fe oxide mineralization in these deposits are poorly constrained, probable ferric oxyhydroxide protolith to the magnetite (Slack et al., 2009) indicates that the depositional site for this protolith was at least minimally oxygenated (e.g., suboxic) in order to allow precipitation of abundant ferric iron from seawater (e.g., Slack et al., 2007). Broken Hill is a proximal deposit with an inferred feeder zone (Groves et al., 2008) that focused hydrothermal fluids onto the sea floor. Hence, the bottom waters there during Pb-Zn and Fe oxide mineralization were probably oxic or suboxic, not anoxic or sulfidic. The other deposits, however, lack documented feeder zones, such that the hydrothermal vent sources for Pb and Zn in the sulfide ores and for Fe in the iron formations could have existed far from each other and from the sites of mineralization. This scenario raises the possibility that the bottom waters surrounding the unidentified vents in the Bhilwara, Namaqua, and Queensland sequences were anoxic, providing a means for transporting dissolved ferrous iron to shallower oxic settings for ferric oxyhydroxide precipitation. Regardless, oxide-dominated iron formations within these intracratonic rift basins at ca. 1800, 1685, 1675, and 1200 Ma suggest that the local bottom waters were not sulfidic, as implied by the model of Canfield (1998), otherwise iron in the exhalites would reside mainly in iron sulfides.

Secular patterns in sedimentary iron deposits

To evaluate the possibility of a secular pattern in sedimentary iron deposits, we divide Earth history into time intervals based on different ocean and atmosphere redox states. The following discussion begins with the modern iron cycle and progress backwards to the Paleoarchean.

Modern iron-rich sediments

Highly oxidizing conditions in modern seawater limit dissolved iron content to ~0.02 to 2 nM (avg 0.5 nM; Bruland and Lohan, 2006). Although most base metals and iron released from hydrothermal vents at mid-ocean ridges and in back-arc systems are deposited in black and white smokers at or immediately above the water-sediment interface, some iron and most manganese disperse via hydrothermal plumes as far as hundreds of kilometers before deposition (e.g., German and Von Damm, 2004). Several deeps in the ca. 6 Ma Red Sea contain hot, anoxic stratified brines derived from rift-hosted hydrothermal systems. Metalliferous sediments containing iron oxides, silicates, sulfides, and carbonates precipitate from these brines (Taitel-Goldman and Singer, 2002). Interestingly, whereas the deep-water brine deposits are dominated by hydrothermal signals, shallow-water deposits of the Shaban deep have Sr, Nd, and REE patterns dominated by a seawater signal (Cocherie et al., 1994).

Modern shallow-water iron-rich sediments are restricted to areas strongly affected by hydrothermal circulation related to active volcanism, such as within Santorini caldera in the Aegean Sea, where biologically mediated, hydrated ferric oxide gels and opaline silica precipitate (Puchelt, 1973; Hanert, 2002), and in Lake Malawi, eastern Africa, where nontronite mud and pellets and limonite with opal oolites are forming (Müller and Förstner, 1973). Significantly, modern analogues of banded silica- and iron-rich iron formations are seemingly unknown, although evidence presented above questions whether there was a depositional rhythmicity to silica and iron banding. Accordingly, we are left to speculate on what comprised the primary compositional structure of BIFs. However, iron ooids and pisoids composed of iron oxides and hydroxides admixed with amorphous silica, with andesitic rock fragments in the center, were described from offshore Mahengetang, Indonesia, in the photic zone (Heikoop et al., 1996), and these could well be modern analogues of GIF. Iron-silicate ooids and peloids were found from Cape Mala Pascua to El Fraile Point, Venezuela, in shallow (~35–40-m depth) waters in an exhalative system connected to ultramafic rocks and transform fault zones (Kimberley, 1994). Iron- and silica-bearing oolites also occur in the bottom sediments of Lake Chad, West Africa, off the Chari delta (Lemoalle and Dupont, 1973).

Low-temperature Si- and Fe-rich hydrothermal deposits generally form in areas of active venting along mid-ocean ridge axes (Corliss et al., 1978; Mills, 1995), at off-axis seamounts (Alt, 1988) or hot-spot and arc and/or back-arc submarine volcanoes (e.g., De Carlo et al., 1983). Such vent deposits do not generally form laterally extensive and thick Fe-Si–rich deposits similar to iron formations. Nevertheless, relatively thick Fe-Si rich hydrothermal deposits have been documented in the recent rock record. For example, silica- and iron-rich deposits as much as 20 m thick have been reported at ODP Site 801 within Jurassic oceanic crust in the western Pacific (Alt et al., 1992; Rouxel et al., 2003), and fossil hydrothermal Si-Fe deposits, with umber, jasper, and iron formation, have been reported in ophiolites as old as 490 Ma (Little et al., 2004).

Phanerozoic ironstones, anoxic events, and VMS deposits

Deposition of Phanerozoic ironstones was mainly restricted to the Ordovician-Devonian and Jurassic-Paleogene, with prominent peaks occurring during the Devonian and Jurassic (Fig. 13). These ironstones are generally up to 2 m thick, although rarely reach 20 m in thickness, and extend for >1,000 km along ancient continental margins in Fennoscandia and the Himalayas, where they demarcate areas of past upwelling (e.g., Garzani, 1993; Sturesson, 2003). Until 1945, Phanerozoic ironstones were important sources of iron in the world

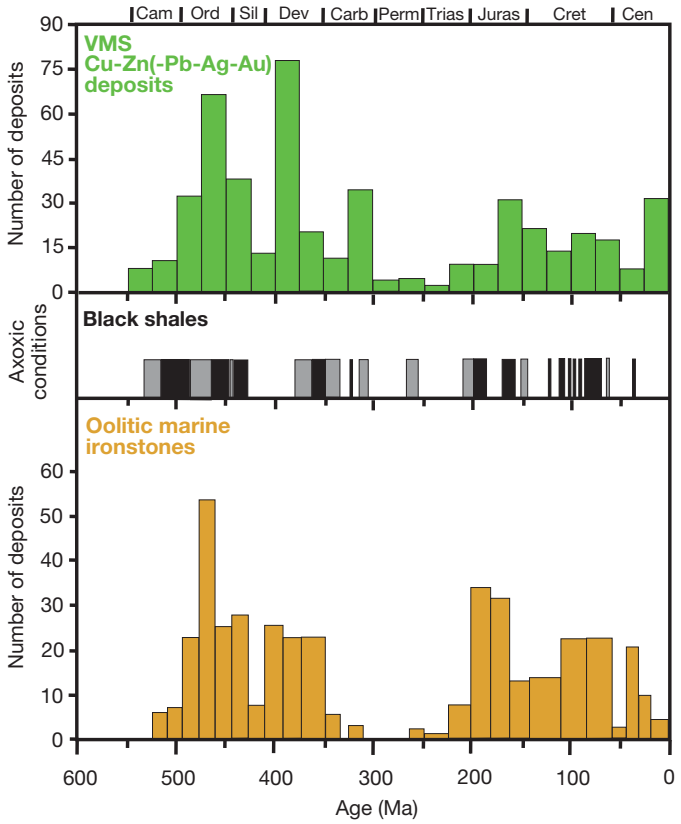

FIG. 13. Secular distribution of Phanerozoic oolitic marine ironstones compared to those of marine anoxic conditions and VMS deposits. Secular trend for ironstones is from Petránek and Van Houten (1997). Data for VMS deposits are from Franklin et al. (2005, App. A2), compiled for time intervals of 25 m.y. Marine anoxic conditions are shown for inferred global periods of anoxia (black bars) and more limited periods of anoxia (gray bars); the latter reflecting less-widespread, regional black shale facies. Data for anoxic conditions during Cambrian through Jurassic periods are from Arthur and Sageman (1994), for Cretaceous from Leckie et al. (2002), and for Cenozoic from Jacobs and Lindberg (1998).

economy (Maynard and Van Houten, 1992). Phanerozoic ironstones contain iron oolites composed of Fe oxyhydroxides (goethite and limonite), Fe silicates (chamosite and berthierite), and minor amounts of amorphous SiO_2. Typically, bulk analyses of Ordovician iron oolites, when normalized to shale composites or local shale, have minor negative to positive Ce anomalies, are enriched in light REEs with respect to heavy REEs, and carry no significant Eu anomalies (e.g., Sturesson, 2003). Ironstones are linked to time intervals with negative seawater Sr isotope excursions (Sturesson, 2003), peaks in formation of VMS deposits (Peter, 2003; Franklin et al., 2005), initial stages of sea-level rise as suggested by their position in Transgressive System Track deposits above hardgrounds (Fig. 6B; Maynard and Van Houten, 1992; Burkhalter, 1995; Taylor et al., 2002), major anoxic events, volcanic events, and quiescences in Earth's magnetic field, and are enriched in apatite or facies equivalents to sedimentary phosphorites (van Houten and Arthur, 1989; Garzani, 1993). Collectively, these associations were linked with superplume events (e.g., Garzani, 1993). Furthermore, ironstones are linked to time periods when seawater was saturated with Mg calcite, rather than with aragonite, and so-called "calcite seas" developed, which correspond with times of rapid sea-floor spreading and greenhouse conditions (Maynard, 1986; Stanley and Hardie, 1998). The formation of berthierite in shallow-water, well-agitated marine environments requires reducing conditions, yet iron sulfides rather than iron silicates would be expected under anoxic and euxinic conditions. However, berthierite and hematite ooids cooccur in ironstones, these minerals even form discrete laminae within individual ooids, indicating fluctuating redox conditions either during deposition or early diagenesis, but before compaction. In addition, glauconite, an abundant sedimentary aluminosilicate mineral with Fe(III) substituting for Al(III), is virtually entirely absent in oolitic ironstones (Maynard, 1986), also suggesting a low redox state in the water column during their deposition (cf. Taylor et al., 2002).

The genesis as well as the iron source for Phanerozoic ironstone deposits remains controversial. Extreme degrees of weathering on continents linked with high sea-level stands during dispersion of supercontinents were inferred by Van Houten and Arthur (1989). However, neither sea-level highstand nor supercontinent dispersal seems to be a necessary condition for deposition of Phanerozoic ironstones (Van Houten, 1985). An alternative model relates ironstones to submarine weathering of volcanic ash (e.g., Sturesson, 2003), although many ironstone units do not contain volcanic ash beds. Reworking of pedogenic ferruginous pisoids into the marine environment has been also suggested but does not explain their restricted stratigraphical position, low Al content in goethitic and hematitic oolites (e.g., Maynard, 1986), or $\varepsilon Nd_{(t)}$ values above those of proximal crustal sources (Sturesson et al., 1999). Aller et al. (1986) proposed a different model for ironstone deposition based on modern Amazon deltaic sediments, invoking high amounts of organic matter loading, anoxia at the sediment-water interface, and intense physical reworking that promoted reoxidation of iron. These features in the Amazon allow for significant burial of reactive iron phases, such as ferric and mixed-valence authigenic iron minerals, despite abundant dissolved sulfate (Aller et al., 1986). The depositional scenario proposed by Aller et al. (1986) is consistent with depositional settings of ironstones but does not explain their episodic secular distribution or much more pronounced iron enrichments in ironstones relative to those in Amazon deltaic sediments. Therefore, the mechanism described by Aller et al. (1986) does not fully explain the genesis of ironstones.

Broad correspondence of the secular distribution of Phanerozoic ironstones and VMS deposits (Fig. 13) offers additional insights into the formation of ironstones and suggests that the iron for ironstone deposition originated in coeval sea-floor hydrothermal systems. In this model, formation of Phanerozoic ironstones is mechanistically linked to times of global ocean anoxia during mantle superplume events. Enhanced hydrothermal activity led to extensive formation of VMS deposits and also contributed to short-term, ocean-wide anoxia and lower seawater sulfate contents. Under anoxic and low seawater sulfate conditions, hydrothermal and diagenetic iron could have been transported by upwelling currents, together with phosphorous and manganese, onto the shelf, where the iron was oxidized biologically or abiologically at a shallow-water dynamic redoxcline. Indeed, low seawater sulfate content during Phanerozoic anoxic events was inferred

from sulfur isotope composition of VMS deposits (Eastoe and Gustin, 1996) and during Cretaceous anoxic events from fluid inclusion data (Timofeeff et al., 2006). Cretaceous anoxic events have been also genetically linked to extensive submarine magmatism based on geochemical evidence (Turgeon and Creaser, 2008) and geologic argument (Sinton and Duncan, 1997; Kerr, 1998). This model implies that hydrothermal iron was transported due to a temporary crash in the size of the seawater sulfate reservoir that prevented formation of significant amounts of sulfide under anoxic conditions. An alternative complimentary to this model is that during times of widespread anoxic conditions, sulfide formation in the deep oceans was limited by organic matter availability, which may have also allowed for iron transport onto the continental shelves while seawater sulfate contents remained at decreased but sufficiently high levels.

Neoproterozoic manganese deposits and iron formations

Manganese deposits and iron formations of Neoproterozoic age are locally developed in association with glacial deposits, whereas iron-rich shales are relatively common in contemporaneous glacially influenced successions (e.g., Young, 2002). The latter relationship was reemphasized by Canfield et al. (2008) to infer a return to Archean anoxic, ferruginous ocean conditions during the late Neoproterozoic. Neoproterozoic iron and manganese deposits are present in the (1) MacKenzie and Ogilvie Mountains of North America (see Figs. 1, 14; Young, 1976; Klein and Beukes, 1993a, b), (2) Urucum district of Brazil (Urban et al., 1992; Trompette et al., 1998; Klein and Ladeira, 2004), (3) Serrania de Mutun in Bolivia (Trompette et al., 1998), (4) southeastern Uruguay (Pecoits et al., 2008), (5) Damara orogen of Namibia (Breitkopf, 1988; Bühn et al., 1992), (6) Adelaide geosyncline of South Australia (Lottermoser and Ashley, 1999), (7) middle Tian-Shan in Kazakhstan, Kyrgyzstan (Zubtsov, 1972), (8) Malyi Khingan in the southern part of the Russian Far East, and (9) Erzin basin in Tuva, Russia, and in adjacent Mongolia (Ilyin, 2009).

Presently available geochronologic constraints and stratigraphic correlations imply that Sturtian and Marinoan glaciations are at least temporally related to the deposition of iron

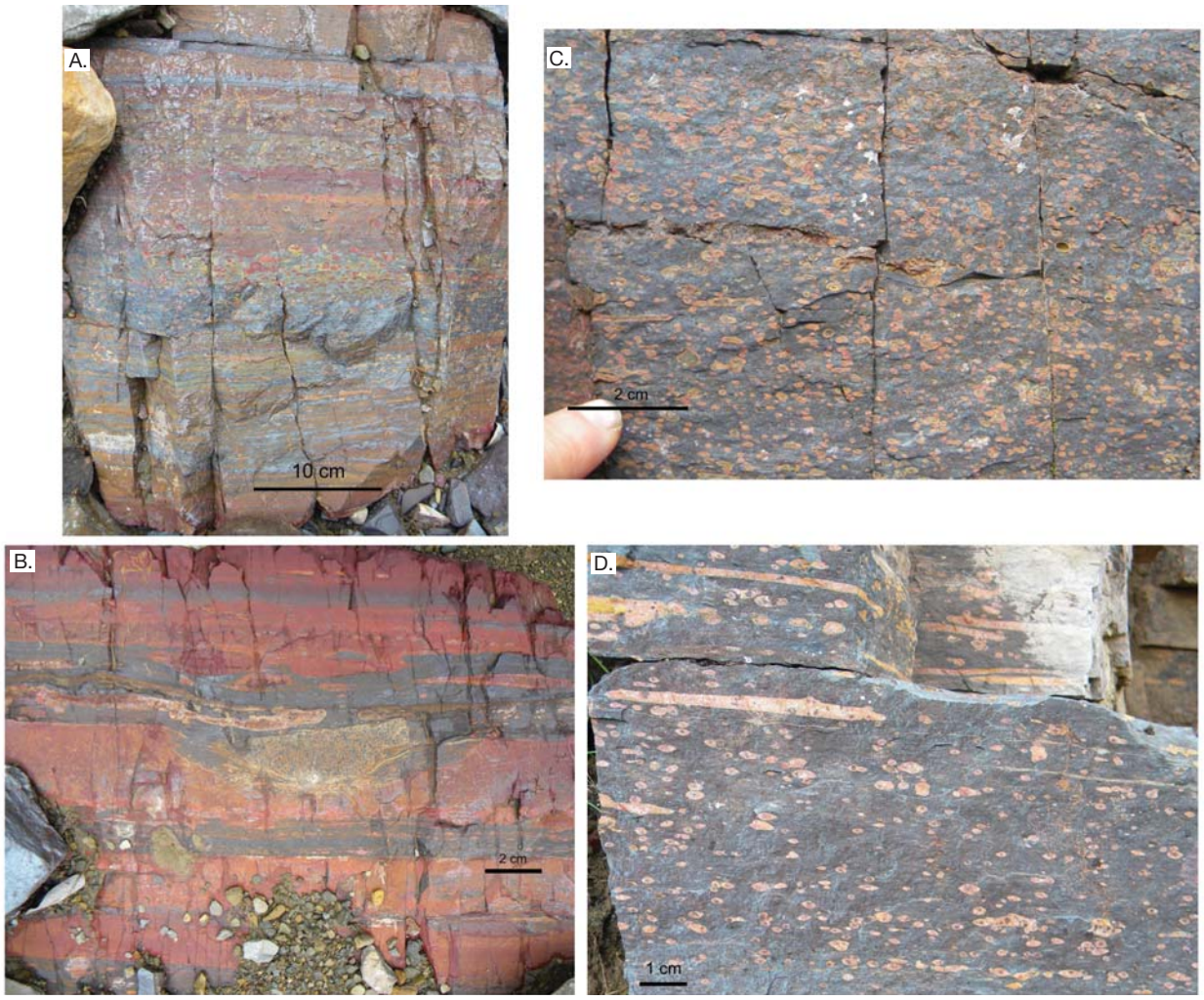

FIG. 14. Rapitan Iron Formation at Cranswick River, Mackenzie Mountains, Northwestern Territories, Canada. A. Nodular and banded jasper interlayered with hematite bands and overprinted by anastomosing hematite. B. Jasper nodules in massive hematite. C. Banded jasper-hematite iron formation with dropstone overprinted by anastomosing hematite. D. Jasper nodules in massive hematite.

formations, although some uncertainty exists about their ages and chemostratigraphically based correlations (e.g., Kendall et al., 2009). The Rapitan Iron Formation and Franklin igneous event on Victoria Island in Canada are ca. 715 Ma (MacDonald et al., 2010), supporting a genetic relationship between mantle processes and deposition of iron formation as discussed above at least on the basin scale. Highly positive sulfur isotope values in shales and manganese formations overlying Neoproterozoic glacial diamictites were explained by the Rayleigh distillation process in the world ocean with low sulfate content, which was therefore highly susceptible to development of anoxic ferruginous conditions and hydrothermal delivery of iron and manganese into shallow basins during mantle plume breakout events (Liu et al., 2006). Importantly, iron formations were deposited during, rather than after, glacial events, as indicated by dropstones in iron formations and interlayering with tillites. Generally poor age constraints for other Neoproterozoic iron formations do not warrant correlation with Neoproterozoic plume events, but there were several mantle plume events during the late Neoproterozoic (e.g., Ernst and Buchan, 2001). Each of the Neoproterozoic iron formations is, however, spatially and temporally linked with submarine mafic volcanic units. Some basins containing Neoproterozoic iron formations also contain VMS deposits of the same age (e.g., Bühn et al., 1992), suggesting a local hydrothermal iron source. Most of the iron formations were deposited in either closed rift basins or on reactivated continental margins (Trompette et al., 1998).

The iron formations generally comprise laminated and nodular hematite, magnetite, hematitic mudstone, and jasper (Fig. 14). Lenticular and nodular chert and jasper are less common but are present within laminated jasper beds (Yeo, 1981). Bedded cherts, similar to those in Archean and Palaeoproterozoic iron formations, are not present. Furthermore, thicknesses of Neoproterozoic iron formations are highly variable over relatively short distances. A GIF and intraformational conglomerates containing hematite pebbles developed locally at the top of the Rapitan Iron Formation and in the Jacadigo Group, Brazil (Klein and Beukes, 1993a; Klein and Ladeira, 2004). The REE patterns for the Neoproterozoic iron formations have no or slightly positive Eu anomalies and no or slightly negative Ce anomalies (Fryer, 1976; Derry and Jacobsen, 1990; Klein and Beukes, 1993a; Lottermoser and Ashley, 1999; Klein and Ladeira, 2004; Liu et al., 2006), indicating a high degree of dilution of locally derived hydrothermal fluid by mildly oxidized seawater, within isolated to semi-isolated basins. Models that are generally accepted for Phanerozoic manganese deposits (e.g., Maynard, 2003) are, therefore, probably also applicable to the origin of Neoproterozoic iron formations. These models infer anoxic conditions in the deeper parts of the isolated to semi-isolated basins with enhanced submarine volcanism and manganese precipitation at the redox boundary on the shallow margins of the basins.

The Neoproterozoic iron formations are notably enriched in phosphorus relative to older iron formations (e.g., Yeo, 1981; Breitkopf, 1988; Klein and Beukes, 1993a). Although seawater phosphorus content may have been higher during the Neoproterozoic than ever before, as also reflected by sedimentary phosphorite deposits of this age, another factor could be a decrease in seawater silica content with respect to Archean and Paleoproterozoic levels (cf. Planavsky et al., in revision) because high seawater silica concentrations impede phosphorus coprecipitation with iron oxyhydroxides as discussed above. Recent discoveries of >740 Ma siliceous microfossils (Porter et al., 2003) imply that a biological sink for silica may have developed during the late Neoproterozoic, which led to a higher efficiency of phosphorus scavenging on ferric oxyhydroxide protoliths to the iron formations.

Proterozoic age gap in major iron-formation deposition

It is generally assumed that after ca. 1.85 Ga, Superior-type iron formations were not deposited for approximately 1.1 b.y. (Isley and Abbott, 1999; Huston and Logan, 2004; Slack and Cannon, 2009). Large deposits during this age gap (1.85–0.75 Ga) are indeed absent, with one notable exception, but several small iron formations and iron-rich lithologic units in sedimentary rock-dominated successions are known. Magnetite and siderite iron formations of the Aok Formation in the Neoproterozoic Shaler Supergroup in the Duke of York and Brock inliers of Victoria Island, Canada, for example, were deposited before the oldest of the Neoproterozoic glacial events at ca. 840 Ma (Rainbird et al., 1994). Older examples within this age gap include the ca. 1.70 Ga Freedom Formation of the Lower Baraboo Series, Wisconsin, which contains in the lower part banded ferruginous chert interlayered with sideritic and kaolinitic slate that has a variable thickness from 60 to 160 m (Weidman, 1904; Leith, 1935; Van Wyck and Norman, 2004) and the likely correlative magnetite-chert iron formation of the Tomiko terrane in Ontario (Easton, 2005). Additionally, the Chuanlinggou Iron Formation in the North China craton, a classic GIF deposit, also appears to be latest Paleoproterozoic (ca. 1.7 Ga; Wan et al., 2003; Dai et al., 2004).

Noteworthy examples of anomalous and small deposits formed during this time gap in northern Australia are the Sherwin Formation and the Munyi Member of the Corcoran Formation, both from the ca. 1.49 Ga Maiwok Subgroup of the Roper basin, Northern Territory (Canavan, 1965; Abbott and Sweet, 2000) and the correlative Constance Range ironstone deposits of the Train Range Member of the Mullera Formation in the South Nicholson basin of Queensland (Harms, 1965). These units consist of ooidal, pisolitic, and peloidal, trough cross-stratified ironstone and ferruginous siliciclastic rocks as much as 23 m thick (Harms, 1965; Abbott and Sweet, 2000). Unweathered samples show grapestones, and ooids as much as 8 mm in diameter (Fig. 4D), with nucleii of quartz or oolitic intraclasts that are composed of hematite and magnetite, although chamosite and greenalite are locally present in a secondary siderite matrix (Abbott and Sweet, 2000). Beds within the ironstone horizons are bounded by erosional surfaces, with sharp compositional contrast between ooidal ironstones and overlying quartz-rich sandstones. The presence of intraclasts and pelloids of iron-rich sediment in quartz-rich sandstone and clasts of ironstone in intraformational conglomerate (Fig. 4B, C) strongly suggests that the sediments were originally iron rich. Many large ironstone intraclasts have a pisolitic coating, testifying to the primary deposition of goethite in the sedimentary environment. The ooids and pelloids formed in an oxidized environment when little or no siliciclastic sediment was introduced. Notably, the

Sherwin Formation and the Munyi Member of the Corcoran Formation enclose black shales of the Velkerri Formation that were used previously to infer a long-term sulfidic state of the coeval deep ocean (Shen et al., 2003; Arnold et al., 2004), based on sulfur isotope composition, iron mineral speciation, and molybdenum isotope composition. Leaving aside whether all available geochemical and geological evidence for the ocean redox state during the Mesoproterozoic is consistent, in general, with the notion of a persistently euxinic deep ocean (e.g., Slack et al., 2007, 2009; Meyer and Kump, 2008), this intricate relationship between ironstones and euxinic black shales strongly suggests that ferruginous and euxinic conditions alternated in the Mesoproterozoic intracontinental Roper and South Nicholson basins on geologically short-time scales.

An important exception to these relatively small iron deposits is the <1.84 Ga Frere Formation in the Earaheedy basin, Western Australia (Goode et al., 1983; Bunting, 1986), which contains a huge tonnage of iron in GIF deposits (App. 1), albeit not in an open-marine basin (Krapež and Martin, 1999). Although economically unimportant at present, the existence of this and other late Paleoproterozoic iron deposits suggest that from ca. 1.84 to 1.45 Ga hydrothermal iron from deep-water oceanic settings was episodically delivered, although in rare cases and in generally small amounts, to shallow-water environments for the deposition of iron formation, ironstone, or iron-rich shale.

Ca. 1.93 to 1.85 Ga iron formations coeval with large VMS deposits

Extensive large iron formations appear after an approximately 500-m.y. gap, at about 1.88 Ga. These are predominantly GIFs and are common in North America, at the margins of the Superior craton (Simonson, 2003), and are coeval with a ca. 1.88 Ga ultramafic LIP (Heaman et al., 1986, 2009; Hulbert et al., 2005), which is potentially related to a mantle plume breakout event (Hamilton et al., 2009; see for a different view Heaman et al., 2009). Recognized now to be correlative based on high-precision geochronology (Findlay et al., 1995; Fralick et al., 2002; Schneider et al., 2002), these iron formations extend discontinuously for more than 3,000 km along the southern and eastern margins of the Superior craton, from Thunder Bay, Ontario, through Minnesota, Wisconsin, and Michigan, to Quebec (Mistassini basin) and to the Labrador trough. Correlative and texturally similar GIFs are also recognized along the western margin of the Superior craton in the Hudson Bay region (Chandler, 1984; Hamilton et al., 2009). All of these iron formations are considered to have been deposited in extensional basins with coeval submarine basaltic volcanism (Ricketts et al., 1982; Fralick et al., 2002; Schulz and Cannon, 2007). A back-arc setting for the iron formations has been proposed by these workers, whereas a foreland basin setting was earlier preferred (Hoffman, 1987; Ojakangas et al., 2001; Schneider et al., 2002). An intriguing and not fully answered question is whether deposition of these iron formations represents local, basin-scale conditions or the composition and redox state of the global ocean. This is an important issue because the occurrence and ages of these iron formations have been used by some workers to infer deep-water anoxic conditions in the coeval global ocean (e.g., Poulton et al., 2004; Slack and Cannon, 2009); if these iron formations reflect more restricted, basin-scale conditions, our understanding of the ocean redox state might be incorrect. Paleogeographic reconstructions are not detailed enough to answer this question; however, tidal signatures have been observed in iron formations and interbedded sedimentary rocks in Minnesota and the Hudson Bay region (Ojakangas, 1983; Chandler, 1984), which are consistent with at least periodic open-marine conditions during iron deposition. Two independent approaches can be used to address this issue. First, do sedimentary successions on the margins of other cratons that have similar ages and had low supply of siliciclastic sediments provide evidence for high concentrations of iron in seawater? Second, do iron oxide exhalites exist in coeval, deep-water, Cu-rich VMS deposits?

Iron formation of the 1.88 Ga Rochford Formation on the eastern margin of the Wyoming craton, a separate entity from the Superior craton during its deposition, although poorly dated and not granular (e.g., Frei et al., 2008), supports deposition of iron formations synchronously on several cratons. In contrast, the precisely dated (1882 ± 3.5 Ma) lower part of the Recluse Group in the Kilohigok basin on the Slave craton, northwestern Canada, lacks evidence for deposition of iron formation (Bowring and Grotzinger, 1992). Instead, organic matter-rich and sulfidic shales are present at this stratigraphic level (Bowring and Grotzinger, 1992). The study of iron mineral speciation and sulfur isotope systematics of these shales is needed to constrain whether the absence of iron formation reflects deposition below the redoxcline or if euxinic conditions prevailed in the open deep ocean during iron deposition in the Animikie basin. Considering the uncertainty in the age of the Rochford Formation, and also the role of upwelling in determining the depositional site of iron formation (e.g., Abbott and Isley, 2001, 2002), this test would unequivocally address the issue.

Deposition of iron formations surrounding the Superior craton is coeval with a peak in tonnages of VMS deposits (Fig. 12), some of which were positioned in arcs adjacent to the craton. The ca. 1.88 Ga VMS deposits are known in the hinterland to the south of the Animikie basin (Schulz and Cannon, 2007), in the Labrador trough (Barrett et al., 1988b), and in the Trans-Hudson orogen (Syme and Bailes, 1993). Recent geochronological studies of the host metavolcanic rocks to VMS deposits in the Pembine-Wausau terrane of northern Wisconsin indicate that these deposits formed at ca. 1875 Ma contemporaneously with GIFs of the Animikie basin (Schulz and Cannon, 2008). These data also suggest that the VMS systems were likely the source of iron for iron formations, consistent with earlier models (e.g., Isley, 1995). Iron oxide exhalites are conspicuously absent at or near these deep-water VMS deposits that formed presumably in open-marine conditions. This observation is unlikely to reflect preservational bias, because slightly younger 1.84, 1.79, and 1.78 Ga Cu-rich VMS deposits that similarly formed in arc settings contain abundant hematite or magnetite exhalites (Slack et al., 2007, Table 2; Slack and Cannon, 2009, table DR2). Although presently inconclusive, this analysis points toward an anoxic ferruginous composition of deep waters in open-marine settings during the time period of ca. 1.93 to 1.88 Ga. In addition, both of these approaches provide a valuable perspective for addressing the composition and redox state of ancient deep seawater and warrant further study.

The Animikie basin of the Lake Superior region also contains another stratigraphic level with regionally extensive iron formations. This level is stratigraphically above the 1850 Ma Sudbury impact ejecta layer and is older than the ca. 1830 Ma regional metamorphic event related to the Penokean orogeny (Cannon et al., 2010). These iron formations are mineralogically and texturally different from the ca. 1880 Ma iron formations of the Animikie basin and were likely deposited in deeperwater, below fair-weather and, probably, storm wave base settings. They are present in the: (1) Marquette Iron Range, Michigan (~60-m-thick Bijiki Iron-Formation Member of the Michigamme Slate containing siderite, chert, iron oxides, and silicates; Ojakangas, 1994; Ojakangas et al., 2001; Cannon et al., 2010), (2) Iron River-Crystal Falls Iron Ranges (~15-m-thick chert-siderite slate of the Stambaugh Formation; James et al., 1968), (3) Gogebic Iron Range, Wisconsin (~47-m-thick iron formation of the Tyler Formation consisting of chert and siderite; Schmidt, 1980; Cannon et al., 2008), and (4) Mesabi Iron Range, Minnesota (~27-m-thick chert-siderite iron formation in the lower part of the Virginia Formation; Lucente and Morey, 1983). Deposition of these iron formations might be genetically related to submarine mafic volcanism in the Animikie basin based on spatial association with, for example, the Badwater Greenstone, but this relationship has not been documented in detail. The iron formations are commonly interbedded with, or overlain by, black sulfidic shales, which likely record the development of euxinic conditions in the Animikie basin (cf. Poulton et al., 2004). Despite poor exposure and limited economic interest, these iron deposits are easily tracable by magnetic anomalies. Their deposition indicates that anoxic and ferruginous seawater redox conditions were reestablished in the Animikie basin after 1850 Ma, in association with mafic volcanism, although evidence for a shallow redoxcline, in this case, is absent and the duration of these conditions was likely short.

Thinly banded, silicate-facies iron formation of similar age, or slightly older, is present in the Pipe Formation of the Thompson nickel belt, Manitoba (Bleeker and Macek, 1996). Also, a 15-m-thick banded chert-magnetite-amphibole, ca. 1905 Ma iron formation is present in the La Ronge-Lynn Lake belt, Saskatchewan (Corrigan et al., 1999). Notably, a ~20-m-thick magnetite-hematite oolitic iron formation is present in the middle member of the Watterson Formation (Hurwitz Group) on the Hearne craton (Miller and Reading, 1993). The age of this oolitic unit is not well constrained, but ages of detrital zircons in the Hurwitz Group suggest it is ca. 1.93 Ga (Davis et al., 2005) and most likely older than the 1.88 Ga iron formations on the margins of the Superior craton.

Iron formations deposited after the GOE and before ca. 1.93 Ga

Giant iron formations (≥10,000 Gt) were not deposited between ca. 2.3 and 1.88 Ga. Nonetheless, Superior- and Algoma-type iron formations are known from this time period. Shortly after the rise of atmospheric oxygen at ca. 2.4 Ga, oolitic hematitic ironstone of the lower Timeball Hill Formation, South Africa, was deposited in shallow-water above fair-weather wave base (Schweigart, 1965; Dorland, 1999). Little geochemical data are available for this unit, partly because it contains significant amounts of siliciclastic material. Its deposition at ca. 2316 Ma (Hannah et al., 2004) may coincide with a felsic magmatic event at ca. 2.32 Ga (e.g., Fetter et al., 2000; Berman et al., 2005; Hartlaub et al., 2007). The significance of this event and whether it is related to mantle processes is unknown. Correlative iron formations are not documented on other continents.

The slightly younger, ca. 2.22 Ga Hotazel Formation, also in South Africa, contains BIF interlayered with manganese-rich sedimentary rocks; this is the largest known manganese deposit (Tsikos et al., 2003). The iron and manganese formation lies above, and is most likely genetically related to, the submarine-emplaced Ongeluk Lavas of mafic to intermediate composition, which are linked with a ca. 2.22 Ga mantle plume breakout event (Ernst and Buchan, 2001). Although volcanic rocks and dikes related to this event are developed on nearly all continents, other iron and manganese formations of this age are unknown. Iron and manganese formations of the Hotazel Formation define three upward-shallowing sequences that were deposited in a slope environment (Schneiderhan et al., 2006). Significantly, the deposits lack positive Eu anomalies but have pronounced negative Ce anomalies, indicating a somewhat oxygenated state of the coeval deep ocean (Tsikos and Moore, 1997). Absence of a significant Eu anomaly is also important because it indicates that the global ocean was not dominated by a hydrothermal component and that Fe and Mn were derived locally, within the basin, by shallow-water alteration of underlying volcanic rocks. Considering that the 2.22 Ga mantle plume breakout event coincides with a positive carbon isotope excursion in seawater composition, the Lomagundi Event, related to high relative burial rates of organic carbon (e.g., Schidlowski et al., 1976; Karhu and Holland, 1996; Bekker et al., 2001), this REE pattern may indicate that significant parts of the oceans were already oxygenated by that time and that Fe and Mn were soluble only in isolated to semiisolated basins overwhelmed by a hydrothermal flux of reductants.

Hematitic oolites and hematite-rich sandstones were deposited in shallow-marine environments during the Lomagundi carbon isotope excursion in South Africa (e.g., Silverton Formation; Schweigart, 1965) and on the Kola Peninsula, Russia (Kuetsjärvi Sedimentary Formation; Akhmedov, 1972a). The BIFs deposited during the Lomagundi excursion include those in the Ijil Group, Mauritania (Bronner and Chauvel, 1979) and the Lomagundi Group, Zimbabwe (Master, 1991). The former belongs to the 2.2 to 2.1 Ga Birimian basin in West Africa that also contains Algoma-type iron and manganese formations in the Francevillian basin, Gabon (Leclerc and Weber, 1980) and in the Nigerian schist belts (Mücke, 2005). The latter developed within the ca. 2.2 to 2.1 Ga Magondi belt (Mapeo et al., 2001). Algoma-type iron formations deposited during the Lomagundi carbon isotope excursion are known in Brazil (e.g., Aimb Formation, Guarinos Group; Resende and Jost, 1995; Itapicuru Complex of the Rio Itapicuru greenstone belt; Dalton de Souza et al., 2003) and Norway (Iddjajav'ri Group, Karasjok greenstone belt; Often, 1985). Considering uncertainty in the ages of these iron formations, it is difficult to relate them to mantle plume breakout events. However, several such events occurred between 2.2 and 2.1 Ga (Ernst and Buchan, 2001).

Following the end of the Lomagundi carbon isotope excursion at 2.1 to 2.0 Ga, small, Algoma-type iron formations were

deposited in several basins in North America (e.g., Homestake Iron Formation, Black Hills, South Dakota; Frei et al., 2008) and Finland (Paakola, 1971; Laajoki and Saikkonen, 1977). Oolitic hematitic ironstone is also present in the Kolasjoki Sedimentary Formation, Kola Peninsula, Russia (Akhmedov, 1972b). Combined, these data suggest that dynamic ocean redox conditions existed during the aftermath of the GOE, with periodically generated upwelling of iron to shallow-water settings above storm and wave base, probably in association with mantle plume breakout events that affected the ocean redox state only on a short-term basis.

First extensive Neoarchean Superior-type iron formations

The oldest extensive and thick Superior-type BIF is the ca. 2.60 Ga Marra Mamba Formation of the Hamersley Province in Australia. It was deposited in a deep-water basinal setting on a passive margin during sea-level highstand of the Marra Mamba Supersequence and has an average thickness of about 210 m (Trendall and Blockley, 1970; Krapež et al., 2003). The BIF carries a pronounced positive Eu anomaly (Alibert and McCulloch, 1993), suggesting a strong hydrothermal imprint on REE systematics of the global ocean during its deposition. Although the Hamersley and Transvaal successions are equivalent in age and are correlative based on sequence stratigraphy, only ankerite-banded chert of the Campbellrand succession corresponds to the Marra Mamba BIF (Beukes and Gutzmer, 2008). A mantle plume breakout event comparable in age to that of the Marra Mamba Formation is unknown. However, the 2575.4 ± 0.7 Ma Great Dyke in Zimbabwe is only slightly younger (Oberthür et al., 2002).

There is only one iron formation (Bruno's Band) in the Hamersley and Transvaal Provinces stratigraphically between the Marra Mamba Iron Formation and the overlying major 2.50 to 2.45 Ga iron formations (Krapež et al., 2003; Beukes and Gutzmer, 2008). In contrast, there are two thin and economically insignificant chert- and early diagenetic siderite-rich beds below the Bruno's Band. This younger episode in deposition of iron formations closely corresponds with volcanism during the 2.50 to 2.45 Ga mantle plume breakout event of global extent (e.g., Heaman, 1997) and immediately preceded a supercontinent assembly (Barley et al., 2005). Deposition of these iron formations occurred on a reactivated continental margin (Krapež et al., 2003), during a rise in sea level. In addition to these time-equivalent iron formations, those in the Quadrilátero Ferrífero region in Brazil, Krivoy Rog area in Ukraine, and Kursk Magnetic Anomaly region in Russia are broadly similar in age based on available geochronologic and chemostratigraphic constraints, as well as on similar patterns of megabanding (Prilutzky et al., 1992; Kulik and Korzhnev, 1997; Bekker et al., 2003; Spier et al., 2007). These iron formations were also deposited on reactivated continental margins and are separated by a prominent unconformity from overlying Paleoproterozoic sequences. These unconformities correspond to long gaps in sedimentation following the supercontinent assembly at ca. 2.4 Ga. Assuming that these formations are similar in age, as much as 70 percent of the total original iron resources in Precambrian iron formations was deposited during the time interval 2.60 to 2.40 Ga. Surprisingly, a corresponding peak in VMS deposits is absent from the geologic record (Fig. 12); in fact, no VMS deposits are known to have formed within this age range (Franklin et al., 2005, App. 1). Texturally, these iron-formation deposits also differ from the older BIFs because they contain intervals having granular textures as well as hematite micro- and nanospheres (Ayres, 1972; Simonson and Goode, 1989; Ahn and Buseck, 1990; Beukes and Klein, 1990; Spier et al., 2007). However, most granules consist of iron silicates and carbonates, although rare hematite granules have been documented (Simonson and Goode, 1989; Beukes and Klein, 1990; Spier et al., 2007). Such features are important because the deposition of these iron formations directly preceded the GOE at ca. 2.4 Ga, and the Animikie GIFs predominantly have hematite as the iron-bearing mineral within the granules. This observation implies that processes responsible for iron-formation deposition before and after the rise of atmospheric oxygen were different, requiring more than one model to explain their formation.

Mesoarchean to Neoarchean BIFs

By ca. 3.1 Ga, a large part of the Kaapvaal craton in southern Africa had tectonically stabilized, and the intracontinental rift and cover successions formed in the Witwatersrand and Pongola basins. Laterally extensive, but rather thin (~10-m-thick) BIF units are preserved in the ca. 2.95 Ga Mozaan Group of the Pongola Supergroup and in the West Rand Group of the Witwatersrand Supergroup, some of which have been used to correlate the two successions (Beukes and Cairncross, 1991). The BIFs are interbedded with ferruginous shales and formed during rapid sea level rises, when large parts of the Kaapvaal craton were submerged and covered by an epicontinental sea. Because there is no direct relationship with volcanic rocks, the BIFs are classified as Superior type. This is in accord with a recent trace element and Nd isotope study of the oldest iron formation of the Mozaan Group (Alexander et al., 2008), which indicates a strong continental contribution to the trace element inventory of these BIFs.

On the Pilbara craton, the ca. 3.02 Ga Cleaverville Formation of the Gorge Creek Group consists predominantly of chert with some intercalations of BIF (Fig. 2A), black shale, and siltstone (Sugitani et al., 2006; Sugahara et al., 2010), and is similar to chert successions in Paleoarchean greenstone belts (see below). Shallow-water to subaerial quartz sandstone is overlain by finely laminated chert and iron formation, suggestive of a deepening-upward sequence. Petrographic and geochemical evidence has been presented for a hydrothermal influence on deposition of this sequence (Sugitani et al., 2006; Sugahara et al., 2010).

Banded iron formations are a distinct component of Mesoarchean to Neoarchean greenstone belts in most other Archean cratons. The majority are classified as Algoma-type deposits, but a large proportion is associated with sedimentary facies of continental-shelf environments, which is a characteristic feature of Superior-type iron formations (e.g., Gross, 1980). Good examples of Superior-type iron formations are found on several cratons that experienced transient crustal stability prior to the global magmatic event at 2.7 Ga. The 2.83 to 2.70 Ga Manjeri Formation of the Zimbabwe craton is a fluvial to shallow-marine succession deposited unconformably on older greenstones and granitoids (Hunter et al., 1998; Hofmann and Kusky, 2004). The BIFs of this unit are intercalated

with quartz arenite, shale, and carbonate strata, and lack obvious links to volcanic rocks of the same age. Similar sequences include the ca. 2.8 Ga Central Slave Cover Group (Bleeker et al., 1999) of the Slave craton, the ca. 2.8 Ga Steep Rock Group in the Wabigoon greenstone belt and correlative sequences in Canada (Wilks and Nisbet, 1988; Tomlinson et al., 2003), and the ca. 2.7 Ga Bababudan Group of the Dharwar craton in India (Srinivasan and Ojakangas, 1986; Trendall et al., 1997). The BIFs of these and similar sequences are usually classified as Superior type. The same assignment applies to iron formations present in the transgressive system tracts of thick sedimentary rock sequences in many Neoarchean greenstone belts, such as the Beardmore-Geraldton area of the Wabigoon subprovince of the Superior province (Fralick and Pufahl, 2006). In contrast, iron formations interlayered with volcanic rocks can be found in most greenstone belts. In several cases, a direct genetic relationship has been observed between volcanic activity and the deposition of iron formation, reflecting volcanic and hydrothermal activity both proximal and distal to volcanic centers (Fyon et al., 1992; Chown et al., 2000).

Paleoarchean BIFs

Paleoarchean BIFs are interbedded with bedded cherts in thick piles of ultramafic to felsic volcanic rocks in greenstone belts of the Kaapvaal and Pilbara cratons. Although bedded cherts are relatively common, true iron formations are rare. Cherts are uniformly underlain by zones of low-temperature sea-floor alteration up to several tens of meters thick (Duchac and Hanor, 1987; Hofmann and Wilson, 2007; Hofmann and Harris, 2008). These zones are characterized by silicification and depletion of many elements, including Fe, Mg, and some transition and base metals, which were likely exhaled by hydrothermal systems to the Paleoarchean ocean, providing a source of dissolved iron (Hanor and Duchac, 1990; Hofmann and Harris, 2008).

The Onverwacht Group of the Barberton greenstone belt, South Africa, which records a time interval of ca. 240 m.y., contains only a single stratigraphic unit of iron formation. The Buck Reef Chert is an unusually thick sequence of predominantly black and white banded chert that contains a unit as much as 100 m thick of banded ferruginous chert, which is composed mainly of microquartz and goethite, although siderite is regarded to be the main iron-bearing mineral at depth (Tice and Lowe, 2004). Whereas most of the Onverwacht Group cherts can be readily linked to hydrothermal activity during their formation (Hofmann and Harris, 2008), hydrothermal influence on the Buck Reef Chert has been debated (Tice and Lowe, 2004; de Vries et al., 2006). Nevertheless, with the evidence for syndepositional volcanism, hydrothermal activity, and extensional deformation in the Buck Reef Chert (Hofmann, 2010), it is difficult to invoke an absence of elevated heat flow during the deposition, making a hydrothermal influence on the deposition of ferruginous cherts probable. In contrast, the southern part of the ca. 3.5 Ga Iron Ore Group, Singhbhum craton, India, deposited in an island-arc setting, contains 120-m-thick iron oxide and carbonate Algoma-type BIF (Mukhopadhyay et al., 2008).

Iron formations are somewhat more common in sedimentary rock sequences overlying the predominantly volcanic rock pile of the Onverwacht Group. In the Barberton greenstone belt, jaspilitic BIF units, several tens of meters thick, are intercalated with ferruginous shale of the 3.26 to 3.23 Ga Fig Tree Group (Heinrichs, 1980; Hofmann, 2005). Felsic volcanic detritus and evidence for hydrothermal activity in rocks interlayered with the iron formation are widespread (Hofmann, 2010). Two thin jaspilitic BIF units interbedded with ferruginous shale also occur at the top of fining-upward sequences within the ca. 3.23 Ga Moodies Group and in association with syndepositional volcanic rocks (Eriksson, 1983). The lower one, within the Clutha Formation, is interlayered with air-fall tuff, accretionary lapilli, and a metabasaltic flow, whereas the upper one, in the Joe's Luck Formation, is immediately above the basaltic unit (Heubeck and Lowe, 1994). Despite the evidence for syndepositional volcanic activity, the presence of iron formations at the top of deepening-upward sequences in the predominantly siliciclastic Moodies Group implies that these BIFs might be the oldest Superior-type iron formations.

Eoarchean BIFs

In the Isua greenstone belt of western Greenland, ca. 3.8 Ga chert and BIF at amphibolite facies metamorphic grade are tectonically interleaved with amphibolite that locally preserves pillow structures (Myers, 2001). The BIF consists predominantly of quartz and magnetite, with cummingtonite and/or grunerite, actinolite, hornblende, and calcite (Dymek and Klein, 1988). Polat and Frei (2005) observed significant enrichments of Fe in Isua pillow basalts, which they attributed to dissolution from oceanic crust and precipitation on the ocean floor from hydrothermal fluids, suggesting that high-temperature hydrothermal alteration of the immediate substrate might have played an important role in deposition of the Isua BIFs.

Quartz-magnetite-grunerite BIF, as much as 30 m in thickness, and other siliceous rocks are intercalated with metasomatized amphibolite in the ca. 3.75 Ga Nuvvuagittuq greenstone belt of the northeastern Superior Province of Canada (Dauphas et al., 2007; O'Neil et al., 2007). The REE + Y profiles and Fe isotope compositions of this BIF are consistent with an origin as marine exhalites.

Controls on Iron Formation Deposition

The analysis presented above allows us to address the fundamental issue of what major controls existed on the deposition of iron formations. Although in some cases it is difficult to resolve whether an iron formation belongs to Algoma or Superior type, Algoma-type deposits are more common, in general, during Earth's early history (>2.5 Ga), probably reflecting higher mantle heat flux and limited size of epicontinental seas. As time progressed, relatively small Superior-type iron formations appeared in the record starting at ca. 3.3 Ga but did not reach significant thickness and extent until 2.6 Ga. An intriguing temporal and, cause-and-effect relationship existed between 2.5 and 2.3 Ga among emplacement of the first true LIPs, a peak in deposition of Superior-type iron formations, atmospheric oxidation, and Paleoproterozoic glaciations. The response of the biosphere to the mantle plume event may have led to the changes in surface environments. Following the atmospheric oxidation, iron and manganese deposition was localized in basins characterized by restricted circulation and intense submarine volcanism.

The later peak in iron-formation deposition at ca. 1.88 Ga was also closely linked in time with the mantle plume breakout event that affected the Superior and other cratons. We infer that at least on the scale of basins that surrounded the Superior craton, the redox state and sulfate content of seawater were lowered enough that the hydrothermal iron flux overwhelmed the oxidizing potential of seawater, with the result that iron was transported to shallow waters where iron compounds precipitated at the dynamic redoxcline. Alternatively, because deeper water marine settings are generally characterized by low productivity, periods of elevated hydrothermal flux of reductants promoted anoxic ferruginous conditions even when seawater sulfate content was still reasonably high. High atmospheric pCO_2 and, consequently, surface temperatures during the mantle plume breakout event, aided stagnant circulation within these basins, if not in the global ocean. In addition, mantle plume breakout events generate higher sea level and sluggish ocean circulation, contributing to anoxia on a basin to global scales (Condie et al., 2001). It was earlier suggested that either oxidation or the development of sulfidic conditions in the deep ocean terminated deposition of iron formations after ca. 1.8 Ga (Holland, 1984; Canfield, 1998). Our analysis, however, suggests that deposition of large iron formations corresponds closely in time with major mantle plume events. Therefore, rather than iron-formation deposition ending by changes in surface conditions, we propose that the development of sulfidic conditions in the Animikie basin, for example, was a consequence of several contemporaneous processes, including a mantle plume event, a significant hydrothermal iron flux, and lowering of the seawater redox state either on a global or basinwide scale. The test of this hypothesis is obvious: shales above the ca. 1.88 Ga iron formations of the Lake Superior region and below the level of the Sudbury impact ejecta blanket (Cannon et al., 2010) would have constrained the seawater redox state after deposition of the iron formations, at least 20 to 50 m.y. before inferred initiation of sulfidic conditions in the deep ocean (cf. Poulton et al., 2004). Episodic development of sulfidic conditions linked with the deposition of iron formations would be consistent with this model.

Although VMS deposits show a corresponding peak in global tonnage at ca. 1.88 Ga, coeval with deposition of Animikie GIFs, sulfide deposits are conspicuously underrepresented for the 2.50 to 2.45 Ga mantle plume event when huge tonnages of iron formation accumulated (Fig. 12). At present, we lack a satisfactory explanation for this. Potentially, long-term global tectonic processes played a role. Whereas volcanic arc systems were established shortly before this time period and were active during the ca.1.88 Ga mantle plume breakout event, deposition of iron formations at 2.50 to 2.45 Ga preceded supercontinent assembly (Barley et al., 2005). Under these conditions, the hydrothermal flux of iron was likely derived predominantly from mid-ocean ridges. Differences between iron formations deposited before and after the GOE, in terms of original textures and settings, imply potentially different modes of iron precipitation. Whereas the Fe-Si protolith for pre-GOE iron formations formed in the deeper parts of basins and was redistributed with density currents throughout basins, post-GOE iron formations record upwelling and oxidation of ferrous iron, precipitation on the shelf and, later, transport by storm and wave currents back into the basin. Although GIFs first appeared at ca. 2.6 Ga or earlier, their predominant mineralogy was not characterized by iron oxides until shortly after the GOE.

Reasons for the later 1.85 to 0.75 Ga gap of 1.1 b.y. in deposition of iron formations are also uncertain, although above we note several exceptions to this gap. If the temporary cessation of plate tectonics (e.g., Silver and Benn, 2008; Condie et al., 2009) was responsible for the gap, then why did both mantle plume events and VMS deposition continue during this time period (Fig. 12)? Mantle plume events do not necessarily require plate tectonic processes, but VMS mineralization does require a submarine heat source in an oceanic environment or at least marine basins that developed on rifted continental or oceanic crust. The secular trend of iron formations clearly deserves more attention. Although precise geochronology has been very successful in dating Precambrian successions, including host strata to iron formations and VMS ores, some major economic iron deposits are still poorly dated; knowing their ages more precisely might critically influence our understanding of oceanic and atmospheric redox states, as well as large-scale evolution of the Earth system. Among these poorly dated deposits (App. 1), Krivoy Rog in Ukraine, the Kursk Magnetic Anomaly in Russia, the Cauê Iron Formation in Brazil, the Frere Iron Formation in Australia, the Chuanlinggou Iron Formation in China, and iron formations in the Chitradurga, Bababudan, and Iron Ore groups in India are critically in need of high-precision geochronology.

Neoproterozoic iron formations are interbedded with glacial deposits, but it is unlikely that Snowball Earth conditions alone led to their deposition (e.g., Kump and Seyfried, 2005). Although long-term ice cover played an important role in lowering the seawater redox state and, potentially, seawater sulfate content, the geologic setting of the giant Rapitan Iron Formation, as well as other Neoproterozoic iron formations (App. 1), provides a strong case for temporal and geographic connection to submarine volcanism. Therefore, for these and other cases, at least three factors were important: seawater redox state, enhanced hydrothermal flux of iron during mantle plume events, and basin configuration including a degree of separation from the global ocean.

Secular relationships among iron formations, VMS deposits, seawater anoxia, and mantle plume events during the Precambrian provide a key framework for interpreting the origin of Phanerozoic ironstones. In contrast to previous studies of ironstones, we emphasize secular links involving ironstones, VMS deposits, organic matter-rich shales, and intervals of enhanced submarine volcanism during mantle plume breakout events. We propose that Phanerozoic ironstones were preferentially deposited during anoxic events when hydrothermal iron was delivered to shallow shelf settings in either isolated basins or on open continental margins. It would, therefore, be instructive to carry out a comparative study of post-GOE Proterozoic GIFs and Phanerozoic ironstones, in order to test whether similar processes were responsible for their respective secular distribution and deposition.

The biosphere also played an important role in the genesis of iron formations. Not only was biological activity involved in direct or indirect precipitation of iron, it also determined the

seawater redox state and seawater sulfate content. In addition, modulation of the biological silica sink during the Precambrian and Phanerozoic increased the silica-influenced scavenging efficiency of phosphorus and metals on ferric oxyhydroxide protoliths to iron formations. However, precipitation and oxidation mechanisms for Archean iron formations are not established. The problem remains that although an iron-rich precursor to BIFs appears probable, it is neither obvious what the texture and mineralogical composition of those sediments were, nor where or how the original sediments were deposited prior to their resedimentation into the basin realm. Certainly, the widespread presence of graded beds within BIFs supports a model in which some of the original sediments were granular, as it is seemingly impossible to produce graded beds from amorphous iron-rich clays, iron-rich gels, or chemically deposited varves, the traditionally inferred precursor sediments to BIF. Whereas recognition that classic BIFs of the Dales Gorge Member, in the Hamersley Province of Western Australia, are density-current deposits is significant, that recognition has made interpretation of the precursor sediments more difficult, because the original depositional site is unknown. The same problem exists for GIFs, because they are essentially clastic sedimentary rocks. As a caveat on these interpretations, petrographic documentation (e.g., Ayres, 1972) has established that iron-rich carbonates grew during burial diagenesis and ore-related alteration and, therefore, iron-rich carbonate was unlikely to have precipitated in the water column.

Our proposed model for iron-formation genesis provides a different perspective on the secular evolution of the ocean redox state. Rather than lagging behind changes in atmospheric oxidation, we suggest that submarine volcanism was directly responsible for generating extensive ocean- and basin-scale anoxia through venting significant fluxes of reductants such as H_2, H_2S, Fe(II), and Mn(II). This perspective applies to both Precambrian and Phanerozoic environments and provides a framework for better understanding ocean evolution and the origin of sedimentary mineral deposits. For future studies continuing to explore the complex interplays among mantle, tectonic, oceanic, and biotic processes that led to the deposition of iron-rich sediments through Earth history, we emphasize the need for a view in which enhanced hydrothermal processes in the deep ocean determined the ocean redox state independently of, or complementary to, the atmospheric oxidation state.

Acknowledgments

AB acknowledges support from NSF grant EAR-05-45484, NASA Astrobiology Institute Award NNA04CC09A, an NSERC Discovery Grant, and the TGI-3 Program operated by the Geological Survey of Canada. JFS thanks Bill Cannon for discussions on iron-formation distribution, setting, and genesis. NP acknowledges support from the NSF-GRF program and thanks Chris Reinhard and Phil Fralick for stimulating discussions on iron formations. BK and AB acknowledge support from an Australian Research Council (ARC) Linkage Grant tied to industry support from BHP Billiton Iron Ore. Bill Cannon, Barry Maynard, and Rich Goldfarb provided constructive, insightful, and timely reviews that helped to clarify and focus the paper. Rob Rainbird and Elizabeth Turner, respectively, supplied photographs for Figures 4A and 14 and are gratefully acknowledged.

REFERENCES

Abbott, D., and Isley, A., 2001, Oceanic upwelling and mantle-plume activity: Paleomagnetic tests of ideas on the source of the Fe in early Precambrian iron formations: Geological Society of America Special Paper 352, p. 323–339.

——2002, The intensity, occurrence, and duration of superplume events and eras over geological time: Journal of Geodynamics, v. 34, p. 265–307.

Abbott, S.T., and Sweet, I.P., 2000, Tectonic control on third-order sequences in a siliciclastic ramp-style basin: An example from the Roper superbasin (Mesoproterozoic), northern Australia: Australian Journal of Earth Sciences, v. 47, p. 637–657.

Ahn, J.H., and Buseck, P.R., 1990, Hematite nanospheres of possible colloidal origin from a Precambrian banded iron formation: Science, v. 250, p. 111–113.

Akhmedov, A.M., 1972a, Iron-rich metasedimentary rock of Pechenga Complex and their genesis: Materials on geology and metallogeny of Kola Peninsula: Apatity, v. 4, p. 125–131 [in Russian].

——1972b, Hematite oolites in sedimentary rocks of the Pechenga Complex: Materials on mineralogy of the Kola Peninsula: Leningrad, Nauka, v. 9, p. 135–137 [in Russian].

Alexander, B.W., Bau, M., Andersson, P., and Dulski, P., 2008, Continentally-derived solutes in shallow Archean seawater: Rare earth element and Nd isotope evidence in iron formation from the 2.9 Ga Pongola Supergroup, South Africa: Geochimica et Cosmochimica Acta, v. 72, p. 378–394.

Alibert, C., and McCulloch, M.T., 1993, Rare earth element and neodymium isotopic compositions of banded iron formations and associated shales from Hamersley, Western Australia: Geochimica et Cosmochimica Acta, v. 57, p. 187–204.

Aller, R.C., Mackin, J.E., and Cox, R.T., 1986, Diagenesis of Fe and S in Amazon inner shelf muds: Apparent dominance of Fe reduction and implications for the genesis of ironstones: Continental Shelf Research, v. 6, p. 263–289.

Alt, J.C., 1988, Hydrothermal oxide and nontronite deposits on seamounts in the Eastern Pacific: Marine Geology, v. 81, p. 227–239.

——2003, Stable isotopic composition of upper oceanic crust formed at a fast spreading ridge, ODP Site 801: Geochemistry, Geophysics, Geosystems, v. 4, doi:10.1029/2002GC000400.

Alt, J.C., France-Lanord, C., Floyd, P.A., Castillo, P., and Galy, A., 1992, Low-temperature hydrothermal alteration of Jurassic ocean crust, Site 801: Proceedings of the Ocean Drilling Program, Scientific Results, v. 129, p. 415–427.

Arnold, G.L., Anbar, A.D., Barling, J., and Lyons, T.W., 2004, Molybdenum isotope evidence for widespread anoxia in Mid-Proterozoic oceans: Science, v. 304, p. 87–90.

Arthur, M.A., and Sageman, B.B., 1994, Marine black shales: Depositional mechanisms and environments of ancient deposits: Annual Review of Earth and Planetary Sciences, v. 22, p. 499–551.

Ayres, D.E., 1972, Genesis of iron-bearing minerals in banded iron formation mesobands in the Dales Gorge Member, Hamersley Group, Western Australia: Economic Geology, v. 67, p. 1214–1233.

Balci, N., Bullen, T.D., Witte-Lien, K., Shanks, W.C., III, Motelica, M., and Mandernack, K.W., 2006, Iron isotope fractionation during microbially stimulated Fe(II) oxidation and Fe(III) precipitation: Geochimica et Cosmochimica Acta, v. 70, p. 622–639.

Barley, M.E., Kerrich R., Krapež, B., and Groves D.I., 1998, The 2.72–2.60 Ga bonanza: Metallogenic and environmental consequences of the interaction between mantle plumes, lithospheric tectonics and global cyclicity: Precambrian Research, v. 91, p. 65–90.

Barley, M.E., Bekker, A., and Krapež, B., 2005, Late Archean to early Paleoproterozoic global tectonics, environmental change and the rise of atmospheric oxygen: Earth and Planetary Science Letters, v. 238, p. 156–171.

Barnes, R.G., 1988, Metallogenic studies of the Broken Hill and Euriowie blocks, New South Wales. 1. Styles of mineralization in the Broken Hill block: New South Wales Geological Survey Bulletin 32, p. 1–115.

Barrett, T.J., Fralick, P.W., and Jarvis, I., 1988a, Rare-earth-element geochemistry of some Archean iron formations north of Lake Superior, Ontario: Canadian Journal of Earth Sciences, v. 25, p. 570–580.

Barrett, T.J., Wares, R.P., and Fox, J.S., 1988b, Two-stage hydrothermal formation of a Lower Proterozoic sediment-hosted massive sulfide deposit, northern Labrabor trough, Quebec: Canadian Mineralogist, v. 26, p. 871–888.

Bau, M., 1993, Effects of syn-depositional and postdepositional processes on the rare-earth element distribution in Precambrian iron-formations: European Journal of Mineralogy, v. 5, p. 257–267.
Bau, M., and Dulski, P., 1996, Distribution of yttrium and rare-earth elements in the Penge and Kuruman Iron-Formations, Transvaal Supergroup, South Africa: Precambrian Research, v. 79, p. 37–55.
Bau, M., Möller, P., and Dulski, P., 1997, Yttrium and lanthanides in eastern Mediterranean seawater and their fractionation during redox-cycling: Marine Chemistry, v. 56, p. 123–131.
Baur, M.E., Hayes, J.M., Studley, S.A., and Walter, M.R., 1985, Millimeter-scale variations of stable isotope abundances in carbonates from banded iron-formations in the Hamersley Group of Western Australia: Economic Geology, v. 80, p. 270–282.
Beal, E.J., House, C.H., and Orphan, V.J., 2009, Manganese- and iron-dependent marine methane oxidation: Science, v. 325, p. 184–187.
Beard, B.L., Johnson, C.M., Cox, L., Sun, H., Nealson, K.H., and Aguilar, C., 1999, Iron isotope biosignatures: Science, v. 285, p. 1889–1892.
Beard, B.L., Johnson, C.M., Von Damm, K.L., and Poulson, R.L., 2003, Iron isotope constraints on Fe cycling and mass balance in oxygenated Earth oceans: Geology, v. 31, p. 629–632.
Beaumont, V., and Robert, F., 1999, Nitrogen isotope ratios of kerogens in Precambrian cherts: A record of the evolution of atmosphere chemistry?: Precambrian Research, v. 96, p. 63–82.
Becker, R.H., and Clayton, R.N., 1972, Carbon isotopic evidence for the origin of a banded iron-formation in Western Australia: Geochimica et Cosmochimica Acta, v. 36, p. 577–595.
Bekker, A., and Kaufman, A.J., 2007, Oxidative forcing of global climate change: A biogeochemical record across the oldest Paleoproterozoic ice age in North America: Earth and Planetary Science Letters, v. 258, p. 486–499.
Bekker, A., Kaufman, A.J., Karhu, J.A., Beukes, N.J., Swart, Q.D., Coetzee, L.L., and Eriksson, K.A., 2001, Chemostratigraphy of the Paleoproterozoic Duitschland Formation, South Africa: Implications for coupled climate change and carbon cycling: American Journal of Science, v. 301, p. 261–285.
Bekker, A., Sial, A.N., Karhu, J.A., Ferreira, V.P., Noce, C.M., Kaufman, A.J., Romano, A.W., and Pimentel, M.M., 2003, Chemostratigraphy of carbonates from the Minas Supergroup, Quadrilátero Ferrifero, Brazil: A stratigraphic record of Early Proterozoic atmospheric, biogeochemical and climatic change: American Journal of Science, v. 303, p. 865–904.
Bekker, A., Holland, H.D., Wang, P. L., Rumble, D., Stein, H.J., Hannah, J.L., Coetzee, L.L., and Beukes, N.J., 2004, Dating the rise of atmospheric oxygen: Nature, v. 427, p. 117–120.
Bekker, A., Barley, M.E., Fiorentini, M.L., Rouxel, O.J., Rumble, D., and Beresford, S.W., 2009, Atmospheric sulfur in Archean komatiite-hosted nickel deposits: Science, v. 326, p. 1086–1089.
Berman, R.G., Sanborn-Barrie, M., Stern, R.A., and Carson, C.J., 2005, Tectonometamorphism at ca. 2.35 and 1.85 Ga in the Rae domain, western Churchill Province, Nunavut, Canada: Insights from structural, metamorphic and in situ geochronological analysis of the southwestern Committee Bay belt: Canadian Mineralogist, v. 43, p. 409–442.
Berman-Frank, I., Cullen, J.T., Shaked, Y., Sherrell, R.M., and Falkowski, P.G., 2001, Iron availability, cellular iron-quotas, and nitrogen fixation in *Trichodesmium*: Limnology and Oceanography, v. 46, p. 1249–1260.
Berman-Frank, I., Quigg, A., Finkel, Z.V., Irwin, A.J., and Haramaty, L., 2007, Nitrogen-fixation strategies and Fe requirements in cyanobacteria: Limnology and Oceangraphy, v. 52, p. 2260–2269.
Beukes, N.J., 1973, Precambrian iron-formations of southern Africa: Economic Geology, v. 68, p. 960–1004.
Beukes, N.J., and Cairncross, B., 1991, A lithostratigraphic-sedimentological reference profile for the Late Archean Mozaan Group, Pongola Sequence: Application to sequence stratigraphy and correlation with the Witwatersrand Supergroup: South African Journal of Geology, v. 94, p. 44–49.
Beukes, N.J., and Gutzmer, J., 2008, Origin and paleoenvironmental significance of major iron formations at the Archean-Paleoproterozoic boundary: Reviews in Economic Geology, v. 15, p. 5–47.
Beukes, N.J., and Klein, C., 1990, Geochemistry and sedimentology of a facies transition—from microbanded to granular iron-formation—in the Early Proterozoic Transvaal Supergroup, South Africa: Precambrian Research, v. 47, p. 99–139.
Beukes, N.J., Klein, C., Kaufman, A.J., and Hayes, J.M., 1990, Carbonate petrography, kerogen distribution, and carbon and oxygen isotope variations in an Early Proterozoic transition from limestone to iron-formation deposition: Transvaal Supergroup, South Africa: Economic Geology, v. 85, p. 663–690.
Bischoff, J.L., and Rosenbauer, R.J., 1987, Phase separation in seafloor geothermal systems: An experimental study on the effects of metal transport: American Journal of Science, v. 287, p. 953–978.
Bjerrum, C.J., and Canfield, D.E., 2002, Ocean productivity before about 1.9 Gyr limited by phosphorous adsorption onto iron oxides: Nature, v. 417, p. 159–162.
Bleeker, W., and Macek, J., 1996, Evolution of the Thompson nickel belt, Manitoba: Setting of Ni-Cu deposits in the western part of the circum Superior boundary zone: Geological Association of Canada-Mineralogical Association of Canada Annual Meeting, Winnipeg, Manitoba, Field Trip Guidebook A1, 44 p.
Bleeker, W., Ketchum, J.W.F., Jackson, V.A., and Villeneuve, M.E., 1999, The Central Slave Basement Complex, Part I: Its structural topology and autochthonous cover: Canadian Journal of Earth Sciences, v. 36, p. 1083–1109.
Bowring, S.A., and Grotzinger, J.P., 1992, Implications of new chronostratigraphy for tectonic evolution of the Wopmay orogen, northwest Canadian Shield: American Journal of Science, v. 292, p. 1–20.
Braterman, P.S., and Cairns-Smith, A.G., 1986, Photoprecipitation and the banded iron-formations—Some quantitative aspects: Origins of Life, v. 17, p. 221–228.
Braterman, P.S., Cairns-Smith, A.G., and Sloper, R.W., 1983, Photooxidation of hydrated Fe^{2+}: Significance for banded iron formations: Nature, v. 303, p. 163–164.
Braun, J.-J., Pagel, M., Muller, J.-P., Bilong, P., Michard, A., and Guillet, B., 1990, Cerium anomalies in lateritic profiles: Geochimica et Cosmochimica Acta, v. 54, p. 781–789.
Breitkopf, J.H., 1988, Iron formations related to mafic volcanism and ensialic rifting in the southern margin zone of the Damara orogen, Namibia: Precambrian Research, v. 38, p. 111–130.
Bronner, G., and Chauvel, J.J., 1979, Precambrian banded iron-formations of the Ijil Group (Kediat Ijil, Reguibat Shield, Mauritania): Economic Geology, v. 74, p. 77–94.
Bruland, K.W., and Lohan, M.C., 2006, Controls of trace elements in seawater: Treatise on Geochemistry, v. 6, p. 23–47.
Bühn, B., Stanistreet, I.G., and Okrusch, M., 1992, Late Proterozoic outer shelf manganese and iron deposits at Otjosondu (Namibia) related to the Damaran oceanic opening: Economic Geology, v. 87, p. 1393–1411.
Buick, R., 1992, The antiquity of oxygenic photosynthesis: Evidence from stromatolites in sulphate-deficient Archaean lakes: Science, v. 255 p. 74–77.
——2008, When did oxygenic photosynthesis evolve?: Philosophical Transactions of the Royal Society of London, v. 363B, p. 2731–2743.
Bullen, T.D., White, A.F., Childs, C.W., Vivit, D.V., and Schulz, M.S., 2001, Demonstration of significant abiotic iron isotope fractionation in nature: Geology, v. 29, p. 699–702.
Bunting, J.A., 1986, Geology of the eastern part of the Nabberu basin: Geological Survey of Western Australia Bulletin, v. 131, 129 p.
Burkhalter, R.M., 1995, Ooidal ironstones and ferruginous microbialites: Origin and relation to sequence stratigraphy (Aalenian and Bajocian, Swiss Jura Mountains): Sedimentology, v. 42, p. 57–74.
Byrne, R., and Sholkovitz, E., 1996, Marine chemistry and geochemistry of the lanthanides, *in* Gschneider, K.A., Jr., and Eyring, L., eds., Handbook on the physics and chemistry of the rare earths: Amsterdam, Elsevier, v. 23, p. 497–593.
Cairns-Smith, A.G., 1978, Precambrian solution photochemistry, inverse segregation, and banded iron formations: Nature, v. 76, p. 807–808.
Cameron, E.M., 1983, Genesis of Proterozoic iron-formation: Sulphur isotope evidence: Geochimica et Cosmochimica Acta, v. 47, p. 1069–1074.
Cameron, V., Vance, D., Archer, C., and House, C.H., 2009, A biomarker based on the stable isotopes of nickel: Proceedings of the National Academy of Sciences, v. 206, p. 10944–10948.
Canavan, F., 1965, Iron and manganese ore deposits of Iron Range, *in* McAndrew, J., ed., Geology of Australian ore deposits: Melbourne, Australasian Institute of Mining and Metallurgy, Eighth Commonwealth Mining and Metallurgical Congress of Australia and New Zealand, p. 391–393.
Canfield, D.E., 1998, A new model for Proterozoic ocean chemistry: Nature, v. 396, p. 450–453.
Canfield, D.E., Poulton, S.W., Knoll, A.H., Narbonne, G.M., Ross, G., Goldberg, T., and Strauss, H., 2008, Ferruginous conditions dominated later Neoproterozoic deep-water chemistry: Science, v. 15, p. 949–952.
Cannon, W.F., LaBerge, G.L., Klasner, J.S., and Schulz, K.J., 2008, The Gogebic Iron Range—a sample of the northern margin of the Penokean fold and thrust belt: U.S. Geological Survey Professional Paper 1730, 44 p.

Cannon, W.F., Schulz, K.J., Horton, J.W.J., and Kring, D.A., 2010, The Sudbury impact layer in the Paleoproterozoic iron ranges of northern Michigan, USA: Geological Society of America Bulletin, v. 122, p. 50–75.

Chandler, F.W., 1984, Metallogenesis of an Early Proterozoic foreland sequence, eastern Hudson Bay, Canada: Journal of the Geological Society, v. 141, p. 299–313.

Chown, E.H., N'Dah, E., and Mueller, W.U., 2000, The relation between iron formation and low temperature hydrothermal alteration in an Archaean volcanic environment: Precambrian Research, v. 101, p. 263–275.

Cloud, P., 1973, Paleoecological significance of banded iron-formation: Economic Geology, v. 68, p. 1135–1143.

Cloud, P.E., 1965, Significance of Gunflint (Precambrian) microflora—photosynthetic oxygen may have had important local effects before becoming a major atmospheric gas: Science, v. 148, p. 27–35.

Cocherie, A., Calvez, J.-Y., and Oudin-Dunlop, E., 1994, Hydrothermal activity as recorded by Red Sea sediments: Sr-Nd isotopes and REE signatures: Marine Geology, v. 118, p. 291–302.

Condie, K.C., Des Marais, D.J., and Abbott, D., 2001, Precambrian superplumes and supercontinents: A record in black shales, carbon isotopes, and paleoclimates?: Precambrian Research, v. 106, p. 239–260.

Condie, K.C., O'Neill, C., and Aster, R., 2009, Evidence and implications for a widespread magmatic shutdown for 250 My on Earth: Earth and Planetary Science Letters, v. 282, p. 294–298.

Corliss, J.B., Lyle, M., Dymond, J., and Crane, K., 1978, The chemistry of hydrothermal mounds near the Galapagos rift: Earth and Planetary Science Letters, v. 40, p. 12–24.

Cornell, D.H., Pettersson, Å, Whitehouse, M.J., and Scherstén, A., 2009, A new chronostratigraphic paradigm for the age and tectonic history of the Mesoproterozoic Bushmanland ore district, South Africa: Economic Geology, v. 104, p. 385–404.

Corrigan, D., Pehrsson, S.J., MacHattie, T.G., Piper, L., Wright, D., Lassen, B., and Chakungal, J., 1999, Lithotectonic framework of the Trans-Hudson orogen in the northwestern Reindeer zone, Saskatchewan: An update from recent mapping along the Reindeer Lake transect: Geological Survey of Canada Current Research, Paper 99–C, p. 169–178.

Croal, L.R., Johnson, C.M., Beard, B.L., and Newman, D.K., 2004, Iron isotope fractionation by Fe(II)-oxidizing photoautotrophic bacteria: Geochimica et Cosmochimica Acta, v. 68, p. 1227–1242.

Crowe, S.A.J., Katsev, C., Magen, S., O'Neill, C., Sturm, A.H., Canfield, D.E., Haffner, G.D., Mucci, A., Sundby, B., and Fowle, D.A., 2008, Photoferrotrophs thrive in an Archean ocean analogue: Proceedings of the National Academy of Sciences, v. 105, p. 15937–15943.

Dai, Y.-D., Song, H.-M., and Shen, J.-Y., 2004, Fossil bacteria in Xuanlong iron ore deposits of Hebei Province: Science in China, ser. D, v. 47, p. 347–356 [in English].

Dalton de Souza, J., Kosin, M., Melo, R.C., Oliveira, E.P., Carvalho, M.J., and Leite, C.M., 2003, Guia de excursão—geologia do segmento norte do orógeno itabuna-salvador-curaçá: Revista Brasileira de Geociências, v. 33 (supplement) p. 27–32.

Dauphas, N., van Zuilen, M., Wadhwa, M., Davis, A.M., Marty, B., and Janney, P.E., 2004, Clues from Fe isotope variations on the origin of Early Archean BIFs from Greenland: Science, v. 306, p. 2077–2080.

Dauphas, N., Cates, N., Mojzsis, S.J., and Busigny, V., 2007, Identification of chemical sedimentary protoliths using iron isotopes in the >3750 Ma Nuvvuagittuq supracrustal belt, Canada: Earth and Planetary Science Letters, v. 254, p. 357–376.

Davis, W.J., Rainbird, R.H., Aspler, L.B., and Chiarenzelli, J.R., 2005, Detrital zircon geochronology of the Paleoproterozoic Hurwitz and Kiyuk Groups, western Churchill Province, Nunavut: Geological Survey of Canada Current Research, Paper 2005–F1, p. 1–13.

Deb, M., and Pal, T., 2004, Geology and genesis of the base metal sulphide deposits in the Dariba-Rajpura-Bethumni belt, Rajasthan, India, in the light of basin evolution, *in* Deb, M., and Goodfellow, W.D., eds., Sediment-hosted lead-zinc sulphide deposits: New Delhi, Narosa Publishing, p. 304–327.

Deb, M., and Thorpe, R.I., 2004, Geochronological constraints in the Precambrian geology of Rajasthan and their metallogenic implications, *in* Deb, M., and Goodfellow, W.D., eds., Sediment-hosted lead-zinc sulphide deposits: New Delhi, Narosa Publishing, p. 246–263.

De Baar, H.J.W., German, C.R., Elderfield, H., and van Gaans, P., 1988, Rare earth element distributions in anoxic waters of the Cariaco Trench: Geochimica et Cosmochimica Acta, v. 52, p. 1203–1219.

De Carlo, E.H., and Green, W.J., 2002, Rare earth elements in the water column of Lake Vanda, McMurdo Dry Valleys, Antarctica: Geochimica et Cosmochimica Acta, v. 66, p. 1323–1333.

De Carlo, E.H., McMurtry, G.M., and Yeh, H.W., 1983, Geochemistry of hydrothermal deposits from the Loihi submarine volcano, Hawaii: Earth and Planetary Science Letters, v. 66, p. 437–449.

Derry, L.A., and Jacobsen, S.B., 1990, The chemical evolution of Precambrian seawater—evidence from REEs in banded iron formations: Geochimica et Cosmochimica Acta, v. 54, p. 2965–2977.

de Vries, S.T., Nijman, W., and Armstrong, R.A., 2006, Growth-fault structure and stratigraphic architecture of the Buck Ridge volcano-sedimentary complex, upper Hooggenoeg Formation, Barberton greenstone belt, South Africa: Precambrian Research, v. 149, p. 77–98.

Dirks, P.H.G.M., Jelsma, H.A., and Hofmann, A., 2002, Thrust-related accretion of an Archaean greenstone belt in the midlands of Zimbabwe: Journal of Structural Geology, v. 24, p. 1707–1727.

Dorland, H.C., 1999, Paleoproterozoic laterites, red beds and ironstones of the Pretoria Group with reference to the history of atmospheric oxygen: Unpublished M.Sc. thesis, Johannesburg, Rand Afrikaans University, 147 p.

Duchac, K.C., and Hanor, J.S., 1987, Origin and timing of metasomatic silicification of an Early Archean komatiite sequence, Barberton Mountain Land, South Africa: Precambrian Research, v. 37, p. 125–146.

Dymek, R.F., and Klein, C., 1988, Chemistry, petrology, and origin of banded iron formation lithologies from the 3800 Ma Isua supracrustal belt, West Greenland: Precambrian Research, v. 39, p. 247–302.

Eastoe, C.J., and Gustin, M.M., 1996, Volcanogenic massive sulfide deposits and anoxia in the Phanerozoic oceans: Ore Geology Reviews, v. 10, p. 179–197.

Easton, R.M., 2005, The Grenvillian Tomiko quartzites of Ontario: Correlatives of the Baraboo quartzites of Wisconsin, the Mazatzal orogen of New Mexico, or unique? Implications for the tectonic architecture of Laurentia in the Great Lakes region [abs.]: Institute on Lake Superior Geology, 51th Annual Meeting, Proceedings, v. 51, pt 1, Proceedings and Abstracts, p. 15–16.

Ehrenreich, A., and Widdel, F., 1994, Anaerobic oxidation of ferrous iron by purple bacteria, a new type of phototrophic metabolism: Applied and Environmental Microbiology v. 60 p. 4517–4526.

Eigenbrode, J.L., and Freeman, K.H., 2006, Late Archean rise of aerobic microbial ecosystems: Proceedings of the National Academy of Sciences, v. 103, p. 15759–15764.

Eigenbrode, J.L., Freeman K.H., and Summons, R.E., 2008, Methylhopane biomarker hydrocarbons in Hamersley Province sediments provide evidence for Neoarchean aerobiosis: Earth and Planetary Science Letters, v. 273, p. 323–331.

Elderfield, H., Gass, G., Hammond, A., and Bear, L.M., 1972, The origin of ferromanganese sediments associated with the Troodos massif of Cyprus: Sedimentology, v. 19, p. 1–19.

Emerson, D., and Moyer, C.L., 2002, Neutrophilic Fe-oxidizing bacteria are abundant at the Loihi seamount hydrothermal vents and play a major role in Fe oxide deposition: and Environmental Microbiology, v. 68, p. 3085–3093.

Eriksson, K.A., 1983, Siliciclastic-hosted iron-formations in the Early Archean Barberton and Pilbara sequences: Journal of the Geological Society of Australia, v. 30, p. 473–482.

Ernst, R.E., and Buchan, K.L., 2001, Large mafic magmatic events through time and links to mantle-plume heads: Geological Society of America Special Paper 352, p. 483–575.

Ewers, W.E., and Morris, R.C., 1981, Studies of the Dales Gorge Member of the Brockman Iron Formation, Western Australia: Economic Geology, v. 76, p. 1929–1953.

Farquhar, J., and Wing, B.A., 2005, The terrestrial record of stable sulphur isotopes: A review of the implications for evolution of Earth's sulphur cycle: Geological Society Special Publication 248, p. 167–177.

Farquhar, J., Bao, H., and Thiemens, M., 2000, Atmospheric influence of Earth's earliest sulfur cycle: Science, v. 289, p. 756–758.

Fetter, A.H., Van Schmus, W.R., Santos, T.J.S., Neto, J.A.N., and Henriarthaud, M., 2000, U-Pb and Sm-Nd geochronological constraints on the crustal evolution and basement architecture of Ceará State, NW Borborema Province, NE Brazil: Implications for the existence of the Paleoproterozoic supercontinent "Atlantica": Revista Brasileira de Geociências, v. 30, p. 102–106.

Findlay, J.M., Parrish, R.R., Birkett, T.C., and Watanabe, D.H., 1995, U-Pb ages from the Nimish Formation and Montagnais glomeroporphyritic gabbro of the central New Quebec orogen, Canada: Canadian Journal of Earth Sciences, v. 32, p. 1207–1220.

Fischer, W.W., and Knoll, A.H., 2009, An iron shuttle for deep-water silica in Late Archean and early Paleoproterozoic iron formation: Geological Society of America Bulletin, v. 121, p. 222–235.

Fischer, W.W., Schroeder, S., Lacassie J.P., Beukes, N.J., Goldberg, T., Strauss, H., Horstmann, U.E., Schrag, D.P., and Knoll, A.H., 2009, Isotopic constraints on the Late Archean carbon cycle from the Transvaal Supergroup along the western margin of the Kaapvaal craton, South Africa: Precambrian Research, v. 169, p. 15–27.

Föllmi, K.B., 1996, The phosphorus cycle, phosphogenesis, and marine phosphate-rich deposits: Earth-Science Reviews, v. 40, p. 55–124.

Foustoukos, D.I., and Bekker, A., 2008, Hydrothermal Fe(II) oxidation during phase separation: Relevance to the origin of Algoma-type BIFs [abs.]: Goldschmidt 2008 Conference, Vancouver, B.C., Canada: Geochimica et Cosmochimica Acta, v. 72, Supplement 1, p. A280.

Fralick, P.W., and Pufahl, P.K., 2006, Iron formation in Neoarchean deltaic successions and the microbially mediated deposition of transgressive systems tracts: Journal of Sedimentary Research, v. 76, p. 1057–1066.

Fralick, P.W., Davis, D.W., and Kissin, S.A., 2002, The age of the Gunflint Formation, Ontario, Canada: Single zircon U-Pb age determinations from reworked volcanic ash: Canadian Journal of Earth Sciences, v. 39, p. 1085–1091.

François, L.M., 1986, Extensive deposition of banded iron formations was possible without photosynthesis: Nature, v. 320, p. 352–354.

Franklin, J.M., Gibson, H.L., Jonasson, I.R., and Galley, A.G., 2005, Volcanogenic massive sulfide deposits: Economic Geology 100th Anniversary Volume, p. 523–560.

Frei, R., Dahl, P.S., Duke, E.F., Frei, K.M., Hansen, T.R., Frandsson, M.M., and Jensen, L.S., 2008, Trace element and isotopic characterization of Neoarchean and Paleoproterozoic iron formations in the Black Hills (South Dakota, USA): Assessment of chemical change during 2.9–1.9 Ga deposition bracketing the 2.4–2.2 Ga first rise of atmospheric oxygen: Precambrian Research, v. 162, p. 441–474.

Frei, R., Gaucher, C., Poulton, S.W., and Canfield, D.E., 2009, Fluctuations in Precambrian atmospheric oxygenation recorded by chromium isotopes: Nature, v. 461, p. 250–254.

Freyer, B.J., 1976, Rare earth evidence in iron-formations for changing Precambrian oxidation states: Geochimica et Cosmochimica Acta, v. 41, p. 361– 367.

Frost, C.D., von Blanckenburg, F., Schoenberg, R., Frost, B.R., and Swapp, S.M., 2007, Preservation of Fe isotope heterogeneities during diagenesis and metamorphism of banded iron formation: Contributions to Mineralogy and Petrology, v. 153, p. 211–235.

Fryer, B.J., 1976, Rare earth evidence in iron-formations forchanging Precambrian oxidation states: Geochimica et Cosmochimica Acta, v. 41, p. 361–367.

Fyon, J.A., Breaks, F.W., Heather, K.B., Jackson, S.L., Muir, T.L., Scott, G.M., and Thurston, P.C., 1992, Metallogeny of metallic mineral deposits in the Superior Province of Ontario: Ontario Geological Survey Special Volume 4, Pt. 2, p. 1091–1174.

Garrels, R.M., and Perry, E.A.J., 1974, Cycling of carbon, sulfur, and oxygen through geologic time, *in* Goldberg, E.A., ed., The sea: New York, Wiley, p. 303–336.

Garvin, J., Buick, R., Anbar, A.D., Arnold, G.L., and Kaufman, A.J., 2009, Isotopic evidence for an aerobic nitrogen cycle in the latest Archean: Science, v. 323, p. 1045–1048.

Garzani, E., 1993, Himalayan ironstones, "superplumes," and the breakup of Gondwana: Geology, v. 21, p. 105–108.

German, C.R., and Elderfield, H., 1990, Application of the Ce-anomaly as a paleoredox indicator: The ground rules: Paleoceanography, v. 5, p. 823–833.

German, C.R., and Von Damm, K.L., 2004, Hydrothermal processes: Treatise on Geochemistry, v. 6, p. 181–222.

German, C.R., Holliday, B.P., and Elderfield, H., 1991, Redox cycling of rare earth elements in the suboxic zone of the Black Sea: Geochimica et Cosmochimica Acta, v. 55, p. 3553–3558.

Giles, D., and Nutman, A.P., 2003, SHRIMP U-Pb zircon dating of the host rocks of the Cannington Ag-Pb-Zn deposit, southeastern Mt. Isa block, Australia: Australian Journal of Earth Sciences, v. 50, p. 295–309.

Glass J.B., Wolfe-Simon, F., and Anbar, A.D., 2009, Coevolution of metal availability and nitrogen assimilation in cyanobacteria and algae: Geobiology, v. 7, p. 100–123.

Godfrey, L.V., and Falkowski, P.G., 2009, The cycling and redox state of nitrogen in the Archaean ocean: Nature Geosciences, v. 2, p. 725–729.

Gole, M.J., and Klein, C., 1981, Banded iron-formation through much of Precambrian time: Journal of Geology, v. 89, p. 169–183.

Golubic, S., and Seong-Joo, L., 1999, Early cyanobacterial fossil record: Preservation, palaeoenvironments and identification: European Journal of Phycology, v. 34, p. 339–348.

Goode, A.D.T., Hall, W.D.M., and Bunting, J.A., 1983, The Nabberu basin of Western Australia: Developments in Precambrian Geology, v. 6., p. 295–323.

Goodwin, A.M., 1973, Archean iron-formations and tectonic basins of the Canadian Shield: Economic Geology, v. 68, p. 915–933.

Goodwin, A.M., Monster, J., and Thode, H.G., 1976, Carbon and sulfur isotope abundances in Archean iron-formations and early Precambrian life: Economic Geology, v. 71, p. 870–891.

Grassineau, N.V., Nisbet, E.G., Fowler, C.M.R., Bickle, M.J., Lowry, D., Chapman, H.J., Mattey, D.P. Abell, P., Yong, J., and Martin, A., 2002, Stable isotopes in the Archaean Belingwe belt, Zimbabwe: Evidence for a diverse microbial mat ecology: Geological Society Special Publication 199, p. 309–328.

Grenne, T., and Slack, J.F., 2003, Paleozoic and Mesozoic silica-rich seawater: Evidence from hematitic chert (jasper) deposits: Geology, v. 31, p. 319–322.

——2005, Geochemistry of jasper beds from the Ordovician Løkken ophiolite, Norway: Origin of proximal and distal siliceous exhalites: Economic Geology, v. 100, p. 1511–1527.

Gross, G.A., 1980, A classification of iron-formation based on depositional environments: Canadian Mineralogist, v. 18, p. 215–222.

——1993, Element distribution patterns as metallogenetic indicators in siliceous metalliferous sediments: International Geological Congress, 29th, Kyoto, Japan, Proceedings, v. 17C, p. 96–106.

Grotzinger, J.P., 1990, Geochemical model for Proterozoic stromatolite decline: American Journal of Science, v. 290A, p. 80–103.

Groves, D.I., Phillips, G.N., Ho, S.E., Houstoun, S.M., and Standing, C.A., 1987, Craton-scale distribution of Archean greenstone gold deposits: Predictive capacity of the metamorphic model: Economic Geology, v. 82, p. 2045–2058.

Groves, I.M., Groves, D.I., Bierlein, F.P., Broome, J., and Penhall, J., 2008, Recognition of the hydrothermal feeder to the structurally inverted, giant Broken Hill deposit, New South Wales, Australia: Economic Geology, v. 103, p. 1389–1394.

Habicht, K.S., Gade, M., Thamdrup, B., Berg, P., and Canfield, D.E., 2002, Calibration of sulfate levels in the Archean ocean: Science, v. 298, p. 2372–2374.

Hamilton, M.A., Buchan, K.L., Ernst, R.E., and Stott, G.M., 2009, Widespread and short-lived 1870 Ma mafic magmatism along the northern Superior craton margin [abs.]: EOS Transactions, American Geophysical Union, 2009 Joint Assembly, Toronto, Canada, Abstract GA11A-01.

Han, T.-M., 1988, Origin of magnetite in Precambrian iron-formations of low metamorphic grade, *in* Zachrisson, E., ed., Proceedings of the Seventh Quadrennial IAGOD Symposium: Stuttgart, E.Schweizerbart'sche Verlagsbuchhandlung, p. 641–656.

Han, T.-M., and Runnegar, B., 1992, Megascopic eukaryotic algae from the 2.1–billion-year-old Negaunee Iron-Formation, Michigan: Science, v. 257, p. 232–235.

Hanert, H.H., 2002, Bacterial and chemical iron oxide deposition in a shallow bay on Palaea Kameni, Santorini, Greece: Microscopy, electron probe microanalysis, and photometry of in situ experiments: Geomicrobiology Journal, v. 19, p. 317–342.

Hannah, J.L., Bekker, A., Stein, H.J., Markey, R.J., and Holland, H.D., 2004, Primitive Os and 2316 Ma age for marine shale: Implications for Paleoproterozoic glacial events and the rise of atmospheric oxygen: Earth and Planetary Science Letters, v. 225, p. 43–52.

Hannington, M.D., Jonasson, I.R., Herzig, P.M., and Petersen, S., 1995, Physical and chemical processes of seafloor mineralization: Geophysical Monograph 91, p. 115–157.

Hannington, M.D., de Ronde, C.E.J., and Petersen, S., 2005, Sea-floor tectonics and submarine hydrothermal systems: Economic Geology 100th Anniversary Volume, p. 111–141.

Hanor, J.S., and Duchac, K.C., 1990, Isovolumetric silicification of Early Archean komatiites: Geochemical mass balances and constraints on origin: Journal of Geology, v. 98, p. 863–877.

Harder, E.C., 1919, Iron-depositing bacteria and their geological relations: U.S. Geological Survey Professional Paper 113, 89 p.

Harms, J.E., 1965, Iron ore deposits of Constance Range, *in* McAndrew, J., ed., Geology of Australian ore deposits: Melbourne, Australasian Institute of Mining and Metallurgy, Eighth Commonwealth Mining and Metallurgical Congress of Australia and New Zealand, p. 264–269.

Hartlaub, R.P., Heaman, L.M., Chacko, T., and Ashton, K.E., 2007, Circa 2.3-Ga magmatism of the Arrowsmith orogeny, Uranium City region, western Churchill craton, Canada: Journal of Geology, v. 115, p. 181–195.

Hatton, O.J., and Davidson, G.J., 2004, Soldiers Cap Group iron-formations, Mt. Isa inlier, Australia, as windows into the hydrothermal evolution of a base-metal-bearing Proterozoic rift basin: Australian Journal of Earth Sciences, v. 51, p. 85–106.

Heaman, L.M., 1997, Global mafic magmatism at 2.45 Ga: Remnants of an ancient large igneous province?: Geology, v. 25, p. 299–302.

Heaman, L.M., Machado, N., Krogh, T.E., and Weber, W., 1986, Precise U-Pb zircon ages for the Molson dyke swarm and the Fox River sill—constraints for Early Proterozoic crustal evolution in northeastern Manitoba, Canada: Contributions to Mineralogy and Petrology, v. 94, p. 82–89.

Heaman, L.M., Peck, D., and Toope, K., 2009, Timing and geochemistry of 1.88 Ga Molson igneous events, Manitoba: Insights into the formation of a craton-scale magmatic and metallogenic province: Precambrian Research, v. 172, p. 143–162.

Heikoop, J.M., Tsujita, C.J., Risk, M.J., Tomascik, T., and Mah, A.J., 1996, Modern iron ooids from a shallow-marine volcanic setting: Mahengetang, Indonesia: Geology, v. 24, p. 759–762.

Hein, J.R., Koski, R.A., Embley, R.W., Reid, J., and Chang, S.-W., 1999, Diffuse-flow hydrothermal field in an oceanic fracture zone setting, northeast Pacific: Deposit composition: Exploration and Mining Geology, v. 8, p. 299–322.

Heinrichs, T., 1980, Lithostratigraphische Untersuchungen in der Fig Tree Gruppe des Barberton greenstone belt zwischen Umsoli und Lomati (Südafrika): Göttinger Arbeiten zur Geologie und Paläontologie, v. 22, p. 1–118.

Heising, S., Richter, L., Ludwig, W., and Schink, B., 1999, *Chlorobium ferrooxidans* sp. nov., a phototrophic green sulfur bacterium that oxidizes ferrous iron in coculture with a "*Geospirillum*" sp. strain: Archives of Microbiology, v. 172, p. 116–124.

Heubeck, C., and Lowe, D.R., 1994, Depositional and tectonic setting of the Archean Moodies Group, Barberton greenstone belt, South Africa: Precambrian Research, v. 68, p. 257–290.

Hinrichs, K., 2002, Microbial fixation of methane carbon at 2.7 Ga: Was an anaerobic mechanism possible?: Geochemistry, Geophysics, Geosystems, v. 3, 10 p.

Hoffman, P.F., 1987. Early Proterozoic foredeeps, foredeep magmatism, and Superior-type iron-formations of the Canadian Shield, *in* Kröner, A., ed., Proterozoic lithospheric evolution: Washington, D.C., American Geophysical Union, and Boulder, Colorado, Geological Society of America, p. 85–98.

Hoffman, P.F., Kaufman, A.J., Halverson, G.P., and Schrag, D.P., 1998, A Neoproterozoic snowball Earth: Science, v. 281, p. 1342–1346.

Hofmann, A., 2005, The geochemistry of sedimentary rocks from the Fig Tree Group, Barberton greenstone belt: Implications for tectonic, hydrothermal and surface processes during mid-Archaean times: Precambrian Research, v. 143, p. 23–49.

——2010, Archaean hydrothermal systems in the Barberton greenstone belt and their significance as a habitat for early life, *in* Golding S., and Glikson, M., eds., Earliest life on Earth: Habitats, environments and methods of detection: Berlin, Springer-Verlag, in press.

Hofmann, A., and Bolhar, R., 2007, The origin of carbonaceous cherts in the Barberton greenstone belt and their significance for the study of early life in mid-Archaean rocks: Astrobiology, v. 7, p. 355–388.

Hofmann, A., and Harris, C., 2008, Stratiform alteration zones in the Barberton greenstone belt: A window into subseafloor processes 3.5–3.3 Ga ago: Chemical Geology, v. 257, p. 224–242.

Hofmann, A., and Kusky, T.M., 2004, The Belingwe greenstone belt: Ensialic or oceanic: Amsterdam, Elsevier, Developments in Precambrian Geology, v. 13, p. 487–537.

Hofmann, A., and Wilson, A.H., 2007, Silicified basalts, bedded cherts and other sea floor alteration phenomena of the 3.4 Ga Nondweni greenstone belt, South Africa: Amsterdam, Elsevier, Developments in Precambrian Geology, v. 15, p. 571–605.

Hofmann, A., Dirks, P.H.G.M., Jelsma, H.A., and Matura, N., 2003, A tectonic origin for ironstone horizons in the Zimbabwe craton and their significance for greenstone belt geology: Journal of the Geological Society of London, v. 160, p. 83–97.

Holland, H.D., 1973, The oceans: A possible source of iron in iron-formations: Economic Geology, v. 68, p. 1169–1172.

——1984, The chemical evolution of the atmosphere and oceans: New York, Princeton University Press, 582 p.

——2005, Sedimentary mineral deposits and the evolution of Earth's near-surface environments: Economic Geology, v. 100, p. 1489–1509.

Hotinski, R.M., Kump, L.R., and Arthur, M.A., 2004, The effectiveness of the Paleoproterozoic biological pump: A $\delta^{13}C$ gradient from platform carbonates of the Pethei Group (Great Slave Lake Supergroup, NWT): Geological Society of America Bulletin, v. 116, p. 539–554.

Hren, M.T., Tice, M.M., and Chamberlain, C.P., 2009, Oxygen and hydrogen isotope evidence for a temperate climate 3.42 billion years ago: Nature, v. 462, p. 205–208.

Hulbert, L.J., Hamilton, M.A., Horan, M.F., and Scoates, R.F.J., 2005, U-Pb zircon and Re-Os isotope geochronology of mineralized ultramafic intrusions and associated nickel ores from the Thompson nickel belt, Manitoba, Canada: Economic Geology, v. 100, p. 29–41.

Hunter, M.A., Bickle, M.J., Nisbet, E.G., Martin, A., and Chapman, H.J., 1998, Continental extensional setting for the Archean Belingwe greenstone belt, Zimbabwe: Geology, v. 26, p. 883–886.

Huston, D.L., and Logan, G.A., 2004, Barite, BIFs and bugs: Evidence for the evolution of the Earth's early hydrosphere: Earth and Planetary Science Letters, v. 220, p. 41–55.

Huston, D.L., Sun, S.-S., Blewett, R., Hickman, A.H., Van Kranendonk, M., Phillips, D., Baker, D., and Brauhart, C., 2002, The timing of mineralization in the Archean North Pilbara terrain, Western Australia: Economic Geology, v. 97, p. 733–755.

Huston, D.L., Pehrsson, S., Eglington, B.M., and Zaw, K., 2010, The geology and metallogeny of volcanic-hosted massive sulfide deposits: Variations through geologic time and with tectonic setting: Economic Geology, v. 105, p. 571–591.

Ilyin, A.V., 2009, Neoproterozoic banded iron formations: Lithology and Mineral Resources, v. 44, p. 78–86.

Isley, A.E., 1995, Hydrothermal plumes and the delivery of iron to banded iron formation: Journal of Geology, v. 103, p. 169–185.

Isley, A.E., and Abbott, D.H., 1999, Plume-related mafic volcanism and the deposition of banded iron formation: Journal of Geophysical Research, v. 104, p. 15,461–15,477.

Jacobs, D.K., and Lindberg, D.R., 1998, Oxygen and evolutionary patterns in the sea: Onshore/offshore trends and recent recruitment of deep-sea faunas: Proceedings of the National Academy of Sciences, v. 95, p. 9396–9401.

Jahnke, R.A., 1984, The synthesis and solubility of carbonate fluorapatite: American Journal of Science, v. 284, p. 57–78.

James, H.L., 1954, Sedimentary facies of iron-formation: Economic Geology, v. 49, p. 235–293.

——1983, Distribution of banded iron-formation in space and time, *in* Trendall, A.F., and Morris, R.C., eds., Iron-formation: Facts and problems: Amsterdam, Elsevier, p. 471–490.

James, H.L., Dutton, C.E., Pettijohn, F.J., and Wier, K.L., 1968, Geology and ore deposits of the Iron River-Crystal Falls district, Iron County, Michigan: U.S. Geological Survey Professional Paper 570, 134 p.

Jaun, B., and Thauer, R.K., 2007, Nickel and its surprising impact in nature, *in* Sigel, A., Sigel, H., and Sigel, R.K.O., eds., Metal ions in life sciences: Chichester, U.K., John Wiley and Sons, v. 2, p. 323–356.

Johnson, C.M., Skulan, J.L., Beard, B.L., Sun, H., Nealson, K.H., and Braterman, P.S., 2002, Isotopic fractionation between Fe(III) and Fe(II) in aqueous solutions: Earth and Planetary Science Letters, v. 195, p. 141–153.

Johnson, C.M., Beard, B.L., Beukes, N.J., Klein, C., and O'Leary, J.M., 2003, Ancient geochemical cycling in the Earth as inferred from Fe isotope studies of banded iron formations from the Transvaal craton: Contributions to Mineralogy and Petrology, v. 144, p. 523–547.

Johnson, C.M., Beard, B.L., and Roden, E.E., 2008a, The iron isotope fingerprints of redox and biogeochemical cycling in the modern and ancient Earth: Annual Reviews of Earth and Planetary Sciences, v. 36, p. 457–493.

Johnson, C.M., Beard, B.L., Klein, C., Beukes, N.J., and Roden, E.E., 2008b, Iron isotopes constrain biologic and abiologic processes in banded iron formation genesis: Geochimica et Cosmochimica Acta, v. 72, p. 151–169.

Kappler, A., Pasquero, C., Konhauser, K.O., and Newman, D.K., 2005, Deposition of banded iron formations by anoxygenic phototrophic Fe(II)-oxidizing bacteria: Geology, v. 33, p. 865–868.

Karhu, J.A., and Holland, H.D., 1996, Carbon isotopes and the rise of atmospheric oxygen: Geology, v. 24, p. 867–870.

Kaufman, A.J., Johnston, D.J., Farquhar, J., Masterson, A.L, Lyons, T.W., Bates, S., Anbar, A.D., Arnold, G.L., Garvin, J., and Buick, R., 2007, Late Archean biospheric oxygenation and atmospheric evolution: Science, v. 317, p. 1900–1903.

Kendall, B., Creaser, R.A., Calver, C.R., Raub, T.D., and Evans, D.A.D., 2009, Correlation of Sturtian diamictite successions in southern Australia and northwestern Tasmania by Re-Os black shale geochronology and the ambiguity of "Sturtian"-type diamictite—cap carbonate pairs as chronostratigraphic marker horizons: Precambrian Research, v. 172, p. 301–310.

Kerr, A.A., 1998, Oceanic plateau formation: A cause of mass extinction and black shale deposition around the Cenomanian-Turonian boundary?: Journal of the Geological Society of London, v. 155, p. 619–626.

Kimberley, M.M., 1989, Exhalative origins of iron formations: Ore Geology Reviews, v. 5, p. 13–145.

——1994, Debate about ironstone: Has solute supply been surficial weathering, hydrothermal convection, or exhalation of deep fluids?: Terra Nova, v. 6, p. 116–132.

Klein, C., and Beukes, N.J., 1989, Geochemistry and sedimentology of a facies transition from limestone to iron-formation deposition in the Early Proterozoic Transvaal Supergroup, South Africa: Economic Geology, v. 84, p. 1733–1774.

——1992, Time distribution, stratigraphy, sedimentologic setting, and geochemistry of Precambrian iron-formations, *in* Schopf, J.W., and Klein, C., eds., The Proterozoic biosphere, a multidisciplinary study: New York, Cambridge University Press, p.139–146.

——1993a, Sedimentology and geochemistry of the glaciogenic Late Proterozoic Rapitan Iron Formation in Canada: Economic Geology, v. 88, p. 542–565.

——1993b, Proterozoic iron-formations, *in* Condie, K.C., ed., Proterozoic crustal evolution: Amsterdam, Elsevier, p. 383–418.

Klein, C., and Ladeira, E.A., 2004, Geochemistry and mineralogy of Neoproterozoic banded iron-formations and some selected, siliceous manganese formations from the Urucum district, Mato Grosso do Sul, Brazil: Economic Geology, v. 99, p. 1233–1244.

Klinkhammer, G., Elderfield, H., and Hudson, A., 1983, Rare-earth elements in seawater near hydrothermal vents: Nature, v. 305, p. 185–188.

Knauth, L.P., and Lowe, D.R., 2003, High Archean climatic temperature inferred from oxygen isotope geochemistry of cherts in the 3.5 Ga Swaziland Supergroup, South Africa: Geological Society of America Bulletin, v. 115, p. 566–580.

Knoll, A.H., Javaux, E.J., Hewitt, D., and Cohen P., 2006, Eukaryotic organisms in Proterozoic oceans: Philosophical Transactions of the Royal Society of London, v. 361B, p. 1023–1038.

Konhauser, K.O., Hamade, T., Morris, R.C., Ferris, F.G., Southam, G., Raiswell, R., and Canfield, D., 2002, Could bacteria have formed the Precambrian banded iron formations?: Geology, v. 30, p. 1079–1082.

Konhauser, K.O., Newman, D.K., and Kappler, A., 2005, Fe(III) reduction in BIFs: The potential significance of microbial Fe(III) reduction during deposition of Precambrian banded iron formations: Geobiology, v. 3, p. 167–177.

Konhauser, K.O., Amskold, L., Lalonde, S.V., Posth, N.R., Kappler, A., and Anbar, A., 2007a, Decoupling photochemical Fe(II) oxidation from shallow-water BIF deposition: Earth and Planetary Science Letters, v. 258, p. 87–100.

Konhauser, K.O., Lalonde, S.V., Amskold, L., and Holland, H.D., 2007b, Was there really an Archean phosphate crisis?: Science, v. 315, p. 1234.

Konhauser, K.O., Pecoits, E., Lalonde, S.V., Papineau, D., Nisbet, E.G., Barley, M.A., Arndt, N.T., Zahnle, K., and Kamber, B.S., 2009, Oceanic nickel depletion and a methanogen famine before the Great Oxidation Event: Nature, v. 458, p. 750–753.

Koschinsky, A., Seifert, R., Halbach, P., Bau, M., Brasse, S., de Carvalho, L.M., and Fonseca, N.M., 2002, Geochemistry of diffuse low-temperature hydrothermal fluids in the North Fiji basin: Geochimica et Cosmochimica Acta, v. 66, p. 1409–1427.

Krapež, B., and Martin, D.McB., 1999, Sequence stratigraphy of the Paleoproterozoic Nabberu Province of Western Australia: Australian Journal of Earth Sciences, v. 46, p. 89–103.

Krapež, B., Barley, M.E., and Pickard, A.L., 2003, Hydrothermal and resedimented origins of the precursor sediments to banded iron formations: Sedimentological evidence from the early Palaeoproterozoic Brockman Supersequence of Western Australia: Sedimentology, v. 50, p. 979–1011.

Kroopnick, P.M., 1985, The distribution of ^{13}C of ΣCO_2 in the world oceans: Deep-Sea Research, v. 32, p. 57–84.

Kulik, D.A., and Korzhnev, M.N., 1997, Lithological and geochemical evidence of Fe and Mn pathways during deposition of Lower Proterozoic banded iron formation in the Krivoy Rog basin (Ukraine): Geological Society Special Publication 119, p. 43–80.

Kump, L.R., and Seyfried, W.E., 2005, Hydrothermal Fe fluxes during the Precambrian: Effect of low oceanic sulfate concentrations and low hydrostatic pressure on the composition of black smokers: Earth and Planetary Science Letters, v. 235, p. 654–662.

Laajoki, K., and Saikkonen, R., 1977, On the geology and geochemistry of the Precambrian iron formations, Väyrylänkylä, South Puolanka area, Finland: Geological Survey of Finland Bulletin 292, p. 1–137.

LaBerge, G.L., 1964, Development of magnetite in iron-formations of the Lake Superior region: Economic Geology, v. 59, p. 1313–1342.

Large, R.R., 1992, Australian volcanic-hosted massive sulfide deposits: Features, styles, and genetic models: Economic Geology, v. 87, p. 471–510.

Leach, D.L., Sangster, D.F., Kelley, K.D., Large, R.R., Garven, G., Allen, C.R., Gutzmer, J., and Walters, S., 2005, Sediment-hosted lead-zinc deposits: Economic Geology 100th Anniversary Volume, p. 561–607.

Leckie, R.M., Bralower, T.J., and Cashman, R., 2002, Oceanic anoxic events and plankton evolution: Biotic response to tectonic forcing during the mid-Cretaceous: Paleoceanography, v. 17, p. 13–1 to 13–29.

Leclerc, J., and Weber, F., 1980, Geology and genesis of the Moanda manganese deposits, Republic of Gabon, *in* Varentsov, I.M., and Grasselly, G., eds., Geology and geochemistry of manganese: Stuttgart, E. Schweizerbart'sche Verlagsbuchhandlung, v. 2, p. 89–109.

Lehours, A.C., Evans, P., Bardot, C., Joblin, K., and Fonty, G., 2007, Phylogenetic diversity of Archaea and bacteria in the anoxic zone of a meromictic lake (Lake Pavin, France): Applied and Environmental Microbiology, v. 73, p. 2016–2019.

Leith, A., 1935, The pre-Cambrian of the Lake Superior region, the Baraboo district, and other isolated areas in the upper Mississippi Valley: Kansas Geological Society Guide Books, v. 9, p. 329–332.

Lemoalle, J., and Dupont, B., 1973, Iron-bearing oolites and the present conditions of iron sedimentation in Lake Chad (Africa): International Union of Geological Sciences, Series A, no. 3, p. 167–178.

Little, C.T.S., Glynn, S.E.J., and Mills, R.A., 2004, Four-hundred-and-ninety-million-year record of bacteriogenic iron oxide precipitation at seafloor hydrothermal vents: Geomicrobiology Journal, v. 21, p. 415–429.

Liu, T.-B., Alten, J., and Maynard, J.B., 2006, Superheavy S isotopes from glacial-associated sediments of the Neoproterozoic of South China: Oceanic anoxia or sulfate limitation: Geological Society of America Memoir 198, p. 205–222.

Lottermoser, B.G., 1989, Rare-earth element study of exhalites within the Willyama Supergroup, Broken Hill block, Australia: Mineralium Deposita, v. 24, p. 92–99.

Lottermoser, B.G., and Ashley, P.M., 1999, Geochemistry, petrology and origin of Neoproterozoic ironstones in the eastern part of the Adelaide geosyncline, South Australia: Precambrian Research, v. 101, p. 49–67.

Lucente, M.E., and Morey, G.B., 1983, Stratigraphy and sedimentology of the Lower Proterozoic Virginia Formation, northern Minnesota: Minnesota Geological Survey Report of Investigations 28, p. 1–28.

Macdonald, F.A., Schmitz, M.D., Crowley, J.L., Roots, C.F., Jones, D.S., Maloof, A.C., Strauss, J.V., Cohen, P.A., Johnston, D.T., and Schrag, D.P., 2010, Calibrating the Cryogenian: Science, v. 327, p. 1241–1243.

Mapeo, R.B.M., Armstrong, R.A., and Kampunzu, A.B., 2001, SHRIMP U-Pb zircon geochronology of gneisses from the Gweta borehole, northeast Botswana: Implications for the Palaeoproterozoic Magondi belt in southern Africa: Geological Magazine, v. 138, p. 299–308.

Master, S., 1991, Stratigraphy, tectonic setting, and mineralization of the Early Proterozoic Magondi Supergroup, Zimbabwe: A review: Johannesburg, University of Witwatersrand, Economic Geology Research Unit Information Circular 238, 75 p.

Maynard, J.B., 1986, Geochemistry of oolitic iron ores, an electron microprobe study: Economic Geology, v. 81, p. 1473–1483.

——2003, Manganiferous sediments, rocks, and ores: Treatise on Geochemistry, v. 7, p. 289–308.

Maynard, J.B., and Van-Houten, F.B., 1992, Descriptive model of oolitic ironstones: U.S. Geological Survey Bulletin 2004, p. 39–40.

Meyer, C., 1988, Ore deposits as guides to geologic history of the Earth: Annual Review of Earth and Planetary Sciences, v. 16, p. 147–171.

Meyer, K.M., and Kump, L.R., 2008, Oceanic euxinia in Earth history: Causes and consequences: Annual Review of Earth and Planetary Sciences, v. 36, p. 251–288.

Miller, A.R., and Reading, K.L., 1993, Iron-formation, evaporite, and possible metallogenetic implications for the Lower Proterozoic Hurwitz Group, District of Keewatin, Northwest Territories: Geological Survey of Canada, Current Research, Part C, v. 93, p. 179–185.

Mills, R.A., 1995, Hydrothermal deposits and metalliferous sediments from TAG, 26°N Mid-Atlantic Ridge: Geological Society Special Publication 87, p. 121–132.
Morey, G.B., 1999, High-grade iron ore deposits of the Mesabi Range, Minnesota: Products of a continental-scale Proterozoic ground-water flow system: Economic Geology, v. 94, p. 133–142.
Mücke, A., 2005, The Nigerian manganese-rich iron-formations and their host rocks—from sedimentation to metamorphism: Journal of African Earth Sciences, v. 41, p. 407–436.
Mukhopadhyay, J., Beukes, N.J., Armstrong, R.A., Zimmermann, U., Ghosh, G., and Medda, R.E., 2008, Dating the oldest greenstone in India: A 3.51-Ga precise U-Pb SHRIMP zircon age for dacitic lava of the southern Iron Ore Group, Singhbhum craton: Journal of Geology, v. 116, p. 449–461.
Müller, G., and Förstner, U., 1973, Recent iron ore formation in Lake Malawi, Africa: Mineralium Deposita, v. 8, p. 277–290.
Murray, J.W., 1979, Iron oxides: Mineralogical Society of America Short Course Notes, v. 6, p. 47–98.
Myers, J.S., 2001, Protoliths of the 3.7–3.8 Ga Isua greenstone belt, West Greenland: Precambrian Research, v. 105, p. 129–141.
Oberthür, T., Davis, D.W., Blenkinsop, T.G., and Höhndorf, A., 2002, Precise U-Pb mineral ages, Rb-Sr and Sm-Nd systematics for the Great Dyke, Zimbabwe—constraints on Late Archean events in the Zimbabwe craton and Limpopo belt: Precambrian Research, v. 113, p. 293–305.
Often, M., 1985, The Early Proterozoic Karasjok greenstone belt, Norway: A preliminary description of lithology, stratigraphy and mineralization: Norges Geologiske Undersøkelse Bulletin 403, p. 75–88.
Ohmoto, H., 2003, Nonredox transformations of magnetite-hematite in hydrothermal systems: Economic Geology, v. 98, p. 157–161.
Ohmoto, H., Watanabe, Y., and Kumazawa, K., 2004, Evidence from massive siderite beds for a CO_2-rich atmosphere before ~1.8 billion years ago: Nature, v. 429, p. 395–399.
Ohmoto, H., Watanabe, Y., Yamaguchi, K.E., Naraoka, H., Haruna, M., Kakegawa, T., Hayashi, K., and Kato, Y., 2006, Chemical and biological evolution of early Earth: Constraints from banded iron formations: Geological Society of America Memoir 198, p. 291–331.
Ojakangas, R.A., 1983, Tidal deposits in the Early Proterozoic basin of the Lake Superior region—the Palms and the Pokegama Formations: Evidence for subtidal shelf deposition of Superior type banded iron formation: Geological Society of America Memoir 160, p. 49–66.
Ojakangas, R.W., 1994, Sedimentology and provenance of the Early Proterozoic Michigamme Formation and Goodrich Quartzite, northern Michigan—regional stratigraphic implications and suggested correlations: U.S. Geological Survey Bulletin 1904-R, p. R1–R31.
Ojakangas, R.W., Morey, G.B., and Southwick, D.L., 2001, Paleoproterozoic basin development and sedimentation in the Lake Superior region, North America: Sedimentary Geology, v. 141–142, p. 319–341.
O'Neil, J., Maurice, C., Stevenson, R., Larocque, J., Cloquet, C., and David, J.F.D., 2007, The geology of the 3.8 Ga Nuvvuagittuq (Porpoise Cove) greenstone belt, northeastern Superior Province, Canada: Developments in Precambrian Geology, v. 15, p. 219–250.
Paakola, J., 1971, The volcanic complex and associated manganiferous iron formation of the Porkonen-Pahtavaara area in Finnish Lapland: Bulletin de la Commission géologique de Finlande, v. 247, 82 p.
Page, R.W., Stevens, B.P.J., and Gibson, G.M., 2005, Geochronology of the sequence hosting the Broken Hill Pb-Zn-Ag orebody, Australia: Economic Geology, v. 100, p. 633–661.
Partridge, M.A., Golding, S.D., Baublys K.A., and Young, E., 2008, Pyrite paragenesis and multiple sulfur isotope distribution in Late Archean and early Paleoproterozoic Hamersley basin sediments: Earth and Planetary Science Letters, v. 272, p. 41–49.
Pecoits, E., Gingras, M.K., Aubet, N., and Konhauser, K.O., 2008, Ediacaran in Uruguay: Palaeoclimatic and palaeobiologic implications: Sedimentology, v. 55, p. 689–719.
Perry, E.C., 1967, The oxygen isotope chemistry of ancient cherts: Earth and Planetary Science Letters, v. 3, p. 62–66.
Perry, E.C., Tan, F.C., and Morey, G.B., 1973, Geology and stable isotope geochemistry of Biwabik Iron Formation, northern Minnesota: Economic Geology, v. 68, p. 1110–1125.
Peter, J.M., 2003, Ancient iron formations: Their genesis and use in the exploration for stratiform base metal sulphide deposits, with examples from the Bathurst mining camp: Geological Association of Canada, GEOTEXT 4, p. 145–176.
Peter, J.M., Goodfellow, W.D., and Doherty, W., 2003, Hydrothermal sedimentary rocks of the Heath Steele belt, Bathurst mining camp, New Brunswick: Part 2. Bulk and rare earth element geochemistry and implications for origin: Economic Geology Monograph 11, p. 391–415.
Petránek, J., and Van Houten, F.B., 1997, Phanerozoic ooidal ironstones: Czech Geological Survey Special Paper 7, 71 p.
Pickard, A.L., 2002, SHRIMP U-Pb zircon ages of tuffaceous mudrocks in the Brockman Iron Formation of the Hamersley Range, Western Australia: Australian Journal of Earth Sciences, v. 49, p. 491–507.
——2003, SHRIMP U-Pb zircon ages for the Palaeoproterozoic Kuruman Iron Formation, Northern Cape Province, South Africa: Evidence for simultaneous BIF deposition on Kaapvaal and Pilbara cratons: Precambrian Research, v. 125, p. 275–315.
Pickard, A.L., Barley, M.E., and Krapež, B., 2004, Deep-marine depositional setting of banded iron formation: Sedimentological evidence from interbedded clastic sedimentary rocks in the early Paleoproterozoic Dales Gorge Member of Western Australia: Sedimentary Geology, v. 170, p. 37–62.
Planavsky, N., Rouxel, O., Bekker, A., and Lyons, T.W., 2008, Rare earth element evidence for redox structure evolution [abs.]: Goldschmidt 2008 Conference, Vancouver, B.C., Canada: Geochimica et Cosmochimica Acta, v. 72, Supplement 1, p. A753.
Planavsky, N., Rouxel, O., Bekker, A., Shapiro, R., Fralick, P., and Knudsen, A., 2009, Iron-oxidizing microbial ecosystems thrived in late Paleoproterozoic redox-stratified oceans: Earth and Planetary Science Letters, v. 286, p. 230–242.
Polat, A., and Frei, R., 2005, The origin of Early Archean banded iron formations and of continental crust, Isua, southern West Greenland: Precambrian Research, v. 138, p. 151–175.
Porter, S.M., Meisterfeld, R., and Knoll. A.H., 2003, Vase-shaped microfossils from the Neoproterozoic Chuar Group, Grand Canyon: A classification guided by modern testate amoebae; Journal of Paleontology, v. 77, p. 409–429.
Poulton, S.W., Fralick, P.W., and Canfield, D.E., 2004, The transition to a sulphidic ocean 1.84 billion years ago: Nature, v. 43, p. 173–177.
Prilutzky, R.E., Suslova, S.N., and Nalivkina, Y.B., 1992, Reconstruction of environmental conditions of Early Proterozoic carbonate deposits of the Ukrainian and Baltic Shields based on isotopic studies: Lithology and Mineral Deposits, v. 5, p. 76–88.
Puchelt, H., 1973, Recent iron sediment formation at the Kameni Islands, Santorini (Greece): International Union of Geological Sciences, Series A, no. 3, p. 227–245.
Pufahl, P.K., and Fralick, P.W., 2004, Depositional controls on Palaeoproterozoic iron formation accumulation, Gogebic Range, Lake Superior region, USA: Sedimentology, v. 51, p. 791–808.
Rainbird, R.H., Jefferson, C.W., Hilderbrand, R.S., and Worth, J.K., 1994, The Shaler Supergroup and revision of the Neoproterozoic stratigraphy in the Amundsen basin, Northwest Territories: Geological Survey of Canada Paper 94–1A, p. 61–70.
Rasmussen, B., Fletcher, I.R., Muhling, J.R., Thorne, W.S., and Broadbent, G.C., 2007, Prolonged history of episodic fluid flow in giant hematite ore bodies: Evidence from in situ U-Pb geochronology of hydrothermal xenotime: Earth and Planetary Science Letters, v. 258, p. 249–259.
Reinhard, C., Raiswell, R., Scott, C., Anbar A.D., and Lyons, T.W., 2009, A Late Archean sulfidic sea stimulated by early oxidative weathering of the continents: Science, v. 326. p. 713–716
Resende, M.G., and Jost, H., 1995, Petrogênese de formações ferríferas e metahidrotermalitos da formação aimbé, Grupo Guarinos (Arqueano), Goiás: Revista Brasileira de Geociencias, v. 25, p. 41–50.
Ricketts, B.D., Ware, M.J., and Donaldson, J.A., 1982, Volcaniclastic rocks and volcaniclastic facies in the middle Precambrain (Aphebian) Belcher Group, Northwest Territories, Canada: Canadian Journal of Earth Sciences, v. 19, p. 1275–1294.
Robert, F., and Chaussidon, M., 2006, A palaeotemperature curve for the Precambrian oceans based on silicon isotopes in cherts: Nature, v. 443, p. 969–972.
Rouxel, O., Dobbek, N., Ludden, J., and Fouquet, Y., 2003, Iron isotope fractionation during oceanic crust alteration (Site ODP 801): Chemical Geology, v. 202, p. 155–182.
Rouxel, O., Bekker, A., and Edwards, K., 2005, Iron isotope constraints on the Archean and Paleoproterozoic ocean redox state: Science, v. 307, p. 1087–1091.
Rouxel, O., Galy, A., and Elderfield, H., 2006, Germanium isotopic variations in igneous rocks and marine sediments: Geochimica et Cosmochimica Acta, v. 70, p. 3387–3400.

Rouxel, O., Shanks, W.C., III, Bach, W., and Edwards, K., 2008, Integrated Fe and S isotope study of seafloor hydrothermal vents at East Pacific Rise 9–10N: Chemical Geology, v. 252, p. 214–227.

Ruttenberg, K.C., and Berner, R.A., 1993, Authigenic apatite formation and burial in sediments from non-upwelling, continental margin environments: Geochimica et Cosmochimica Acta, v. 57, p. 991–1007.

Sangster, D.F., 1978, Exhalites associated with Archaean volcanogenic massive sulphide deposits: University of Western Australia, Geology Department and Extension Service Publication 2, p. 70–81.

Schidlowski, M., Eichmann, R., and Junge, C.E., 1976, Carbon isotope geochemistry of the Precambrian Lomagundi carbonate province, Rhodesia: Geochimica et Cosmochimica Acta, v. 40, p. 449–455.

Schmidt, R.G., 1980, The Marquette Range Supergroup in the Gobebic iron district, Michigan and Wisconsin: U.S. Geological Survey Bulletin 1460, 96 p.

Schneider, D.A., Bickford, M.E., Cannon, W.F., Schulz, K.J., and Hamilton, M.A., 2002, Age of volcanic rocks and syndepositional iron formations, Marquette Range Supergroup: Implications for the tectonic setting of Paleoproterozoic iron formations of the Lake Superior region: Canadian Journal of Earth Sciences, v. 39, p. 999–1012.

Schneiderhan, E.A., Gutzmer, J., Strauss, H., Mezger, K., and Beukes, N.J., 2006, The chemostratigraphy of a Paleoproterozoic MnF-BIF succession—the Voelwater Subgroup of the Transvaal Supergroup in Griqualand West, South Africa: South African Journal of Geology, v. 109, p. 63–80.

Schrum, H.N., Spivack, A.J., Kastner, M., and D'Hondt, S., 2009, Sulfate-reducing ammonium oxidation: A thermodynamically feasible metabolic pathway in subseafloor sediment: Geology, v. 37, p. 939–942.

Schulz, K.J., and Cannon, W.F., 2007, The Penokean orogeny in the Lake Superior region: Precambrian Research, v. 157, p. 4–25.

——2008, Synchronous deposition of Paleoproterozoic Superior-type banded iron-formations and volcanogenic massive sulfides in the Lake Superior region: Implications for the tectonic evolution of the Penokeon orogen [abs.]: Geological Society of America Abstracts with Programs, v. 40, p. 385.

Schweigart, H., 1965, Genesis of the iron ores of the Pretoria Series, South Africa: Economic Geology, v. 60, p. 269–298.

Scott, C., Lyons, T.W., Bekker, A., Shen, Y., Poulton, S.W., Chu, X., and Anbar, A.D., 2008, Tracing stepwise oxygenation of the Proterozoic ocean: Nature, v. 452, p. 456–459.

Severmann, S., Johnson, C.M., Beard, B.L., German, C.R., Edmonds, H.N., Chiba, H., and Green, D.R.H., 2004, The effect of plume processes on the Fe isotope composition of hydrothermally derived Fe in the deep ocean as inferred from the Rainbow vent site, Mid-Atlantic Ridge, 36°14N: Earth and Planetary Science Letters, v. 225, p. 63–76.

Severmann, S., Lyons, T.W., Anbar, A., McManus, J., and Gordon, G., 2008, Modern iron isotope perspective on the benthic iron shuttle and the redox evolution of ancient oceans: Geology, v. 36, p. 487–490.

Sharpe, R., and Gemmell, J.B., 2002, The Archean Cu-Zn magnetite-rich Gossan Hill volcanic-hosted massive sulfide deposit, Western Australia: Genesis of a multistage hydrothermal system: Economic Geology, v. 97, p. 517–539.

Shen, Y., Knoll, A.H., and Walter, M.A., 2003, Evidence for low sulfate and anoxia in a mid-Proterozoic marine basin: Nature, v. 423, p. 633–635.

Shen, Y., Pinti, D., and Hashizume, K., 2006, Biogeochemical cycles of sulfur and nitrogen in the Archean ocean and atmosphere: Geophysical Monograph 164, p. 305–320.

Sherrell, R.M., Field, M.P., and Ravizza, G., 1999, Uptake and fractionation of rare earth elements on hydrothermal plume particles at 9°45′N, East Pacific Rise: Geochimica et Cosmochimica Acta, v. 63, p. 1709–1722.

Siever, R., 1992, The silica cycle in the Precambrian: Geochimica et Cosmochimica Acta, v. 56, p. 3265–3272.

Silver, P.G., and Behn, M.D., 2008, Intermittent plate tectonics?: Science, v. 319, p. 85–88.

Simonson, B.M., 2003, Origin and evolution of large Precambrian iron formations: Geological Society of America Special Paper 370, p. 231–244.

Simonson, B.M., and Goode, A.D.T., 1989, First discovery of ferruginous chert arenites in the early Precambrian Hamersley Group of Western Australia: Geology, v. 17, p. 269–272.

Simonson, B.M., and Hassler, S.W., 1996, Was the deposition of large Precambrian iron formations linked to major marine transgressions?: Journal of Geology, v. 104, p. 665–676.

Simonson, B.M., Schubel, K.A., and Hassler, S.W., 1993, Carbonate sedimentology of the early Precambrian Hamersley Group of Western Australia: Precambrian Research, v. 60, p. 287–335.

Sinton, C.W., and Duncan, R.A., 1997, Potential links between oceanic plateau volcanism and global ocean anoxia at the Cenomanian-Turonian boundary: Economic Geology, v. 92, p. 836–842.

Slack, J.F., and Cannon, W.F., 2009, Extraterrestrial demise of banded iron formations 1.85 billion years ago: Geology, v. 37, p. 1011–1014.

Slack, J.F., Grenne, T., Bekker, A., Rouxel, O.J., and Lindberg, P.A., 2007, Suboxic deep seawater in the late Paleoproterozoic: Evidence from hematitic chert and iron formation related to seafloor-hydrothermal sulfide deposits, central Arizona, USA: Earth and Planetary Science Letters, v. 255, p. 243–256.

Slack, J.F., Grenne, T., and Bekker, A., 2009, Seafloor-hydrothermal Si-Fe-Mn exhalites in the Pecos greenstone belt, New Mexico, and the redox state of ca. 1720 Ma deep seawater: Geosphere, v. 5, p. 302–314.

Søgaard, E.G., Medenwaldt, R., and Abraham-Peskir, J.V., 2000, Conditions and rates of biotic and abiotic iron precipitation in selected Danish freshwater plants and microscopic analysis of precipitate morphology: Water Reasearch, v. 34, p. 2675–2682.

Spier, C.A., de Oliveira, S.M.B., Sial, A.N., and Rios, F.J., 2007, Geochemistry and genesis of the banded iron formations of the Cauê Formation, Quadrilátero Ferrífero, Minas Gerais, Brazil: Precambrian Research, v. 152, p. 170–206.

Spry, P.G., Peter, J.M., and Slack, J.F., 2000, Meta-exhalites as exploration guides to ore: Reviews in Economic Geology, v. 11, p. 163–201.

Srinivasan, R., and Ojakangas, R.W., 1986, Sedimentology of quartz pebble conglomerates and quartzites of the Archean Bababudan Group, Dharwar craton, South India: Evidence for early crustal stability: Journal of Geology, v. 94, p. 199–214.

Stalder, M., and Rozendaal, A., 2004, Apatite nodules as an indicator of depositional environment and ore genesis for the Mesoproterozoic Broken Hill-type Gamsberg Zn-Pb deposit, Namaqua Province, South Africa: Mineralium Deposita, v. 39, p. 189–203.

Stanley, S.M., and Hardie, L.A., 1998, Secular oscillations in the carbonate mineralogy of reef-building and sediment-producing organisms driven by tectonically forced shifts in seawater chemistry: Palaeogeography, Palaeoclimatology, Palaeoecology, v. 144, p. 3–19.

Staton, S., Amskold, L., Gordon, G., Anbar, A., and Konhauser, K., 2007, Iron isotope fractionation during photooxidation of aqueous ferrous iron [abs.]: American Geophysical Union, Fall Meeting, Abstracts, p. V44A-04b.

Steinhoefel, G., Horn, I., and von Blanckenburg, F., 2009, Micro-scale tracing of Fe and Si isotope signatures in banded iron formation using femtosecond laser ablation: Geochimica et Cosmochimica Acta, v. 73, p. 5343–5360.

Straub, K.L., Rainey, F.A., and Widdel, F., 1999, *Rhodovulum iodosum* sp. nov. and *Rhodovulum robiginosum* sp. nov., two new marine phototrophic ferrous-iron-oxidizing purple bacteria: International Journal of Systematic Bacteriology, v. 49, p. 729–735.

Sturesson, U., 2003, Lower Palaeozoic iron oolites and volcanism from a Baltoscandian perspective: Sedimentary Geology, v. 159, p. 241–256.

Sturesson, U., Dronov, A., and Saadre, T., 1999, Lower Ordovician iron ooids and associated oolitic clays in Russia and Estonia: A clue to the origin of iron oolites?: Sedimentary Geology, v. 123, p. 63–80.

Sugahara, H., Sugitani, K., Mimura, K., Yamashita, F., and Yamamoto, K., 2010, A systematic rare-earth elements and yttrium study of Archean cherts at the Mount Goldsworthy greenstone belt in the Pilbara craton: Implications for the origin of microfossil-bearing black cherts: Precambrian Research, v. 177, p. 73–87.

Sugitani, K., Yamashita, F., Nagaoka, T., Yamamoto, K., Minami, M., Mimura, K., and Suzuki, K., 2006, Geochemistry and sedimentary petrology of Archaean clastic sedimentary rocks at Mt. Goldsworthy, Pilbara craton, Western Australia: Evidence for the early evolution of continental crust and hydrothermal alteration: Precambrian Research, v. 147, p. 124–147.

Syme, E.C., and Bailes, A.H., 1993, Stratigraphic and tectonic setting of Early Proterozoic volcanogenic massive sulfide deposits, Flin Flon, Manitoba: Canadian Journal of Earth Sciences, v. 88, p. 566–589.

Taitel-Goldman, N., and Singer, A., 2002, Metastable Si-Fe phases in hydrothermal sediments of Atlantis II Deep, Red Sea: Clay Minerals, v. 37, p. 235–248.

Taylor, D., Dalstra, H.J., Harding, A.E., Broadbent, G.C., and Barley, M.E., 2001, Genesis of high-grade hematite orebodies of the Hamersley Province, Western Australia: Economic Geology, v. 96, p. 837–873.

Taylor, K.G., Simo, J.A., Yakum, D., and Leckie, D.A., 2002, Stratigraphic significance of ooidal ironstones from the Cretaceous western interior

seaway: The Peace River Formation, Alberta, Canada, and the Castlegate Sandstone, Utah, U.S.A.: Journal of Sedimentary Research, v. 72, p. 316–327.

Thode, H.G., and Goodwin, A.M., 1983, Further sulfur and carbon isotope studies of Late Archean iron-formations of the Canadian Shield and the rise of sulfate reducing bacteria: Precambrian Research, v. 20, p. 337–356.

Tice, M.M., and Lowe, D.R., 2004, Photosynthetic microbial mats in the 3,416-Myr-old ocean: Nature, v. 431, p. 549–552.

Timofeeff, M.N., Lowenstein, T.K., Augusta Martins da Silva, M., and Harris, N.B., 2006, Secular variation in the major-ion chemistry of seawater: Evidence from fluid inclusions in Cretaceous halites: Geochimica et Cosmochimica Acta, v. 70, p. 1977–1994.

Tomlinson, K.Y., Davis, D.W., Stone, D., and Hart, T.R., 2003, U-Pb age and Nd isotopic evidence for Archean terrane development and crustal recycling in the south-central Wabigoon subprovince, Canada: Contributions to Mineralogy and Petrology, v. 144, p. 684–702.

Trendall, A.F., 1973, Varve cycles in the Weeli Wolli Formation of the Precambrian Hamersley Group, Western Australia: Economic Geology, v. 68, p. 1089–1097.

Trendall, A.F., and Blockley, J.G., 1970, The iron formations of the Precambrian Hamersley Group, Western Australia with special reference to the crocidolite: Geological Survey of Western Australia Bulletin 119, 366 p.

Trendall, A.F., de Laeter, J.R., Nelson, D.R., and Mukhopadhyay, D., 1997, A precise zircon U-Pb age for the base of the BIF of the Mulaingiri Formation (Bababudan Group, Dharwar Supergroup) of the Karnataka craton: Journal of the Geological Society of India, v. 50, p. 161–170.

Trompette, R., Alvarenga, C.J.S., and de Walde, D., 1998, Geological evolution of the Neoproterozoic Corumbá graben system (Brazil): Depositional context of the stratified Fe and Mn ores of the Jacadigo Group: Journal of South America Earth Sciences, v. 11, p. 587–597.

Tsikos, H., and Moore, J.M., 1997, Petrography and geochemistry of the Paleoproterozoic Hotazel iron-formation, Kalahari manganese field, South Africa: Implications for Precambrian manganese metallogenesis: Economic Geology, v. 92, p. 87–97.

Tsikos, H., Beukes, N.J., Moore, J.M., and Harris, C., 2003, Deposition, diagenesis, and secondary enrichment of metals in the Paleoproterozoic Hotazel iron-formation, Kalahari manganese field, South Africa: Economic Geology, v. 98, p. 1449–1462.

Turgeon, S.C., and Creaser, R.A., 2008, Cretaceous oceanic anoxic event 2 triggered by a massive magmatic episode: Nature, v. 454, p. 323–326.

Tyrrell, T., 1999, The relative influences of nitrogen and phosphorus on oceanic primary production: Nature, v. 400, p. 525–531.

Urban, H., Stribrny, B., and Lippolt, H.J., 1992, Iron and manganese deposits of the Urucum district, Mato Grosso do Sul, Brazil: Economic Geology, v. 87, p. 1375–1392.

Valaas Hyslop, E., Valley, J.W., Johnson, C.M., and Beard, B.L., 2008, The effects of metamorphism on O and Fe isotope compositions in the Biwabik Iron Formation, northern Minnesota: Contributions to Mineralogy and Petrology, v. 155, p. 313–328.

van den Boorn, S.H.J.M., van Bergen, M.J., Nijman, W., and Vroon, P.Z., 2007, Dual role of seawater and hydrothermal fluids in Early Archean chert formation: Evidence from silicon isotopes: Geology, v. 35, p. 939–942.

Van Houten, F.B., 1985, Oolitic ironstones and contrasting Ordovician and Jurassic paleogeography: Geology, v. 13, p. 722–724.

Van Houten F.B., and Arthur M.A., 1989, Temporal patterns among Phanerozoic oolitic ironstones and oceanic anoxia: Geological Society Special Publication 46, p. 33–49.

Van Wyck, N., and Norman, M., 2004, Detrital zircon ages from Early Proterozoic quartzites, Wisconsin, support rapid weathering and deposition of mature quartz arenites: Journal of Geology, v. 112, p. 305–315.

Vargas, M., Kashefi, K., Blunt-Harris, E.L., and Lovley, D.R., 1998, Microbiological evidence for Fe(III) reduction on early Earth: Nature, v. 395, p. 65–67.

Veizer, J., 1976, Evolution of ores of sedimentary affiliation through geologic history: Relations to the general tendencies in evolution of the crust, hydrosphere, atmosphere, and biosphere, *in* Wolf, K.H., ed., Handbook of strata-bound and stratiform ore deposits: Amsterdam, Elsevier, v. 3, p. 1–41.

Von Damm, K.L., 1995, Controls on the chemistry and temporal variability of seafloor hydrothermal fluids: Geophysical Monograph 91, p. 222–247.

Walker, J.C.G., 1984, Suboxic diagenesis in banded iron formations: Nature, v. 309, p. 340–342.

Walter, X.A., Picazo, A., Miracle, R.M., Vicente, E., Camacho, A., Aragno, M., and Zopfi, J., 2009, Anaerobic microbial iron oxidation in an ironmeromictic lake [abs.]: Goldschmidt2009 Conference, Davos, Switzerland: Geochimica et Cosmochimica Acta, v. 73, Supplement 1, p. A1405.

Wan, Y.-S., Zhang, Q.-D., and Song, T.-R., 2003, SHRIMP ages of detrital zircons from the Changcheng System in the Ming Tombs area, Beijing: Constraints on the protolith nature and maximum depositional age of the Mesoproterozoic cover of the North China craton: Chinese Science Bulletin, v. 48, p. 2500–2506 [in English].

Weidman, S., 1904, The Baraboo iron-bearing district of Wisconsin: Wisconsin Geological and Natural History Survey Bulletin 13, 190 p.

Welch, S.A., Beard, B.L., Johnson, C.M., and Braterman, P.S., 2003, Kinetic and equilibrium Fe isotope fractionation between aqueous Fe(II) and Fe(III): Geochimica et Cosmochimica Acta, v. 67, p. 4231–4250.

Weyer, S., Anbar, A.D., Gerdes, A., Gordon, G.W., Algeo, T.J., and Boyle, E.A., 2008, Natural fractionation of $^{238}U/^{235}U$: Geochimica et Cosmochimica Acta, v. 72, p. 345–359.

Wheat, C.G., Feely, R.A., and Mottl, M.J., 1996, Phosphate removal by oceanic hydrothermal processes: An update of the phosphorus budget in the oceans: Geochimica et Cosmochimica Acta, v. 60, p. 3593–3608.

Whitehouse, M.J., and Fedo, C.M., 2007, Microscale heterogeneity of Fe isotopes in >3.71 Ga banded iron formation from the Isua greenstone belt, southwest Greenland: Geology, v. 35, p. 719–722.

Widdel, F., Schnell, S., Heising, S., Ehrenreich, A., Assmus, B., and Schink, B., 1993, Ferrous iron oxidation by anoxygenic phototrophic bacteria: Nature, v. 362, p. 834–836.

Wilks, M.E., and Nisbet, E.G., 1988, Stratigraphy of the Steep Rock Group, northwestern Ontario: A major Archean unconformity and Archean stromatolites: Canadian Journal of Earth Sciences, v. 25, p. 370–391.

Williams, L.B., and Ferrell, R.E., Jr., 1991, Ammonium substitution in illite during maturation of organic matter: Clays and Clay Minerals, v. 39, p. 400–408.

Williams, P.J., Barton, M.D., Johnson, D.A., Fontbote, L., de Haller, A., Mark, G., Oliver, N.H.S., and Marschik, R., 2005, Iron oxide copper-gold deposits: Geology, space-time distribution, and possible modes of origin: Economic Geology 100th Anniversary Volume, p. 371–405.

Winter, B.L., and Knauth, L.P., 1992, Stable isotope geochemistry of cherts and carbonates from the 2.0 Ga Gunflint Iron Formation: Implications for the depositional setting, and the effects of diagenesis and metamorphism: Precambrian Research, v. 59, p. 283–313.

Xiong, J., 2006, Photosynthesis: What color was its origin?: Genome Biology 2006, v. 7 (245), 5 p.

Yeo, G.M., 1981, The Late Proterozoic Rapitan glaciation in the northern Cordillera: Geological Survey of Canada Paper 81-10, p. 25–46.

Young, G.M., 1976, Iron formation and glaciogenic rocks of the Rapitan Group, Northwest Territories, Canada: Precambrian Research, v. 3, p. 137–158.

——2002, Geochemical investigation of a Neoproterozoic glacial unit: The Mineral Fork Formation in the Wasatch Range, Utah: Geological Society of America Bulletin, v. 114, p. 387–399.

Zahnle, K.J., Claire, M.W., and Catling, D.C., 2006, The loss of mass-independent fractionation of sulfur due to a Paleoproterozoic collapse of atmospheric methane: Geobiology, v. 4, p. 271–283.

Zerkle, A.L., House, C.H., Cox, R.P., and Canfield, D.E., 2006, Metal limitation of cyanobacterial N_2 fixation and implications for the Precambrian nitrogen cycle: Geobiology, v. 4, p. 285–297.

Zubtsov, Y.I., 1972, Precambrian tillites in the Tien Shan, and their stratigraphic value: Byulleten' Moskovskogo Obshchestva Ispytateley Prirody, Otdel Geologicheskiy, v. 47, p. 42–56 [in Russian].